MICROFILTRATION MEMBRANE FOULING IN WATER TREATMENT: IMPACT OF CHEMICAL ATTACHMENTS

by

Haiou Huang

A dissertation submitted to The Johns Hopkins University

in conformity with the requirements for the degree of

Doctor of Philosophy

Baltimore, Maryland

September 29, 2006

Abstract

Microfiltration Membrane Fouling in Water Treatment:
Impact of Chemical Attachments
by Haiou Huang

Membrane fouling is the loss of membrane permeability as a result of the accumulation of aquatic materials on membrane surfaces. It was hypothesized in this study that the origin of MF membrane fouling is the chemical attachment of these materials on membrane surfaces, which is variable with varying solution chemistry. This hypothesis was tested using model simulation and experimental work.

A mathematical model was first developed based on analyses of particle attachments in MF and a hydraulic model that relates the extent of membrane fouling to the mass of particles attaching to different areas of the membrane. The model simulation results indicate that depositional attachment is primarily responsible for membrane fouling. However, increase in coagulational attachment can reduce the occurrence of pore blocking type of fouling, thereby lowering the extent of the total fouling. Particle size has secondary effects on membrane fouling and generally affects its extent. Particles with radii in a range of 1/6 ~ 1/2 of membrane pore diameter cause the greatest fouling when they are sticky to membrane surfaces. These findings were subsequently validated using a polyvinylidene fluoride (PVDF) MF membrane and monodisperse polystyrene latex particles with predetermined sizes and chemical stabilities.

This model was finally applied to the understanding of natural organic matter (NOM) fouling of the PVDF membrane. The combined results from model simulation, membrane fouling experiments, and various analytical techniques suggests that the model NOM consists of three major components, each with different relevance to membrane

fouling. Component A has sizes close to membrane pores and can cause substantial fouling regardless of the solution chemistry. Component B has sizes and stabilities that vary with varying solution chemistry, and therefore, can foul the membrane to a different extent. Component C does not directly cause membrane fouling due to its small size.

Overall, this study established a mechanistic model useful in the understanding of MF membrane fouling, with potential applications to other low pressure membranes. The results suggest that particle-membrane attachment is the primary reason for irreversible MF membrane fouling, which should be of primary concern in the research, design and operation of MF systems.

Thesis Advisor:

Professor Charles R. O'Melia

Readers:

Professor Charles R. O'Melia

Professor William P. Ball

Professor Eugene Shchukin

Dr. Joseph G. Jacangelo

Acknowledgements

Despite all the technical terms and scientific jargon used, this study is really about a simple aspect of human life, i.e., affordability. More specifically, it carries out the mission of making a relatively novel technology, microfiltration, affordable to everyone who wants to have enough drinkable water for his/her daily life. This mission fits reasonably well into the basic needs of mankind, but does not perfectly match the language of "pure" science. Therefore, the readers have to accept the author's apology for covering the core mission under verbose descriptions of theories and experimentations throughout this essay.

Before letting the readers rush into the forest (and eventually get lost), the author would like to first express his gratitude to his academic advisor and mentor, Dr. Charles R. O'Melia, for his insightful guidance and incredible patience in allowing a student to spend so many years on toy bricks in his lab and explore the nature of science. CROM's scholarship and altruism set the standard for the author to follow in his own career. Second, the author would like to thank his family for their long term support to his study, even though it has made their own lives so "unaffordable," both financially and emotionally. Hopefully, all their sacrifices will be rewarded eventually. Third, the spiritual support from Prof. Long-ping Yuan should be acknowledged. Although he never knows the author (one of the hundreds of audiences listening to his talk in Tsinghua University back in 1998), yet it is his dedication to his career and contribution to his people that convinced the author that the bright part of science does shine over the dark clouds of agonies and personal sufferings. Special thanks also go to Dr. Joseph G.

Jacangelo and Prof. Eugene Shchukin. Their generous support helped the author to enter a broader area of his discipline and career.

The author would like to thank the readers of this thesis, Professors William P. Ball, Eugene Shchkin, and Joseph G. Jacangelo, for their helpful comments and suggestions, which strengthen the scientific value of this work.

Other professors and colleagues in DoGEE deserve many, many thanks for making the tough life of a researcher bearable and fruitful. The author will remember Dr. Wolman's remarks on the conflicts of equality and efficiency in the history of mankind. The author will also remember the discussions on "politics" with Adrian Penisson, who, unfortunately, left us before we could end the talks... Meanwhile, Mr. Rodrigue Spinette gave a lot of useful suggestions during this study, which is crucial in the formation of the conceptual model discussed in this thesis.

Finally, the author gratefully acknowledge the support from the industrial partners. US Filter/Memcor kindly provided the hollow fiber membranes; Arkema/Atofina donated the Kynar samples used in the study. US Filter also provided partial funding to this study through the Olivieri fellowship.

Table of Contents

List of Figures

List of Tables

Chapter One

BACKGROUND

1.1 SCOPE AND OBJECTIVES

The objectives of the study are: 1) to develop a model that is useful in assessing the effects of physiochemical/chemical attachment on the fouling of microfiltration (MF) membranes, 2) to validate the model experimentally using monodisperse polystyrene latex particles with predetermined colloidal stabilities, 3) to examine the applicability of the model to the fouling of MF membranes by pedogenic natural organic matter (NOM) under varied chemical conditions; and 4) based on the experimental results and model calculations, to determine the potential presence of critical conditions for chemical attachment of NOM that are relevant to the fouling, especially hydraulically irreversible fouling, of MF membranes used in the treatment of natural surface waters.

Within the scope of the study, a fundamental assumption was tested: *the fouling of microfiltration membranes is primarily attributed to the chemical attachment of aquatic materials among themselves and on membrane surfaces, which may vary with varying solution chemical conditions.* The experimental work was conducted in the three steps mentioned above in order to test this assumption. The mathematical model provides a numerical tool to qualitatively evaluate the impacts of particle size, depositional (particle-membrane) stability, and coagulational (particle-particle) stability on membrane fouling, together with their relative importance. Next, the major findings were validated in fouling experiments with well-defined colloidal particles. The results were further compared to the fouling behavior of NOM in order to explore the possibility of differentiating the roles of different organic fractions in the fouling process.

The background of the study and the hypothesis is introduced in the following sections.

1.2 APPLICATION OF MICROFILTRATION IN WATER TREATMENT

1.2.1 The History

The history of the development and application of MF technology can be summarized in Figure 1-1 [1]. The earliest extensive application of MF membranes related to the quality of potable water was as a method for rapid testing of microorganism contamination of water supplies. This technique was developed and used in Germany for military purposes during World War II. Before the mid-1960s, however, MF membranes were almost exclusively applied in laboratory or small-scale industrial uses. MF began to be used in biological and pharmaceutical manufacturing (1960s and 1970s) and for dust control in microelectronics (1980s). A common feature of these industries is the high commercial value of their final products. Therefore, single-use and disposable membranes were technically simple and economically affordable. The efficacy of MF in the sterilization of waters has also been proved during its application in these industries. This is a particularly important driving force technically for the introduction of MF into the area of water treatment in the U.S. as the regulations on drinking water quality have been tightened [2]. Unlike previous applications, single-use membranes are not suitable for large-scale potable water treatment as a result of high membrane costs and low productivity of clean water. This problem is discussed in detail in the next section.

The application of MF in water treatment has grown rapidly since the end of the last century. The total installed capacity of MF was approximately 200 million gallon per

day (mgd) in water industries worldwide by 2000 [3], mostly in Europe and the US. According to a survey conducted by the US EPA in 2001, more than half of the full-scale MF plants in the US had installed capacity of less than 0.5 mgd as of April, 2000. Reasons for this include: ease of operation, excellent finished water quality, high degree of automation that reduces the need of continual staffing, and modular design that does not require custom engineering. All these factors are attractive to small communities [2]. Recently, both the capacity and number of MF plants installed have increased dramatically, both in the US and worldwide. Water treatment plants with mgd capacities have been in service or under construction.

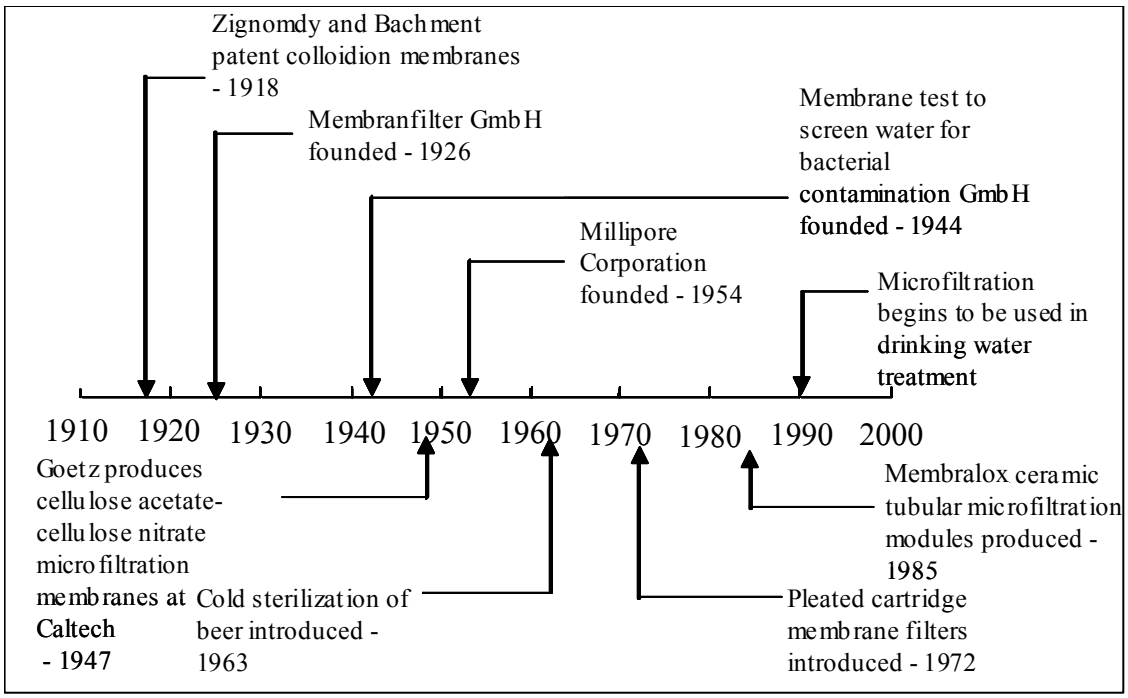

Figure 1-1. History of MF technology. Adapted from [1], page 268, with some modifications.

MF can be used in potable water treatment to disinfect water and remove turbidity. Madaeni [4] reviewed the application of MF and other membrane filtration techniques in water disinfection. Except for some scarce reports on the passage of certain types of bacteria through some model systems, most studies have confirmed the reliability of MF in removing bacteria and cysts or oocysts. For the purpose of water and wastewater treatment, however, MF is typically used as a post-treatment subsequent to other chemical or biological processes. Chemical pretreatment, especially coagulation, has been commonly used to enhance the removal of viruses [5] and other aquatic contaminants by MF membranes, such as disinfection byproduct (DBP) precursors (NOM) [6] and arsenic [7]. On the other hand, MF is also used as a pretreatment for nanofiltration (NF) and Reverse Osmosis (RO) systems to reduce their solid loads and exposures to microorganisms. The latter is usually relevant to the control of biofouling [8, 9]. It is expected that the application of MF in water treatment will continue to grow at an accelerated speed in the next few years, together with other low pressure membrane technologies [2, 3].

1.2.2 MF Membrane Properties

The membrane is the key to the operation and efficiency of MF techniques. MF membranes are porous membranes that rely on the dimension of pores to selectively separate dispersed materials from their dispersions [10]. The properties of MF membranes can be classified into two basic categories: structural properties and functional properties. Structural properties include membrane bulk material, surface chemistry (e.g., surface functionality and hydrophilicity), pore geometry (e.g., size and

shape), porosity, and surface roughness. These properties are generally specified by the individual manufacturing processes, but can also be modified to improve membrane performance, especially fouling resistance. Comparatively, functional properties are not intrinsic. Rather, they are "manifested" properties that are only observed during the utilization of MF membranes. Among these, hydraulic permeability and nominal pore size are the primary concerns for the application of MF in water treatment. The former determines the water productivity of a membrane system; the latter is relevant to the removal of aquatic contaminants of concern by the membrane. In order to maintain a balance between permeability and removal efficiency, commercial MF membranes used in water treatment usually have high permeability (low working transmembrane pressures of less than 100 kPa) and nominal pore sizes of 0.1 or 0.2 μm (measured by microsphere rejection, bubble point tests, and others). More recently, chemical compatibility, particularly chlorine tolerance, has become another important functional property of these MF membranes, primarily as a result of the application of chemical cleaning in fouling control. Overall, the structural and functional properties of MF membranes are strongly related to each other. The possibility of engineering the structure of membranes to meet the needs of specific functions required for water treatment is one of the advantages of membrane filtration techniques over conventional processes.

1.3 MEMBRANE FOULING IN PRACTICE

From the practical point of view, membrane fouling means the "permanent" loss of system productivity over time when natural waters are filtered using a microfiltration unit. In other words, less cleaned water can be produced at given energy input or higher energy

has to be consumed to maintain a desirable water productivity, as a result of membrane contamination by materials in the feedwater. Because hydraulic backwashing and/or pneumatic shaking of membranes are inherent in the routine cycle of microfiltration, fouling is oftentimes considered as the performance loss that remain after periodic hydraulic cleaning. This is comparable to the concept of *hydraulically irreversible fouling* used later in this thesis.

The occurrence of fouling is almost universal for large-scale microfiltration systems. Therefore, fouling control or reduction is an unavoidable challenge to both membrane design and system operation. This is evidenced by the fast evolution of membranes used by industries. Since the industrial operation of the first microfiltration facility in late 1980s, commercial membranes have evolved from the first generation of hydrophobic and less chlorine tolerant membranes (e.g., polypropylene membranes) to a new generation of hydrophilic and chlorine tolerant membranes (e.g., modified polyvinylidene fluoride and polyethersulfone). The driving force for the evolution is primarily fouling control. Comparing the two generations of membranes, the new generation typically has less hydraulically irreversible fouling and is more compatible to chemical cleaning using oxidants. Moreover, despite the advance of membrane design, proper operation is still crucial to the fouling control of large scale systems. It is often found that membrane fouling can be reduced by pretreating (e.g., coagulating) the feedwater to partially remove some foulants, lowering permeate flux and/or recovery, and/or increasing the frequency of chemical backwashing/cleaning. With the integration of these design and operation strategies, most large-scale microfiltration plants are now capable of maintaining their productivity in long-term operation, which has boosted the

application of MF and other low pressure membrane filtration in water purification and reclamation. There are still, however, "spacious" rooms to be filled in for the control of fouling, both economically and technically, to facilitate the development and application of this new technology.

1.4 Mechanistic Investigation of Membrane Fouling by Aquatic Contaminants

1.4.1 NOM Characteristics

Natural organic matter (NOM) is a global term for naturally occurring organic materials found in the environment. They have been considered a major category of foulant to microfiltration membranes. Therefore, some properties of NOM are herein introduced.

In natural waters typically used in potable water treatment, including lake waters, river waters, and groundwaters, two major sources of NOM are usually found, namely, soils and waters bodies [11-13]. The associated NOM are referred to as "pedogenic/allochthonous" and "aquagenic/autochthonous", respectively. Pedogenic NOM in surface waters consists primarily of fulvic acids (FA); aquagenic NOM is comprised of polymers such as proteins and polysaccharides that are produced and released by the primary producers in aquatic environments [14]. The concentration of aquagenic polysaccharides is generally low because they are readily decomposed by other organisms in waters [14] or form sediments associated with colloidal particles [11, 12]. In contrast, pedogenic NOM usually prevails in natural waters due to its high resistance to biodegradation, capability in stabilizing inorganic colloids [14], and

consistent inputs from surrounding soils [13]. However, high concentrations of aquagenic NOM can be found in eutrophic lakes in summer [12].

Most aquatic NOM has properties of polyelectrolytes due to the presence of ionizable functional groups on their chemical structures. These functional groups are reactive with other aquatic species, including proton, calcium, and other multivalent ions [15, 16]. Pedogenic NOM found in aquatic systems is usually smaller in size and molecular weight but more negatively charged than aquagenic NOM [17]. Meanwhile, NOM extracted directly from soils is found to have higher molecular weight than NOM found in aquatic environments [18]. Because of the presence of these functional groups, the conformation and configuration of NOM are subject to change with varied solution chemistry, both in the bulk aqueous phase and at solid/water interfaces [19].

Another direct result of varying solution chemistry is the variation of NOM adsorption at solid/water interfaces. Most information available so far is limited to mineral oxide/water interfaces, where the complexation interactions (ligand exchanges) between the neutral surface sites of oxides and the deprotonated functional groups of NOM seem to dominate the adsorption process [19]. Another study looked at the adsorption of proteins on hydrophilic ultrafiltration (UF) membrane surfaces under different pHs and ionic strengths [20]. The results indicated that the kinetics of protein adsorption are primarily limited by surface interactions, rather than diffusive transport. Electrostatic interactions appeared to be the governing factor under varied solution chemical conditions. Besides the chemistry of ambient media, the surface chemistry of solid surfaces seems to also affect the adsorption of proteins [21]. The impacts of long

range surface interactions on protein transport through porous membranes have been reviewed by Zydney and Pujar [22].

1.4.2 Recent Advances in the Understanding of Membrane Fouling

MF membrane fouling is defined in the study as *the loss of MF membrane permeability due to the accumulation of exogenous substances on membrane surfaces or inside their porous structures during the MF of natural waters*. Membrane fouling will decrease the productivity of MF membrane systems and/or increase the cost of their operation and maintenance. Recent advances in the understanding of membrane fouling can be summarized in four basic aspects: 1) identification of major aquatic components in natural waters (e.g., NOM) that are primarily responsible for the fouling of MF membranes, 2) development of conceptual or phenomenological models for membrane fouling, 3) establishment of mathematical models to describe or predict fouling, and 4) development of fouling control strategies. The four aspects are oftentimes intertwined in the studies reported.

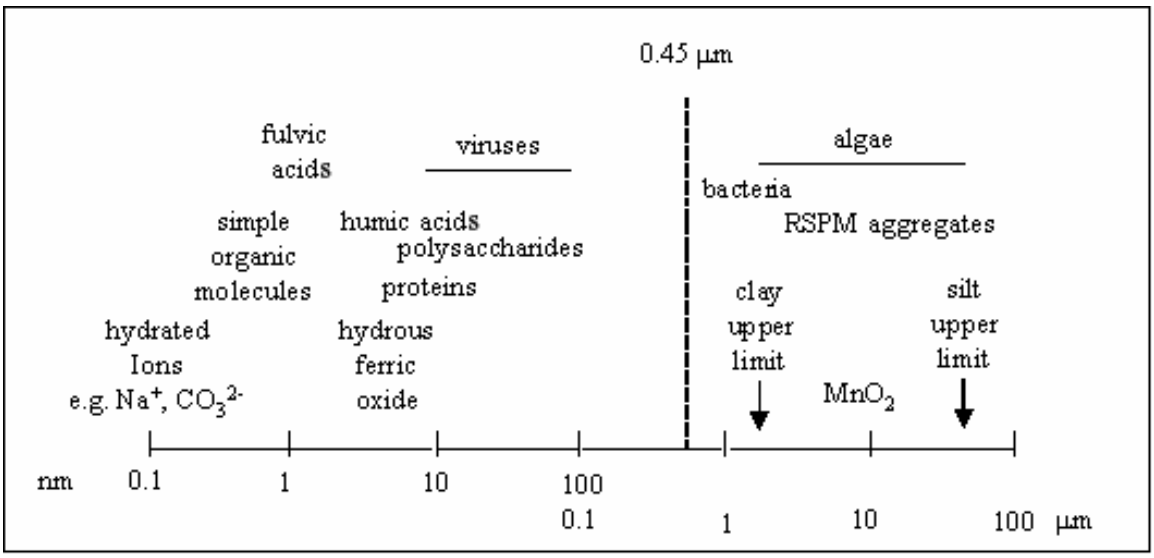

Figure 1-2. Approximate sizes of chemical and biological components of natural surface waters. RSPM means riverine suspended particulate matter at moderate flow; the MnO_2 particle size refers to lake water precipitates. Adapted from [23], page 36.

Figure 1-2 summarizes major components of natural waters and their approximate sizes. As shown in the figure, MF membranes with nominal pore sizes of 0.1 or 0.2 μm should be effective in removing clays, algae, bacteria, protozoa, MnO_2, and some suspended aggregates. However, several recent studies showed that the major foulants of MF membranes are generally smaller than the nominal pore size of MF membranes. In the study by Carroll *et al.* [24], NOM in Moorabool River water was concentrated and then separated into four fractions: strongly hydrophobic (34 % of total DOC), weakly hydrophobic (or transphilic, 18 % of total DOC), charged hydrophilic (33 % of total DOC), and neutral hydrophilic (15 % of total DOC). The last fraction was organic materials that passed through all ion exchange resins used for fractionation. The hydrophilic neutral organics produced the greatest fouling compared to all of the fractions that can be adsorbed by the resins, and the amount of fouling was close to that of unfractionated water samples. In a follow-up study [25], size fraction of the hydrophilic

neutral organics was conducted using the same source of natural water used by Carrol *et al.*. The results showed that this organic fraction is comprised of mostly high molecular weight (HMW) substances. On the other hand, Lee *et al.* [26] performed size fractionation of NOM in natural waters, the filtrates, and backwashing waters through different types of low pressure MF/UF membranes. They found that the high molecular weight/colloidal fraction of NOM had the most dramatic changes after filtration, coincident with the loss and the restoration of membrane permeability. Therefore, this particular fraction was presumed to be an important component of foulants in MF. Both aforementioned studies suggested that aquagenic NOM (non-humic substances) is more important than pedogenic NOM (mostly humic substances) in causing membrane fouling. The authors' recent works [27] showed that aquatic colloids are even more effective than aquagenic NOM in the fouling of MF membranes. This is consistent with an earlier works done by Howe and Clark [28]. In that study, the authors compared the effects of particulate, colloidal and dissolved organic matter in the fouling of MF membranes. They found that the majority of fouling was ascribed to colloidal materials in a size range of 3 – 20 nm. Elemental analysis of the foulants revealed that these colloidal size materials contained primarily organics as well as some inorganic colloids. The actual composition varied depending on the sources of the natural waters.

Given this evidence of the role of small colloidal materials in membrane fouling, adsorption becomes a "physically realistic explanation" for the fouling mechanism considering the fact that membrane pores are substantially larger than the size of these colloids [28]. A direct consequence of this reasoning is that, by reducing the adsorption of these colloids on membrane surfaces, the fouling should be mitigated as well. This has

been realized in two different ways: membrane modification and pretreatment of the raw water using adsorption. Carroll *et al.* [29] modified the surface of a polypropylene (PP) membrane by introducing a layer of uncharged or charged hydrophilic polymer, and no fouling was observed in the filtration of natural surface waters by modified membranes with grafted anionic hydrophilic polymers. On the other hand, Clark *et al.* prepared a polymeric adsorbent that was claimed to be capable of adsorbing these colloidal materials and reducing fouling. However, all these studies did not show how hydrodynamic conditions can affect their results, albeit all "adsorptions" occurred in the presence of water flow, either through the modified membranes or the polymeric adsorbent. In one of our preliminary tests, no fouling by Dismal Swamp water NOM was observed in the absence of calcium when the permeation flux was as low as 5 gal/ft^2-day (gfd); fouling was seen when the permeate flux was increased to the range of 10 – 36 gfd and the fouling rates were approximately the same. In comparison, membrane fouling occurred even at a permeate flux of 5 gfd in the presence of 1 mM of calcium. This suggests the important role of hydrodynamic conditions in the fouling of MF membranes and its correlation with solution chemistry. Similar effects were also observed by other researchers in the MF of inorganic colloidal suspensions or protein solutions [30, 31]. The fouling experiments reported in this thesis were conducted at a permeate flux of approximately 50 gfd (90 L/m^2-hr). This is expected to be greater than the "critical flux" for the NOM fouling to occur if it exists.

In comparison to the concept of membrane fouling by small colloids, Yuan and Zydney [32] studied the impact of NOM aggregation on the fouling of MF membranes. The results showed that, under solution chemical conditions favorable for the aggregation

of a soil derived humic acid, the fouling of MF membranes became severe. In the meantime, prefiltration of NOM solutions containing these aggregates substantially alleviated NOM fouling. However, there is not enough evidence to support the presence of humic aggregates in natural waters. Therefore, it is unclear whether their finding is applicable to the fouling of MF membranes by aquatic humic substances. On the other hand, protein aggregates larger than the pore size of MF membranes may exist in certain aqueous conditions, thereby playing a dominant role in membrane fouling [31, 33]. For these large materials, fouling is likely to occur by blocking the open pores on membrane surfaces and/or forming a cake layer that results in additional hydraulic resistance. The actual picture will be more complicated because of the complex structure of membrane pores [34].

1.5 MATHEMATICAL MODELS FOR MEMBRANE FOULING

Pursuant to the understanding of different roles of aquatic components in membrane fouling, different mathematical models have been developed to emphasize the importance of large and/or small materials. The most widely used empirical model is the cake filtration model that focuses on the role of materials larger than membrane pore size. A general function for the hydrodynamic resistance of cake layers [R_c, m^{-1}] can be written as:

$$R_c = \hat{R}_c \cdot m_d \tag{1}$$

where $\hat{R}_c$ [m/kg] is the specific resistance of the particle deposit or cake layer on the membrane surface, and m_d [kg/m^2] is the mass of deposits accumulated on unit surface

area of membranes. The corresponding permeate flux (J, m^3/m^2-s) is expressed using Darcy's law and a resistant-in-series model:

$$J = \frac{\Delta P}{\mu\left(R_m + R_c\right)} \tag{2}$$

where ΔP (Pa) is transmembrane pressure (TMP), μ (Pa-s) is the solution viscosity, and R_m (1/m) is the hydrodynamic resistance of clean membranes. Additional work has been done in order to relate $\hat{R}_c$ to the structure of cake layers formed by particles or aggregates [35, 36]. The cake filtration model has been used to fit field filtration data and reasonable results have been obtained [37]. This does not explain the mechanism of fouling, but indicates the presence of proportionality between the increase of hydrodynamic resistance and the mass of deposits on MF membranes as the filtration proceeds under some practical conditions. The values of $\hat{R}_c$ vary from 10^{10} to 10^{16} m/kg for different aquatic substances [38]. Babel *et al.* [39] found that $\hat{R}_c$ for a Chlorella algae culture changed from 10^{11} m/kg to 10^{12} m/kg when the growth condition became inhibitive. Foley [40] reviewed different factors affecting the permeability of cake layers formed in dead-end MF of microbial suspensions. It was found that $\hat{R}_c$ is dependent on cell morphology, surface properties, operating pressure, ageing time, and etc., and can vary substantially even for the same bacterium.

Kosvintsev *et al.* [41] developed another model to describe the fouling of MF membranes by materials larger than membrane pore sizes as a result of the physical sieving effect. According to their analysis, membrane fouling by cake filtration does not start right after the onset of filtration, and the fouling is rather dominated by pore blocking until the membrane surface is covered by 12 layers of latex particles. A

dimensionless form of the mathematical equation can be written in the case of constant pressure MF as follows:

$$V^* = \frac{1}{\beta}\ln\left(1+\beta t^*\right) \tag{3}$$

where V^* is the dimensionless permeate volume, β is the ratio between the area of influence above a pore and the pore area itself, and t^* is the dimensionless filtration time. V^* and t^* are made dimensionless basically by normalizing the cumulative permeate volume to the entire volume of the membrane, and the filtration time to the time for the permeate to pass through the entire membrane at the flowrate of time zero (Q_0 as in the Zydney's model), respectively. β is the only fitting parameter in this model, and is varied by the chemistry of the filtration system. β is larger than one in the presence of favorable interactions between the membrane surface and particles. Subsequent to pore blockage, the fouling will shift to cake layer filtration mentioned above. More details of the model has been presented in their recent works [42].

Zydney *et al.* combined two fouling processes in a "pore-blockage – cake filtration model" to describe the fouling of MF membranes by proteins and humic acids [43, 44]. Again, this model is established by assuming that the fouling is caused primarily by large particles, primarily the aggregates of proteins and humic acids. The mathematical manipulation is based on constant pressure and varying flux systems. A general equation for the fouling of MF membranes with non-interconnected pore structure is written as:

$$\frac{Q}{Q_0} = \exp\left(-\frac{k_b \Delta P C_b}{\mu R_m} t\right) + \frac{R_m}{R_m + R_{po} + R' m_p}\left[1 - \exp\left(-\frac{k_b \Delta P C_b}{\mu R_m} t\right)\right] \tag{4}$$

where Q and Q_0 (m^3/s) are volumetric filtrate flow rates at filtration time of t and 0, respectively, k_b (m^2/kg) is a pore blockage parameter and equals the membrane area blocked per unit mass of aggregates convected to the membrane, C_b (kg/m^3) is the bulk concentration of large aggregates and depends upon the chemistry of the protein and buffer solution, R_m (1/m) is the clean membrane resistance, R_{po} is the initial resistance of the first particle/aggregate (1/m), m_p (kg) is the total mass of aggregates retained by the membrane, and ΔP is the transmembrane pressure (Pa). The RHS of the equation includes two terms that are related to pore blockage and cake formation, respectively. The first term (pore blocking) will dominate at the early stage of fouling, and the second term (cake filtration) will govern at longer times. This equation can be altered to account for composite membranes and isotropic membranes as well. In the meantime, the impact of solution chemistry on membrane fouling was not directly included in the model, but was rather considered as a prerequisite for the aggregation of proteins or humic acids.

In comparison to the aforementioned models, the adsorptive fouling of MF membranes by materials smaller than membrane pore sizes has also been interpreted in some model studies. The impact of the adsorption layer on the permeability of MF membranes can be estimated using a modified form of Hagen-Poiseulle capillary filtration model [45]:

$$\frac{J}{J_0} = \left(1 - \frac{\delta'}{r_p}\right)^4 \tag{5}$$

where J and J_0 (m^3/m^2-s) are the permeate fluxes before and after the formation of the adsorptive fouling layer under the given transmembrane pressure, respectively, δ' (m) is the thickness of the adsorption layer, and r_p (m) is the pore radius of membranes. The

major difficulty in applying the adsorptive fouling model to the MF of natural surface waters lies in the complex nature of aquatic NOM. In other words, the value of δ' is not easy to obtain either theoretically or experimentally. This problem is further complicated by the heterogeneity of membrane surface properties.

1.6 CHEMICAL ATTACHMENT RELEVANT TO MICROFILTRATION

An important problem behind this study is the question: *what is the origin of the attachment of foulants on membrane surfaces?* To physicists, the answer is simple. There are only four (may even less) types of forces that can contribute to "attachment", namely, universal attractive force, weak interaction, strong interaction, and electromagnetic force [46]. These forces apply to material entities at different scales, and it is the electromagnetic force that is most relevant to our question. However, there has not been a way for engineers to directly apply this understanding to the microfiltration of natural waters. In fact, the summation of all electromagnetic forces involved in such a system is too complicated to be solved even with the most powerful computers in the world. Therefore, some approximations used by chemists have to be employed in order to simplify the problem and find some useful guidance for engineering applications.

1.6.1 Chemical Attachment by Dispersion Interaction

Foulants stay together on membrane surfaces most likely due to the presence of physiochemical interactions, such as the dispersion interaction between aqueous entities. In the classical view of DLVO theory, the dispersion interaction is attractive across water

and is balanced by the electrostatic repulsion due to the presence of surface charges. The presence of a primary well in the interaction energy curve determines the existence of relatively "irreversible" attachment; comparatively, more "reversible" attachment may be established if there is another energy well, i.e., secondary well on the interaction energy curve. The major difference between deposition in the primary and the secondary energy wells is the presence of an energy barrier for the primary well. The height of the energy barrier depends not only on how strong the attractive interaction is, but also on the magnitude of the repulsive electrostatic interaction. Therefore, it is usually considered beneficial to increase the charge density of the likely charged interacting entities to reduce attachment. Quantitative analysis of the interactions is possible for some model systems using existing numerical approaches. As an example, Table 1-1 lists the Hamaker constants (a measure of the van del Waals interaction) between polystyrene latex particles and representative membrane materials across water, calculated using the macroscopic approach [46]. The Hamaker constant at zero frequency, $A_{\nu=0}$, is related to the dielectric constants, and can be partially screened out if concentrated electrolytes are present in the aqueous phase. The magnitude of $A_{\nu=0}$ is always less than $\frac{3}{4}kT$. Therefore, attention should be paid to the Hamaker constants at frequencies above zero, $A_{\nu>0}$, which is related to the three refractive indices, or fundamentally, the dispersion interaction between these surfaces. As shown in the table, the minimum and the maximum $A_{\nu>0}$ values are observed with PTFE and alumina, respectively; the dispersion interaction between latex and PVDF (the major material of the membrane used in the study) is slightly less than half of that between two latex particles. However, if the material is uniform, it should be noticed that the attractive force or energy due to

dispersion interaction between two identical spherical particles is half of that between a spherical particle and a flat surface. Consequently, the dispersion interaction between a latex particle and a PVDF membrane is approximately equivalent to that between two latex particles. This does not mean that the interaction energy curves will be the same in the two cases because the electrostatic repulsion varies as the surface charge densities of the latex particle and the PVDF membrane are different.

Table 1-1. Non-retarded Hamaker constants calculated using the Lifshitz approach for representative particle-membrane interaction systems (assuming the absorption frequency, $\nu_e = 3\times10^{15}$ s^{-1})

Interaction System[1] (1-3-2)	Dielectric Constant, kHz[2]			Refractive Index[3]			Hamaker Constant × 10^{21}, J		
	ε1	ε3	ε2	n1	n3	n2	$A_{v=0}$	$A_{v>0}$	A_{tot}
Latex-water-PTFE	2.55	80	2.1	1.557	1.333	1.359	2.75	1.55	4.30
Latex-water-PVDF	2.55	80	6.4	1.557	1.333	1.42	2.47	5.12	7.59
Latex-water-CA	2.55	80	4.5	1.557	1.333	1.475	2.59	8.27	10.9
Latex-water-PP	2.55	80	1.5	1.557	1.333	1.49	2.79	9.12	11.9
Latex-water-cellulose nitrate	2.55	80	6.4	1.557	1.333	1.51	2.47	10.2	12.7
Latex-water-PES	2.55	80	3.5	1.557	1.333	1.55	2.65	12.5	15.1
Latex-water-latex	2.55	80	2.55	1.557	1.333	1.557	2.72	12.8	15.6
Latex-water-PC	2.55	80	2.95	1.557	1.333	1.586	2.69	14.4	17.1
Latex-water-Alumina	2.55	80	11.6	1.557	1.333	1.75	2.16	22.9	25.1
Latex-water-fused quartz	2.55	80	3.8	1.557	1.333	1.448	2.63	6.74	9.37

Note: [1] the Acronyms for membrane materials mean: PTFE (polytetrafluoroethylene), PVDF (polyvinylidene fluoride), CA (cellulose acetate), PP (polypropylene), PES (polyethersulfone), PC (polycarbonate); [2] dielectric constant information was obtained from http://www.clippercontrols.com/info/dielectric_constants.html; [3] Refractive index values were adapted from http://www.texloc.com/closet/cl_refractiveindex.html; [4] Lifshitz equation for the calculation of Hamaker constant [46]:

$$A_{tot} = A_{v=0} + A_{v>0}$$

$$\approx \frac{3}{4}kT\left(\frac{\varepsilon_1-\varepsilon_3}{\varepsilon_1+\varepsilon_3}\right)\left(\frac{\varepsilon_2-\varepsilon_3}{\varepsilon_2+\varepsilon_3}\right)+\frac{3h\nu_e}{8\sqrt{2}}\frac{\left(n_1^2-n_3^2\right)\left(n_2^2-n_3^2\right)}{\left(n_1^2+n_3^2\right)^{1/2}\left(n_2^2+n_3^2\right)^{1/2}\left\{\left(n_1^2+n_3^2\right)^{1/2}+\left(n_2^2+n_3^2\right)^{1/2}\right\}}$$

1.6.2 Physiochemical Attachment by "Polar" Interactions

Surface interactions across aqueous media are oftentimes more complicated than what depicted by the classical DLVO theory, mostly because liquid water is a structured medium, a result of the presence of hydrogen bonding between water molecules [46].

Different types of interactions have been proposed to be included in order to extend the DLVO theory into aqueous phase. van Oss postulated the concepts of polar and apolar interactions to classify and predict these interactions [47]. The apolar interaction mainly consists of the aforementioned dispersion interaction; the polar (or Lewis acid-base) interaction, meanwhile, is comprised of the interactions between all Lewis acid-base pairs in the system, including the two interacting entities and surrounding water molecules. It is useful in explaining the advantage of hydrophilizing the membrane surface to reduce the irreversible attachment of particles and other fouling materials on membrane surface. According to the concept of apolar/polar interactions, the strength of chemical attachment depends not only on the dispersion interaction (apolar), but also, or even more dominantly, on the polar interactions. The latter can be either attractive or repulsive based on the hydrophilicity of the two interacting surfaces. For two hydrophilic surfaces, the polar interaction is repulsive and counteracts the attractive dispersion interaction. Therefore, the total interaction becomes either weakly attractive or repulsive even in the absence of electrostatic repulsion. In this case, the interacting system is thermodynamically stable with respect to coagulation or deposition. In comparison, the polar interactions would be fairly attractive between hydrophobic surfaces, which are additive to the attractive dispersion interactions. Consequently, electrostatic repulsion becomes the dominant factor in balancing the attractions and preventing the occurrence of physiochemical attachment. In this case, the interacting system is kinetically stable with respect to coagulation and deposition. Therefore, there are in principle at least two possible approaches to make the membrane less vulnerable to the attachment of aquatic contaminants (hence membrane fouling): one is the hydrophilization of membrane

surfaces (to enhance thermodynamic stability), and the other is the ionization of membrane surfaces (to achieve kinetic stability). Both approaches have been investigated in other studies [29, 48-52].

The presence of polar interactions has also been used to explain the different affinities of silica and latex particles on hydrophilic membranes [53]. In this study, hydrophobic polystyrene latex particles showed less affinity to three commercial hydrophilic membranes than to silica particles, as measured using atomic force microscopy. The hydrogen bonding attraction between silica particles and membrane surfaces was speculated to be the primary reason for the greater attachment. Regardless of the true mechanisms, such results suggest that the molecular structure of membranes and aquatic particles can be important to their interactions.

1.6.3 Chemical Attachment in the Presence of NOM

Another complicated problem is the universal presence of NOM in natural water as introduced previously. The sorption or deposition of NOM moieties on particle and membrane surfaces can form an additional polymeric layer at solid/water interfaces. Two major consequences on the physiochemical attachment are usually considered: one is the shrinkage of membrane pore structures that affects the occurrence of internal attachment and fouling [54]; the other is possible modification of the properties of membrane surfaces by the adsorbed polymer layer [54-56].

Besides these "indirect" effects, NOM is also a potential foulant by itself; as stated in the review of previous studies. It is anticipated that the occurrence and extent of NOM fouling are dependent on several factors, including the size of NOM and its affinity

to membrane surfaces. Overall, it is usually believed that different NOM fractions may play different roles in the fouling of MF membranes, as well as other low pressure membranes [25, 26, 57-59]. This is discussed in detail in Chapter 4.

1.6.4 Chemical Attachments between Heterogeneous Surfaces

All previous discussions on chemical attachment are based on a simple assumption that the interacting surfaces have homogeneous surface properties, thus can be characterized using some global parameters, such as charge density, hydrophobicity, and Hamaker constant. However, this may or may not be appropriate in reality. On the one hand, a small piece of cell wall or other structures from aquatic organisms can have heterogeneous surface compositions so that different parts of its surface have different affinities to the membrane. As found by Saha *et al.* [60], the fouling of various ultrafiltration membranes used in the filtration of a sugarcane juice was dominated by a high molecular weight fraction of polysaccharide (~130 kD) that contained protein moieties potentially responsible for the attachment of the entire moiety on membrane surfaces. On the other hand, membrane surfaces, especially those modified as introduced previously, are also likely to have heterogeneous surface properties relevant to foulant attachment. This heterogeneity can be attributed to different physical and/or chemical origins. For instance, Bowen and Sharif [61] simulated the attachment of particles at the entrances of membrane pores with different shapes. They found that membrane pores with round corners are the least vulnerable to colloidal fouling compared to those with sharp and spiky corners as a result of enhanced electrostatic repulsion. This result suggests that particles are more likely to attach and block pores with certain corner

shapes. Brant *et al.* [62] studied the surface heterogeneity of two NF and RO membranes using chemical force microscopy, a modified technique based on regular AFM to obtain lateral distribution of surface energies/stickiness. It was found that the surfaces of the two membranes used were chemically heterogeneous and that the heterogeneity became more significant below micron-sized dimensions. This implies that the stickiness of membrane surfaces to foulants can be localized, rather than uniform as considered previously.

For the scope of this study, the heterogeneity of membrane surfaces has to be neglected in order to simplify the mathematical description of the model introduced in the following chapter. But it is always worthwhile to remember the heterogeneous nature of real membrane filtration systems, as well as the complicated origins of chemical interactions involved in membrane fouling. These challenges will be active research areas in the near future.

Chapter Two

A CHEMICAL ATTACHMENT BASED MEMBRANE FOULING MODEL

2.1 INTRODUCTION

A common shortcoming of the models discussed in the previous chapter is the insufficient consideration of the chemical aspects of the fouling process. The relative size of contaminants and membrane pores is usually regarded as the primary factor in determining the occurrence of surface fouling (cake layer formation or pore blocking) and adsorptive internal plugging. Moreover, fouling is oftentimes treated as a direct consequence of contaminant rejection, assuming that all contaminants rejected can cause the loss of membrane permeability. In both cases, the importance of chemical attachment of contaminants on membrane surfaces has not been clearly accounted. On the other hand, studies that emphasized the sorption of small contaminants and the resulting fouling are in general short of relevant description on the transport of contaminants inside or outside the porous bodies of microfiltration membranes. Consequently, a model that can depict the coupled effects of chemical and physical factors in membrane fouling is in great need for a deeper understanding of this important phenomenon.

A new model on the fouling of MF membranes has been developed in the study. The main objective of the model was to incorporate both chemical and physical aspects of membrane fouling in a simple but distinctive way. The foundations of this model are the collision and chemical attachment of aquatic contaminants on membrane external and internal surfaces and the Hermia model discussed in the Appendix.

2.2 PHYSICAL DESCRIPTION

Since membrane fouling is the interplay between aquatic contaminants and porous membranes, it is necessary to start the discussion with a brief review of the properties of membranes and aquatic materials. Commercial MF membranes used in water treatment are usually "non-homogeneous" membranes with three-dimensional porous structures. As an example, Figure 2-1 shows a polyvinylidene fluoride (PVDF) membrane with a nominal pore size of 0.1 μm. This membrane has a rough top surface with mean pore size of approximately 1 μm, which is substantially larger than the nominal pore size of 0.1 μm determined using the bubble point test (400 kPa). The cross-sectional picture of the membrane reveals that the three dimensional porous structure exists not only on the outside surface, but also deep in the membrane. The pores or pore openings (so-called "throats") that determine the size exclusion rating of the membrane are "buried" below the top layer of 3-D pores. Therefore, aquatic materials must be able to penetrate the top layer in order to block these throats. This is different from the polycarbonate membranes with circular cylindrical pores used by others [41]. For the latter, pore blocking and/or cake formation occur more readily on the outside surface of the membranes. The presence of such a coarse surface is common for porous membranes, including other membranes with presumably relative tight pore structures, such as nanofiltration and ultrafiltration membranes. This explains why the membrane pore size determined by various surface characterization techniques is in general much larger than the pore size rating measured by solute rejection tests.

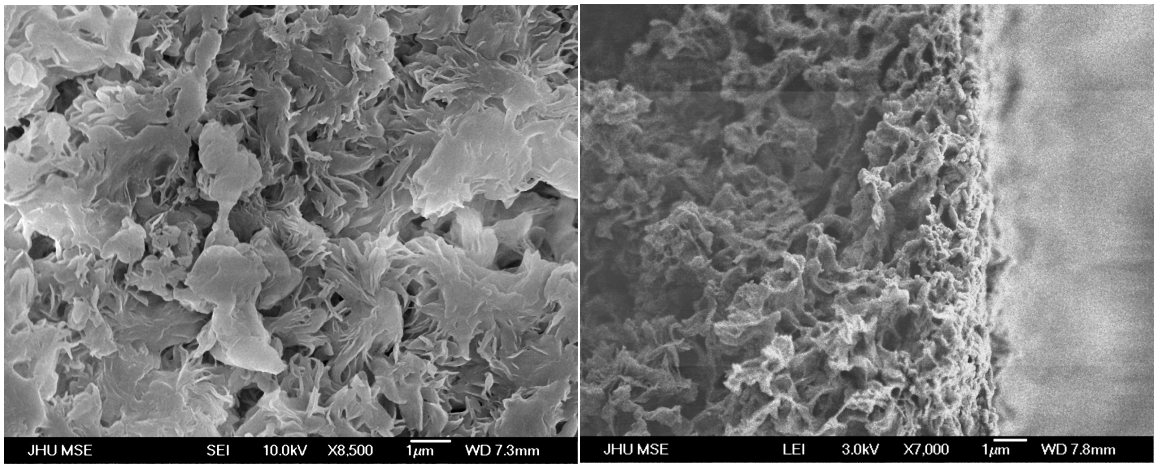

Figure 2-1. Scanning electron micrograms of the top (left) and the cross-sectional (right) surfaces of a polyvinylidene floride (PVDF) MF membrane. The 3-D porous structure of the membrane is clearly shown herein. The left-hand side of the membrane shown on the right is exposed to the feedwater.

Now the properties of aquatic contaminants need to be considered. As depicted previously, studies conducted so far have not determined what components of aquatic contaminants play major roles in the fouling of MF membranes. However, most available results have indicated that colloidal (1 nm –1 μm) aquatic materials, especially NOM with corresponding sizes, are likely to have dominant impacts on the fouling process. When waters containing these colloidal sized materials (herein referred to as "particles") are filtered with a clean MF membrane such as shown in Figure 2-1, particles will be able to penetrate into the 3-D pores; some particles will collide with the wall of the 3-D porous top layer, and be retained if they can chemically attach onto the surface. Other particles will continue to move through this layer and collide with either solid surfaces or pore throats deep in the membrane, or pass through the membrane. At this stage, particles may be rejected not only by chemical attachment and retention, but also by steric exclusion if they are larger than the size of pores or throats. The collision between particles and membrane solid surfaces (herein referred to as surface collision) is

similar to the scenario of packed bed filtration although the local distribution of water flow may be different as a result of different porous structures. On the other hand, the collision between particles and membrane pore throats (herein referred to as pore collision) is a unique feature of membrane filtration in which the dimensions of particles and pores are close enough for this to happen. In comparison, the pore dimension of packed bed filters is usually substantially larger than aquatic colloidal materials.

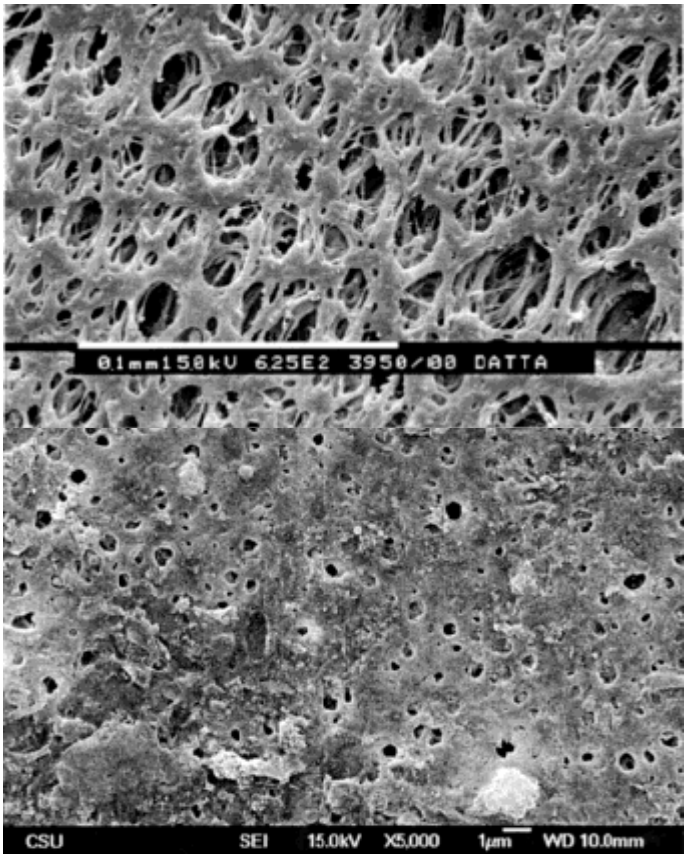

Figure 2-2. Scanning electron micrograms of a polyethersulfone MF membrane before (top) and after (below) being fouled by bovine serum albumin (BSA) protein solution at a concentration of 12 g/L [50]. The porous structure of the membrane was substantially changed due to the attachment of protein.

For surface collision, the general rule of convection-diffusion transport is likely to be applicable with necessary modifications to take into account the variation of collector geometries. Comparatively, the conceptual picture of sieving effects envisioned by

Kosvintsev *et al.* may be applicable to ideal "surface" filters where the retention of aquatic materials and the resulting fouling only happen on the outside surface of membranes [41, 42].

Regardless of the means of collision, whether a particle can become a part of a irreversible fouling layer depends predominantly on the physiochemical interactions between this particle and the membrane surface as the attachment in this case must overcome not only the thermodynamic tendency of back-diffusion, but also the mechanical and hydrodynamic forces encountered during backwashing processes. The importance of chemical attachment to particle retention by MF membranes and the consequent changes to the hydraulic permeability of the porous media is somewhat comparable to that of packed bed filtration. The major difference is that the collisions between particles and membrane pore openings can also result in retention (not irreversible attachment) entirely due to steric exclusion, which is less likely to occur in packed bed filters.

With the fouling of a clean membrane, more and more particles attach to membrane surfaces or pores, and the structural property of the membrane changes accordingly (see Figure 2-2). The attachment to membrane pores becomes less and less important as the number of available pores subject to blocking (collision) depletes. In the meantime, surface collision continues although more and more collisions occur between incoming particles and other particles that have already attached to membrane bare surfaces. At this time, the physiochemical interactions between particles become increasingly important. If favorable particle-particle interactions exist, fouling layers comprised of multilayers of particles are likely to build up on membrane surfaces. For

particles larger than the membrane pore size, it is expected that the formation of multilayers results in the fouling of membranes in a way similar to cake layer filtration, but most likely not only outside membrane external surfaces (i.e., formation of cake layer) but also in the void space inside the top layer of membranes. The overall effect is smoothing of the rough membrane outside surfaces, as reported in other studies using surface characterization techniques. For particles smaller than the membrane pore size, the formation of multilayers also appears outside the membranes as explained later.

The reason why multilayers of small particles are difficult to form deep inside membrane pores can be explained as follows. Since the relevant pore size rating (close to the maximum size of pore throats) of MF membrane used in water treatment is in general less than 200 nm, the small particles discussed herein will be dozens of nm in diameter at most. Aggregation of these submicron particles is dominated by Brownian motion. The half-life of aggregation is reciprocally proportional to particle number concentration as found by in classical theories of perikinetic coagulation. If the foulants are comprised of 1 mg/L monodisperse suspension of completely destabilized particles with sizes of 10 to 100 nm and a density close to water, 1.0 g/cm^3, then the half-life of aggregation would be approximately 0.08 seconds for 10 nm particles to 80 seconds for 100 nm particles. Such a time scale is fairly short compared to the hydraulic retention time of these particles encountered in most natural or engineering systems. Therefore, it is expected that small particles are more likely to form aggregates before reaching membrane surfaces than to build up multilayers inside membrane pore walls once they lose their coagulational stability. This tendency becomes stronger with decreasing particle sizes or increasing

particle concentrations. Consequently, the formation of multilayer on membrane pore walls deep inside the membrane is neglected in the model.

It is noteworthy that particle retention and membrane fouling are correlated but different concepts. From the standpoint of mass transport, the former and the latter are related to the transport of dispersed materials and dispersion media, separately. Membrane fouling occurs when chemical attachment of particles on membrane surfaces makes it more difficult for water to flow through the porous body of MF membranes, or increases their hydrodynamic resistance. A practical example would be the retention of the aggregates of completely destabilized hydrophobic particles on membrane surfaces. In this case, the increase in the hydrodynamic resistance of the membrane is minimized while the retention is maximized. In other words, the removal and accumulation of these particle aggregates have little direct contribution to membrane fouling. Theoretically speaking, during the MF of natural waters, water flows through membranes driven by the hydraulic pressure gradient across the membrane. When a particle attaches onto a membrane surface, an interfacial region between the particle and the flowing water is formed. The interfacial regions between the particle and water will generate additional viscous force to overcome the permeation of water. Meanwhile, when a particle completely blocks a pore throat of a membrane, water will no longer be able to flow through the open channel beneath. This causes the redistribution of water flow to other open channels. Water will travel through the remaining open channels at a faster mean velocity under the condition of constant flow filtration, which in turn increases the viscous force hindering water flow. In both cases, the hydrodynamic resistance of

membranes increases, and the membrane permeability decreases as a result of particle attachment to the membrane surface.

It has been widely believed that, when one particle is rejected by a MF membrane, the loss of membrane pore areas (pore blockage) has more dramatic impacts on the reduction of membrane permeability than introduction of new interfacial area (e.g., formation of cake layers) [42]. Figure 2-3 shows the blockage of membrane pores and formation of cake layer during the MF of latex particles. The fouling rate was faster during pore blockage than in cake layer formation. To take into accounts these different effects, Hermia introduced the idea of complete, standard, and intermediate pore blocking, as well as cake formation, to describe the efficiency of different types of blockage/fouling in reducing membrane permeability [63]. In them, complete pore blocking means that all particles delivered to membrane surfaces attach solely to the membrane outside surface, and therefore the particle-particle collision mentioned above does not exist. It is also assumed that all particles can block all pores inside their projected area on membrane surfaces. This type of fouling is theoretically the fastest in all types of foulings. In comparison, the intermediate pore blocking takes into account the presence of collisions between incoming particles and particles that have already attached to membrane pores. Particles become less efficient in causing fouling as fewer particles can reach membrane pore openings. Finally, internal pore plugging is defined as the standard pore blocking. In this case, particles will penetrate and fill up membrane pores, and cause pore constriction. Unlike complete pore blocking, standard pore blocking occurs in three dimensional pore spaces. It is therefore less effective than the former although all particles can participate in the blocking process. Overall, the Hermia model does not

consider chemical aspects of fouling, but it provides a useful preliminary evaluation on the efficiency of different types of particle attachments on fouling once they occur. Details of this model are provided in the Appendix.

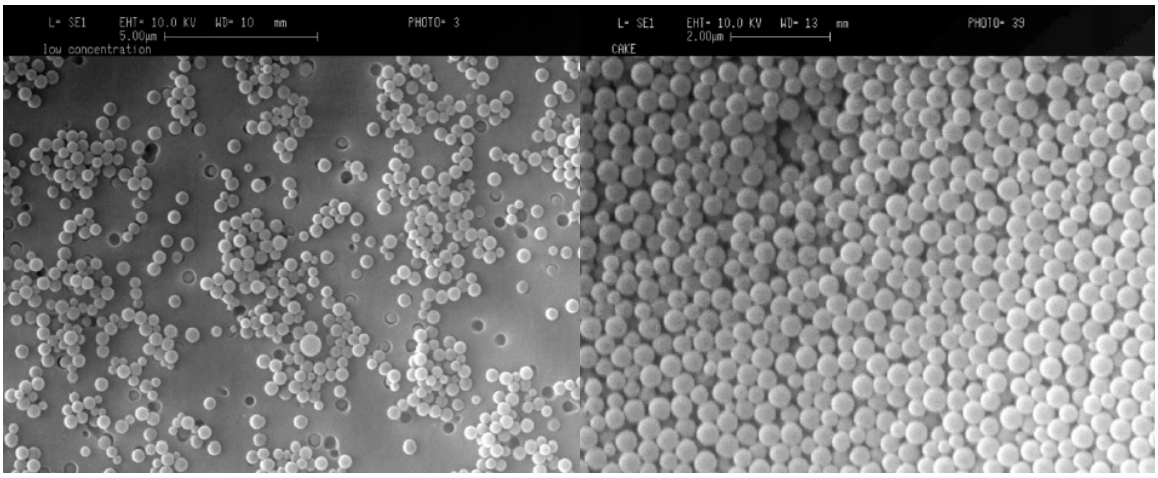

Figure 2-3. Pore blockage (left) and cake layer formation (right) on the surface of a polycarbonate (PC) membrane during the filtration of latex suspensions [42]. The decrease of membrane permeability was found to be more substantial during pore blockage than in cake layer formation. The left image also shows that the deposition of latex particles on membrane outside surface and pore openings happened randomly and simultaneously.

A special case of cake layer formation may happen if the fouling material can form a gel-like structure that is extremely impermeable to water flows. This phenomenon is unlikely to occur with hydrophobic spherical particles, typically used in bench scale studies, but can be found when the fouling is caused by hydrophilic colloids or some aquatic macromolecules such as alginate that are rich in polar groups,. The presence of some divalent ions including calcium can enhance the formation of the gel-like layer by forming intramolecular/intermolecular cross-linkages. The permeability of the gel layer is much lower than normal cake layers given the same amount of materials attaching onto membrane surfaces. The formation of gel-like layers is not addressed in the study as it is

a more sophisticated process than the fouling by hydrophobic colloids. However, the effects of different types of interactions, i.e., solute-membrane and solute-solute interactions, are comparable to the interactions involving particles. As found by Laabs *et al.*, the gel-like layer formed by "hydrophilic" fraction of aquatic colloids appeared to be more sticky to membrane surfaces than other fractions of the colloids isolated [64].

2.3 MATHEMATICAL MODELING

In order to develop a model based on the conceptual picture of membrane fouling described previously, it is beneficial to treat fouling as three consecutive steps: collision, attachment, and increase of hydrodynamic resistance. This approach will make it convenient to improve the specific numerical analysis used for each step in future study.

2.3.1 Model Membrane and Aquatic Contaminant

First of all, it is necessary to simplify the structures of the membrane and the particle, the two major parts of membrane fouling. As found in other works [42, 45], the mathematical model will become extremely complicated if the real structures of membranes and aquatic particles are used directly [65]. More likely, additional parameters have to be introduced and validated. These are beyond the scope of the study as the chemical aspects of fouling are of primary concern here. Therefore, some appropriate assumptions on the physical and chemical properties of MF membranes is made in order to establish a simple but useful mathematical model to evaluate the importance of chemical attachment in the fouling of MF membranes.

Geometrical Assumptions

In the context of this study, aquatic contaminants are regarded as monodispersed, non-deformable, spherical particles owning uniform surface properties. The radius of particles (a) can be either greater or smaller than the membrane pore size. If it is greater or equivalent to membrane pore size, fouling will occur on the membrane surface in means of pore blocking and/or cake layer formation. In the case of surface pore blocking, the projected area of a particle on the membrane surface (σ) simply equals πa^2. For a particle smaller than the membrane pores, membrane porous structure will be changed by this particle as additional solid volume ($4\pi a^3/3$) and surface area ($4\pi a^2$) are introduced inside the membrane. Therefore, the projected area of a unit mass of the particles on membrane surface, σ [m^2/kg] is calculated as:

$$\sigma = \frac{0.75}{\rho a} \tag{6}$$

where ρ [kg/m^3] is the particle density.

On the other hand, the structure of MF membranes is simplified as porous bodies with uniform circular cylindrical pores. The diameter of the pores, D_m[m], is related to the mean pore size of the commercial membrane used in the study as determined in solute rejection tests. The surface porosity of the membrane, ε_s, is assumed to equal its bulk porosity. The latter is determined for a hollow fiber membrane using the following relationship:

$$\text{Bulk Porosity} = 1 - \frac{\text{Mass of Fibers}}{\rho_{\text{m}}} \times \frac{4}{\pi(\Phi_{out}^2 - \Phi_{in}^2)(\text{Length of Fibers})}$$

where ρ_m is the density of membrane materials, and Φ_{out} and Φ_{in} are the outside and inside diameters of the membrane fibers, respectively. The number density of membrane pores, N_m [1/m^2] is thereby calculated using ε_s and D_m:

$$N_m = \frac{4\varepsilon_s}{\pi D_m^2} \tag{7}$$

Meanwhile, the length of membrane pores, L_m [m], is estimated using the following equation:

$$L_m = \frac{\pi D_m^4 R_m N_m}{128} \tag{8}$$

where R_m [m^{-1}] is the hydraulic resistance of a clean membrane, which can be determined experimentally. For a membrane that has porous structure as shown in Figure 2-1, the length of membrane pores calculated using (8) is usually less than the physical thickness of the membrane because of the presence of pore spaces much larger than the size of pore throats.

Chemical Attachment Assumptions

The attachment probabilities between a particle and the membrane and between two particles are assumed to be α_{pm} and α_{pp}, respectively. In other words, we have:

$$\text{The probability for a particle to attach onto the membrane surface} \equiv \alpha_{pm}$$
$$= \frac{\text{rate at which particles attach on membrane surfaces}}{\text{rate at which particles colloid with membrane surfaces}}$$

$$\text{The probability for a particle to attach to another particle} \equiv \alpha_{pp}$$
$$= \frac{\text{rate at which particles attach to each other}}{\text{rate at which particles colloid with each other}}$$

These two attachment probabilities are the key parameters of the model. It is assumed that the entire surface of the model membrane has homogeneous chemical properties and therefore the attachment probability between the membrane and a particle (α_{pm}) is the same for particles attaching everywhere inside and outside the membrane, including solid surface and pore openings. Likewise, it is also assumed that the attachment probability (α_{pp}) is uniform for particles in the feedwater or between a particle in the feed stream and a particle attached on membrane surfaces. As depicted in the previous chapter, both assumptions mentioned above are substantial simplifications compared to the complicated nature of the interfacial interactions involved.

2.3.2 Collision and Attachment: Large Particles

As discussed in the physical description of the model, three types of collisions can happen on membrane outside surfaces, i.e., collision between a particle and the membrane solid surface, collision between a particle and another particle attached on membrane solid surface, and collision between a particle and the membrane pore. They are complimentary, and thus a conservative function can be written for the corresponding collision probabilities as follows:

$$\beta_S + \beta_P + \beta_{pp} = 1 \tag{9}$$

where β_S, β_P, and β_{pp} [dimensionless] refer to the collision probability between a particle and the membrane surface, the membrane pores, and other particles, respectively.

These values can be obtained by analyzing the trajectory of particle motion induced by the permeation flow. For the collision probability between one particle and

the pores on a clean membrane, β_{P0} [dimensionless], is simply the surface porosity (ε_s) of the model membrane:

$$\beta_{P0} = \varepsilon_s = \frac{\pi N_m D_m^2}{4} \tag{10}$$

In the meantime, β_{pp} equals zero, and $\beta_{S0} + \beta_{P0}$ equals unity. After the onset of membrane surface fouling by means of either pore blocking or cake layer formation, particles that have already attached to the membrane surface will prohibit further attachment of incoming particles on the region inside four times of their projected areas on the surface, and increase the probability of particle-particle collisions. In this case, β_{pp} is proportional to the ratio of the membrane surface area covered effectively by particles (A_{covered}) to that of the entire membrane (A_m). The way to determine the collision probabilities is to determine the uncovered membrane surface area first. The approach is similar to what is presented in the Appendix for the derivation of "intermediate pore blocking" equations.

$$dA_t = -4^{\alpha_{pp}} \sigma dm_t A_t \tag{11}$$

where A_t [dimensionless] is the total uncovered or open membrane surface area at any filtration time normalized to the total membrane surface area, and m_t [kg/m^2] is the total mass of particles delivered to a unit membrane surface area. Unlike what is used in "intermediate pore blocking", the RHS of Eqn (11) includes a factor of ($4^{\alpha pp}$), which reflects the fact that a particle landing on the open area of a membrane can collide with incoming particles moving into a cyclic area up to 4 times that of the projected particle area; therefore, the effective loss of open area equals ($4^{\alpha pp}$)σdm_t. α_{pp} is the attachment probability and ranges between zero and unity. It is used as an impacting factor for the

negative effects of particle-particle attachment on pore blocking. When α_{pp} equals zero, the colloidal particles are stable with respect to coagulational attachment; thus the ring-like area with radii of a to $2a$ surrounding a particle on the membrane surface is still accessible by incoming particles. In this case, the effective loss of open membrane area decreases to σdm_t, indicating that incoming particles can "slide" off the surface of the attached particles after collision and arrive at the uncovered membrane surface. Comparatively, if α_{pp} increases to unity, the colloidal particles become completely unstable with respect to particle-particle attachment; therefore, incoming particles moving in an area of $4\sigma dm_t$ above the attached particles will attach to these particles and prevent the open membrane areas (hence the pores in these areas) underneath them to from being reached by other incoming particles.

Now, we can solve Eqn (11) using the boundary condition: $A_t = 1$ when $m_t = 0$, and obtain:

$$A_t = \exp\left(-4^{\alpha_{pp}} \sigma m_t\right) \tag{12}$$

Herein it is assumed that the surface porosity of the clean membrane is maintained in the open area. The collision probabilities for the fouled membrane can thus be written as follows:

$$\beta_{pp} = 1 - A_t = 1 - \exp\left(-4^{\alpha_{pp}} \sigma m_t\right) \tag{13}$$

$$\beta_P = \varepsilon_s \exp\left(-4^{\alpha_{pp}} \sigma m_t\right) \tag{14}$$

$$\beta_S = \left(1 - \varepsilon_s\right) \exp\left(-4^{\alpha_{pp}} \sigma m_t\right) \tag{15}$$

The subsequent attachment of particles is calculated based on the collision probability and the attachment probability discussed above. The mass of particles

attaching to membrane pores in a unit membrane surface area, m_p [kg/m^2], can be expressed using a differential equation:

$$dm_p = \alpha_{pm}\beta_P dm_t \tag{16}$$

Bringing Eqn (14) into Eqn (16), and solving the differential equation, we obtain:

$$m_p = \frac{\alpha_{pm}\varepsilon_s}{4^{\alpha_{pp}}\sigma}\left[1-\exp\left(-4^{\alpha_{pp}}\sigma m_t\right)\right] \tag{17}$$

Consequently, the total mass of particles on a unit membrane surface area that contribute to cake formation (m_c) is simply:

$$m_c = m_t - m_p = m_t - \frac{\alpha_{pm}\varepsilon_s}{4^{\alpha_{pp}}\sigma}\left[1-\exp\left(-4^{\alpha_{pp}}\sigma m_t\right)\right] \tag{18}$$

These particles, however, may or may not remain on the membrane surface after hydraulic backwashing. In order to predict the amount of particles relevant to hydraulically irreversible fouling, the type of particle attachment in the cake layer has to be considered. On the one hand, some particles directly attach to the solid surface of the membrane and their mass on a unit membrane surface area, m_s [kg/m^2], is related to particle-membrane collision probability and attachment probability:

$$dm_s = \alpha_{pm}\beta_S dm_t \tag{19}$$

This equation can be solved by inserting Eqn (15), and the final result is:

$$m_s = \frac{\alpha_{pm}\left(1-\varepsilon_s\right)}{4^{\alpha_{pp}}\sigma}\left[1-\exp\left(-4^{\alpha_{pp}}\sigma m_t\right)\right] \tag{20}$$

Similarly, the mass of particles attaching to other particles on the membrane surface normalized to a unit membrane surface area, m_{pp} [kg/m^2], can be obtained by bringing Eqn (13) into the following equation:

$$dm_{pp} = \alpha_{pm}\beta_{pp} dm_t \tag{21}$$

The final expression is:

$$m_{pp} = \alpha_{pp} m_t - \frac{\alpha_{pp}}{4^{\alpha_{pp}} \sigma}\left[1 - \exp\left(-4^{\alpha_{pp}} \sigma m_t\right)\right] \tag{22}$$

If Eqns (17), (20), and (22) are added up, we have:

$$m_p + m_s + m_{pp} = \alpha_{pp} m_t - \frac{\alpha_{pp} - \alpha_{pm}}{4^{\alpha_{pp}} \sigma}\left[1 - \exp\left(-4^{\alpha_{pp}} \sigma m_t\right)\right] \tag{23}$$

Apparently, the LHS of the equation is always less than the total mass of particles retained by the membrane, m_f, except when $\alpha_{pm} = \alpha_{pp} = 1$. Meanwhile, the mass of particles in the cake is obtained:

$$m_c = m_s + m_{pp} = \alpha_{pp} m_t + \frac{\alpha_{pm}\left(1 - \varepsilon_s\right) - \alpha_{pp}}{4^{\alpha_{pp}} \sigma}\left[1 - \exp\left(-4^{\alpha_{pp}} \sigma m_t\right)\right] \tag{24}$$

2.3.3 Collision and Attachment: Small Particles without Pore Constriction

Unlike particles that are larger the membrane pores, the "collision" between a particle smaller than the membrane pores and a membrane pore leads not to the blockage of the pore, but to penetration of the particle inside the pore. The particle can collide with the pore wall as a result of Brownian motion once it enters the pore (note that there is not water flow in the radial direction). To assess the collision and attachment of small particles on pore walls, it is easier to simplify the problem to the convective transport of small particles inside cylindrical tubes under steady state conditions, similar to the approach used to describe the Brownian coagulation of colloidal particles [66].

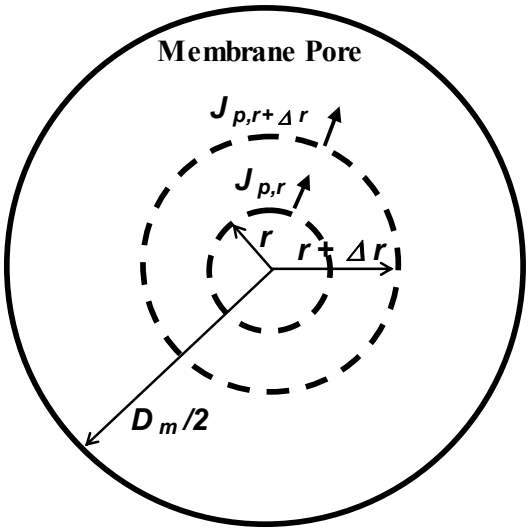

Figure 2-4. Schematic Top View of a Cylindrical Membrane Pore. The ring-like control space is between r and $r+\Delta r$. $J_{p,r+\Delta r}$ and J_r represent the particle flux at r and $r+\Delta r$, repectively.

First, a mass balance equation can be established for a ring-like slice of space in the pore channel as shown in Figure 2-4:

$$J_{p,r+\Delta r}\left[2\pi\left(r+\Delta r\right)L_m\right]-J_{p,r}\left(2\pi rL_m\right)=0 \tag{25}$$

where J_p [kg/m^2-s] is the particle flux due to Brownian diffusion, and r [m] is the radius of the ring-like slice. Rearrange Eqn (25), we obtain:

$$\frac{J_{p,r+\Delta r}-J_{p,r}}{\Delta r}=-\frac{J_{p,r+\Delta r}}{r} \tag{26}$$

Let $\Delta r \to 0$, Eqn (26) is transformed into a differential form:

$$\frac{dJ_p}{dr}=-\frac{J_p}{r} \tag{27}$$

Solving Eqn (27), we have:

$$J_p=\frac{K}{r},\ K=\text{constant} \tag{28}$$

Now Fick's first law in diffusion can be applied to the diffusion of particles in the radial direction:

$$J_p = -D_p \frac{dC_p}{dr} \tag{29}$$

where D_p [m^2/s] is the diffusion coefficient of colloidal particles, and C_p [kg/m^3] is the particle concentration. Combining Eqns (28) and (29), and solving for the constant K with boundary conditions $C_p = 0$ at $r = D_m/2$ and $C_p = C_a$ at $r = a$ (here a is the particle radius):

$$K = \frac{C_a D_p}{\ln\left(\frac{D_m}{2a}\right)} \tag{30}$$

By inserting Eqn (30) into Eqn (28), we find that the particle flux at the pore wall is as follows:

$$J_{p,D_m/2} = \frac{2C_a D_p}{D_m \ln\left(\frac{D_m}{2a}\right)} \tag{31}$$

Next, the change of particle concentration along the axial direction of the pore can be calculated. For a slice of disk-like space inside the pore with a diameter of D_m and a thickness of dl, assuming that the mean particle concentration on the top and the bottom side of the disk is half of the corresponding particle concentrations at $r = a$, i.e., $C_{a,l}$ and $C_{a,l+\Delta l}$, we can establish another mass balance equation for this controlled space under steady state condition:

$$\frac{C_{a,l}}{2} Q_1 = \frac{C_{a,l+\Delta l}}{2} Q_1 + \alpha_{pm} J_{p,D_m/2} \left(\pi D_m \Delta l\right) \tag{32}$$

Here Q_1 is the permeate flowrate in one membrane pore and is related to the total permeate flowrate with the following equation:

$$Q_1 = \frac{Q}{A_m N_m} = \frac{J}{N_m} \tag{33}$$

where Q and J are the permeate flowrate and flux, respectively. Both are known operational conditions.

Eqn (32) does not take into account the Brownian diffusion in the axial direction because it is negligible compared to convective transport under conditions relevant to microfiltration. This equation can be further converted into a differential form:

$$\frac{dC_{a.l}}{dl} = -\frac{2J_{p,D_m/2}\alpha_{pm}}{Q_1}\left(\pi D_m\right) \tag{34}$$

Inserting Eqn (31) into Eqn (34), we obtain:

$$\frac{dC_{a.l}}{dl} = -\frac{4\pi\alpha_{pm}D_p}{Q_1 \ln\left(\frac{D_m}{2a}\right)}C_{a,l} \tag{35}$$

Integration of Eqn (35) yields:

$$\frac{C_{a,L}}{C_{a,0}} = \exp\left(-\frac{4\pi\alpha_{pm}D_p}{Q_1 \ln\left(\frac{D_m}{2a}\right)}L_m\right) \tag{36}$$

Since we have assumed that the mean particle concentration at any cross section of a membrane pore is half of that at r = a, the ratio of the mean concentrations of particles at the inlet and the outlet of the membrane pore should equal to that of the local concentrations at $r = a$, we obtain:

$$\frac{C_{out}}{C_{in}} = \frac{C_{a,out}}{C_{a,in}} = \exp\left[-\frac{4\pi\alpha_{pm}D_p}{Q_1 \ln\left(\frac{D_m}{2a}\right)}L_m\right] = \exp\left[-\frac{4\alpha_{pm}D_p}{Q_1 D_m \ln\left(\frac{D_m}{2a}\right)}\left(\pi D_m L_m\right)\right] \tag{37}$$

where C_{out} and C_{in} are the mean particle concentrations at the inlet and outlet of the membrane pore, respectively, which in turn are equivalent to the particle concentrations

in the feedwater and the permeate, separately. Eqn (37) is comparable to the clean bed efficiency model developed for packed bed filtration. If the membrane is fouled due to particle attachment onto pore walls, this equation is no longer valid. Further inspection of the equation shows that the term of ($\pi D_m L_m$) on the RHS is indeed the total area of pore wall in a pore available for deposition. Apparently, it will continuously decrease as internal fouling proceeds. During the process of membrane fouling, Eqn (37) should be generalized as:

$$\frac{C_{out}}{C_{in}} = \exp\left[-\frac{4\alpha_{pm} D_p A_{w,1}(V_1)}{Q_1 D_m \ln\left(\frac{D_m}{2a}\right)}\right] = \exp\left(-\alpha_{pm} B A_{w,1}(V_1)\right) \qquad (38)$$

where $A_{w,1}(V_1)$ is the surface area of the pore wall when the permeate volume reaches V_1 and B [m^{-2}] is a mass transfer coefficient clustering all parameters in the exponential term on the RHS of the equation except α_{pm} and the variable, $A_{w,1}$. It will be shown later that the value of B is in the order of 10^{16} (m^{-2}) under the experimental microfiltration conditions. This means that, for a membrane with a pore diameter of 60 nm, 99 percent of the particles will be rejected by traveling a distance into the pore even less than their diameter if they are unstable with respect to deposition.

Now it is possible to calculate the mass of particles attaching to the wall of one membrane pore, $m_{w,1}$ [kg] as below:

$$dm_{w,1} = C_{in} Q_1 \left(1 - \frac{C_{out}}{C_{in}}\right) dt_1 = C_{in} \left(1 - \frac{C_{out}}{C_{in}}\right) dV_1 \qquad (39)$$

Similar to the pore blocking on the membrane outside surface, the area of pore wall occupied by particles is approximately (when $\alpha_{pp} = 0$):

$$dA_{w,1}(V_1) = -\sigma dm_{w,1} = -\sigma C_{in}\left(1 - \frac{C_{out}}{C_{in}}\right)dV_1 \tag{40}$$

Combining Eqns (38) and (40) and solving for $A_{w,1}$, we obtain:

$$A_{w,1}(V_1) = \frac{1}{\alpha_1 B}\ln\left\{1 + \left[\exp\left(\pi D_m L_m B\alpha_{pm}\right) - 1\right]\exp\left(-\sigma\alpha_{pm}BC_{in}V_1\right)\right\} \tag{41}$$

Because $\exp\left(\pi D_m L_m B\alpha_1\right) >> 1$ under the conditions of concern, Eqn (41) can be further simplified:

$$A_{w,1}(V_1) = \frac{1}{\alpha_1 B}\ln\left[1 + \exp\left(\pi D_m L_m B\alpha_{pm} - \sigma\alpha_{pm}BC_{in}V_1\right)\right] \tag{42}$$

Thus,

$$m_{w,1} \cong \frac{\pi D_m L_m - A_{w,1}}{\sigma} = \frac{1}{\sigma\alpha_1 B}\left\{\pi D_m L_m B\alpha_{pm} - \ln\left[1 + \exp\left(\pi D_m L_m B\alpha_{pm} - \sigma\alpha_{pm}BC_{in}V_1\right)\right]\right\} \tag{43}$$

Eqn (43) can be extended to the entire membrane by considering the following relationships:

$$m_{w,1} = \frac{m_w}{N_m} \tag{44}$$

$$V_1 = \frac{V_s}{N_m} \tag{45}$$

where m_w [kg/m^2] is the mass of the particles attaching to the pore walls in all membrane pores normalized to unit membrane surface area, V_s [m^3/m^2] is the permeate throughput, or the volume of permeate filtered through unit surface area of the membrane, and N_m, once again, is the pore density in the membrane.

By inserting Eqns (44) and (45) into Eqn (43), we obtain:

$$m_w = \frac{N_m}{\sigma\alpha_1 B}\left\{\pi D_m L_m B\alpha_{pm} - \ln\left[1+\exp\left(\pi D_m L_m B\alpha_{pm} - \frac{\sigma\alpha_{pm}B}{N_m}C_{in}V_s\right)\right]\right\} \quad (46)$$

This equation is valid when α_{pm} does not equal zero, otherwise $m_w \equiv 0$. As shown in Eqn (46), the attachment of small particles on the pore walls will eventually reach a maximum of $\frac{\pi D_m L_m N_m}{\sigma}$ as fouling proceeds. The radius of the particles should not exceed one sixth of the pore diameter, i.e., $a < D_m/6$ in order to apply Eqn (46); otherwise, the constriction of pore entrances by particles attached will prohibit other incoming particles from traveling deeper into the pores. Although physically sound, the numerical calculation using this equation is not straightforward because it involves a large exponential term. When $C_{in}V_s$ is small, the exponential term can be much greater than 10^{100}, the upper limit for a double precision number to be handled by most computer programs. Therefore, it is necessary to simplify the calculation of m_w.

Figure 2-5 shows the minimum values of α_{pm} for the removal of 90 percent of the particles within a lateral traveling distance of $2a$ as calculated using Eqn (38). The results indicate that the deposition of particles on the pore walls of the membrane is almost complete until the pore wall is gradually filled up by the particles; given that the particles are somewhat unstable with respect to deposition, i.e., $\alpha_{pm} > 0.1$. In this case, it is reasonable to assume that the removal of particles is consistently complete, and thus:

$$m_w = C_{in}V_s \quad (47)$$

and $m_w \le \frac{\pi D_m L_m N_m}{\sigma}$. Interestingly, the relationship manifested by Eqn (47) is the assumption used in the Hermia model as discussed in the Appendix. However, the

maximum value for m_w and the related chemical conditions were not presented in that model.

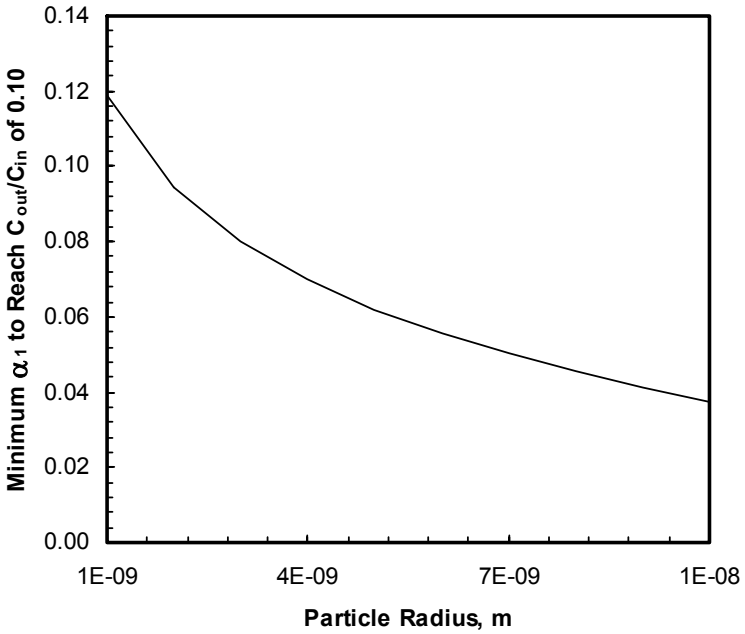

Figure 2-5. Variation of the Minimum Depositional Attachment Probability Required for the Removal of 90 Percent of Incoming Particles within a Pore Depth of 2a, as a Function of Particle Radius Calculated Using Eqn (38). $D_m = 5.8\times10^{-8}$ m, $Q_1 = 9.44\times10^{-20}$ m^3/s, and D_p is calculated using Einstein's Equation at a temperature of 25 °C.

2.3.4 Collision and Attachment: Small Particles with Pore Constriction

It is also noteworthy that Eqn (46) does not take into account the effect of pore constriction on the size exclusion of incoming particles. In other words, it is assumed that particles being attached to the pore wall only affect the attachment of other particles inside their projected areas on the wall, but do not inhibit their movement through the pore channel. In order to meet this requirement, the radius of the particles should not exceed one sixth of the pore diameter, i.e., $a < D_m/6$. It can be anticipated that m_w will be much less if pore constriction causes more particles to be retained on the outside surface of the membrane. When this happens, the retention and attachment of small particles can

be treated just as surface fouling, similar to that of large particles discussed in previous section, since unstable particles cannot travel significantly deep into membrane pores as we learn from Eqn (38). In this case, the membrane property that determines the fouling rate is not the thickness of the effective membrane layer, but the number of pore entrances on the membrane surface and their sizes. Considering the chemical condition that $\alpha_{pp} \neq 0$, the equations for large particles can be rewritten for small particles attaching on membrane surface as follows:

$$m_p = \frac{\alpha_{pm}\varepsilon_s}{\sigma}\left[1-\exp\left(-\sigma m_t\right)\right] \tag{48}$$

$$m_c \text{ (total)} = m_t - m_p = m_t - \frac{\alpha_{pm}\varepsilon_s}{\sigma}\left[1-\exp\left(-\sigma m_t\right)\right] \tag{49}$$

$$m_c \text{ (irreversible)} = m_s = \frac{\alpha_{pm}\left(1-\varepsilon_s\right)}{\sigma}\left[1-\exp\left(-\sigma m_t\right)\right] \tag{50}$$

2.3.5 Reduction of Membrane Permeability: Large Particles ($a \geq D_m/2$)

The reduction of membrane permeability is dominated by pore blockage and cake layer formation if the fouling is caused by particles larger than the pore size. As discussed in the Appendix, the following expressions can be used to describe the increase of relative transmembrane pressure (P') as a function of the mass of particles retained by the membrane (m_f') in constant flow filtration:

$$\frac{dP'}{dm_f'} = \frac{\hat{R}_c}{R_m} \text{ (cake layer formation)} \tag{51}$$

$$\frac{dP'}{dm_f'} = \sigma P'^2 \text{ (complete pore blocking)} \tag{52}$$

where $\hat{R}_c$ is the specific cake resistance as introduced in the Appendix. The integral forms of Eqns (51) and (52) are written as follows after replacing corresponding m_f':

$$P' = 1 + \frac{\hat{R}_c}{R_m} m_c \text{ (cake layer formation)} \tag{53}$$

$$P' = \frac{1}{1 - \sigma m_p} \text{ (complete pore blocking)} \tag{54}$$

One important correction has to be made before the expression for mass retention was introduced into Eqn (54). As elucidated in the Appendix, the decrease of membrane permeability due to pore blocking by large particles is in fact a function of the loss of membrane pore area, instead of the projected area of particles on membrane surface. Therefore, Eqn (54)should be revised as:

$$P' = \frac{\varepsilon_s}{\varepsilon_s - \sigma\left(\frac{D_m^2}{4a^2}\right) m_p} \tag{55}$$

where $\left(\frac{D_m^2}{4a^2}\right)$ is the ratio of the area of a pore to the projected area of the particle that covers the pore. If $D_m > 2a$ as in the case of small particles after pore constriction, this correction becomes unnecessary. Subsequent to the correction, the increase of relative transmembrane pressure due to pore blocking is obtained by inserting Eqn (17) into Eqn (55) and also noting that $m_t = C_f V_s$ (C_f is the mass concentration of particles in the feedwater):

$$P' = \frac{\varepsilon_s}{\varepsilon_s - \frac{\alpha_{pm} \varepsilon_s D_m^2}{4^{1+\alpha_{pp}} a^2}\left[1 - \exp\left(-4^{\alpha_{pp}} \sigma C_f V_s\right)\right]} \tag{56}$$

As for cake layer formation, the hydraulic reversibility is recognized. The relative transmembrane pressure before hydraulic backwashing is obtained by combining Eqns (18) and (53):

$$P' = 1 + \frac{\hat{R}_c}{R_m}\left\{ C_f V_s - \frac{\alpha_{pm}\varepsilon_s}{4^{\alpha_{pp}}\sigma}\left[1 - \exp\left(-4^{\alpha_{pp}}\sigma C_f V_s\right)\right]\right\} \tag{57}$$

In comparison, the corresponding relationship for the pressure after hydraulic backwashing is derived by bringing Eqn (24) into Eqn (53):

$$P' = 1 + \frac{\hat{R}_c}{R_m}\left\{ \alpha_{pp} C_f V_s + \frac{\alpha_{pm}\left(1-\varepsilon_s\right) - \alpha_{pp}}{4^{\alpha_{pp}}\sigma}\left[1 - \exp\left(-4^{\alpha_{pp}}\sigma C_f V_s\right)\right]\right\} \tag{58}$$

The total fouling of a membrane can be obtained by assuming that different types of fouling have additive impacts. Therefore, the summation of Eqns (56) and (57) defines the total fouling before hydraulic backwashing, and the summation of Eqns (56) and (58) gives the hydraulically irreversible fouling. Note that hydraulically reversible fouling due to pore blocking is considered insignificant in the model as elucidated in the physical description.

2.3.6 Reduction of Membrane Permeability: Small Particles ($a < D_m/6$)

Unlike large particles, the fouling caused by small particles with radii less than (D_m/6) is predominantly internal fouling, or "standard pore blocking" as mentioned in the Hermia model. In this case, the relationship between the relative transmembrane pressure and the mass of particles attaching on pore walls is described as:

$$\frac{dP'}{dm_f'} = \left(\frac{2}{L_m \rho}\right) P'^{3/2} \text{ (standard pore blocking)} \tag{59}$$

or by an integrated expression:

$$P' = \frac{1}{\left(1 - \frac{m_w}{\rho L_m}\right)^{\frac{1}{2}}} \text{ (standard pore blocking)} \qquad (60)$$

By bringing Eqn (46) into Eqn (60), it is obtained that:

$$P' = \frac{1}{\left\{1 - \frac{N_m}{\sigma\rho\alpha_{pm} B L_m}\left\{\pi D_m L_m B \alpha_{pm} - \ln\left[1 + \exp\left(\pi D_m L_m B \alpha_{pm} - \frac{\sigma\alpha_{pm} B}{N_m} C_{in} V_s\right)\right]\right\}\right\}^{1/2}} \qquad (61)$$

Here the meaning of the coefficient B is given in Eqn (38). Again, note that Eqn (61) does not apply when α_{pm} equals zero. If α_{pm} equals zero, P' will remain unity since $m_w \equiv 0$. If the particles are unstable with respect to deposition, i.e., $\alpha_{pm} > 0.1$, a simple relationship can be used to substitute for Eqn (61). It is derived by inserting Eqn (47) into Eqn (60):

$$P' = \frac{1}{\left(1 - \frac{C_f V_s}{\rho L_m}\right)^{\frac{1}{2}}} \qquad (62)$$

On the other hand, surface fouling of the membrane by small particles is insignificant in the absence of increasing surface retention of particles as a result of pore constriction effect. Without significant pore constriction, the surface fouling is primarily cake layer formation caused by particles attached to the solid surface outside the membrane, and their impact to membrane permeability is negligible compared to internal fouling.

2.3.7 Reduction of Membrane Permeability: Small Particles ($D_m/6 < a < D_m/2$)

Due to the existence of the pore constriction effect, the fouling of a membrane by small particles with radii between $D_m/2$ and $D_m/6$ is primarily surface fouling as introduced previously. Pore blocking type of fouling is therefore determined by the following relationship:

$$P' = \frac{\varepsilon_s}{\varepsilon_s - \sigma m_p} \tag{63}$$

Compared to Eqn (55), Eqn (63) does not include the correctional factor since particles are smaller than membrane pores. By inserting Eqn (48) into Eqn (63), we obtain:

$$P' = \frac{1}{1 - \alpha_{pm}\left[1 - \exp\left(-\sigma C_f V_s\right)\right]} \tag{64}$$

On the other hand, the total fouling caused by cake layer formation is represented by:

$$P' = 1 + \frac{\hat{R}_c}{R_m}\left\{C_f V_s - \frac{\alpha_1 \varepsilon_s}{\sigma}\left[1 - \exp\left(-\sigma C_f V_s\right)\right]\right\} \tag{65}$$

Likewise, the hydraulically irreversible fouling caused by cake layer is expressed as:

$$P' = 1 + \frac{\hat{R}_c}{R_m} \cdot \frac{\alpha_{pm}\left(1 - \varepsilon_s\right)}{\sigma}\left[1 - \exp\left(-\sigma C_f V_s\right)\right] \tag{66}$$

Note herein that $\alpha_{pp} = 0$.

2.4 MODEL SIMULATION

2.4.1 Basic Modeling Conditions

Table 2-1. List of parameters used in the final expressions of the fouling model.

Category	Parameter	Symbol	Values or Calculation Methods*
Physical	Membrane surface porosity	ε_s	0.70
	Diameter of circular cylindrical pores of the model membrane	D_m	58 nm
	Radius of model spherical particles	a	Variable in three levels
	Membrane surface area covered by unit mass of particles	σ	Calculated using Eqn (6) with $\rho = 1.055$
	Particle mass concentration in the feedwater	C_f	20 mg/L
	Hydraulic resistance of clean membranes	R_m	1.70×10^{11} m^{-1}
	Specific cake resistance	$\hat{R}_c$	$(4\times10^{20})a$ (a in m)$^+$
	Diffusion coefficient of particles in unrestricted space	D_p	Variable, estimated using Einstein's Eqn at a 25 °C
	Pore density of clean membranes	N_m	2.65×10^{14} m^{-2} (Eqn (7))
	Permeate flowrate in single pore	Q_1	9.44×10^{-20} m^3/s (Eqn (33))
	Effective membrane thickness	L_m	1.25×10^{-5} (Eqn (8))
Chemical	Attachment probability between particles and membrane surfaces (including membrane pores), related to depositional stability of particles	α_{pm}	Variable between 0 and 1
	Attachment probability between two particles, related to coagulational stability of particles	α_{pp}	Variable between 0 and 1

Note: * known values for the membrane used in the experimental part of the study are herein presented. Details are provided in the next chapter. + specific cake resistance is estimated using the empirical equation determined based on the fouling of a PVDF membrane by 93 nm latex particles, which is extended to other particle sizes by assuming that the hydraulic resistance by those particles is a constant if normalized to their particle surface areas.

In order to apply the fouling model, some basic modeling conditions need to be chosen beforehand. It is of primary concern to understand the impacts of attachment probabilities on the fouling process. Therefore, the two related parameters, α_{pm} and α_{pp}, should be allowed to vary in a valid range of 0 to 1. On the other hand, particle size is considered from its relevance in the occurrence of either internal or external attachment of particles. Based on our previous discussion, three levels of particle sizes can be selected: $a \geq D_m/2$, $D_m/2 > a \geq D_m/6$, and $a < D_m/6$. At the first level, surface fouling dominates, and particles are modeled as "large particles". At the second level, membrane

fouling begins with internal plugging, but quickly shifts to surface fouling due to substantial pore constriction. At the third level, pore plugging is the predominant fouling mechanism during the entire filtration process. Other modeling conditions can also be set based on feasible experimental conditions as shown in Table 2-1.

2.4.2 Fouling by Large Particles

The fouling of the model membrane by 100 nm ($a = 5\times10^{-8}$ m) particles is simulated herein using the model. Figure 2-6 shows an example of the predicted increase of the specific mass of particles contributing to pore blocking or cake layer formation with the increasing permeate throughput. It is noticed that most of the particles are present in the cake layer, not on membrane pores throughout the fouling process; the difference becomes greater as more particles are delivered to the membrane surface. However, as illustrated in Figure 2-7, the small fraction of particles attaching to membrane pores has greater impact to membrane permeability than the majority of particles present in the cake. Also the hydraulically irreversible fouling is dominated by pore blocking because the coagulational attachment probability equals zero in this particular case. The same calculation and comparison can be made for other physiochemical conditions by varying either the depositional attachment probability or the coagulational attachment probability.

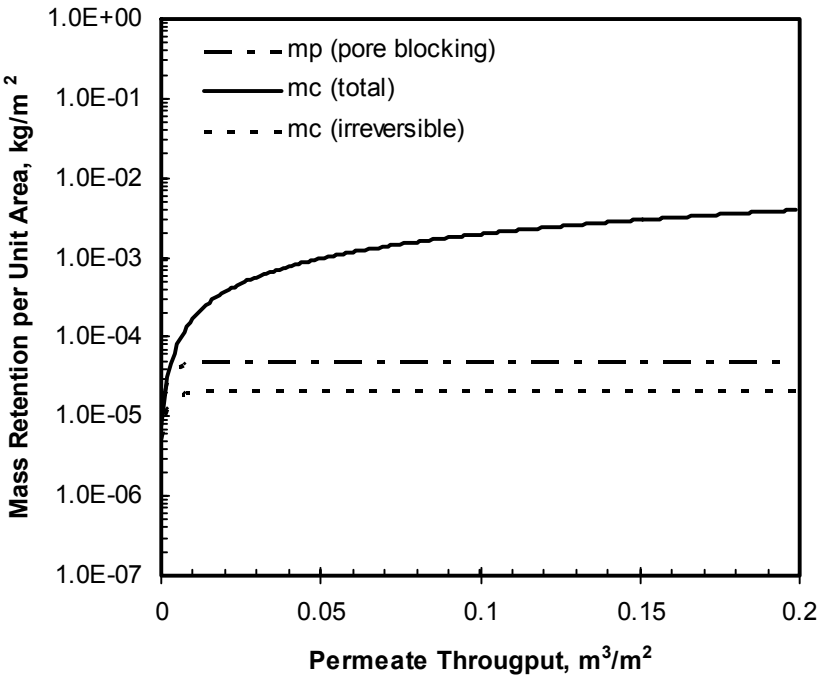

Figure 2-6. Specific Mass of Particles Contributing to Pore Blocking, Total and Irreversible Cake Formation as Function of Permeate Throughput. Depositional attachment probability, $\alpha_{pm} = 1$, and coagulational attachment probability, $\alpha_{pp} = 0$.

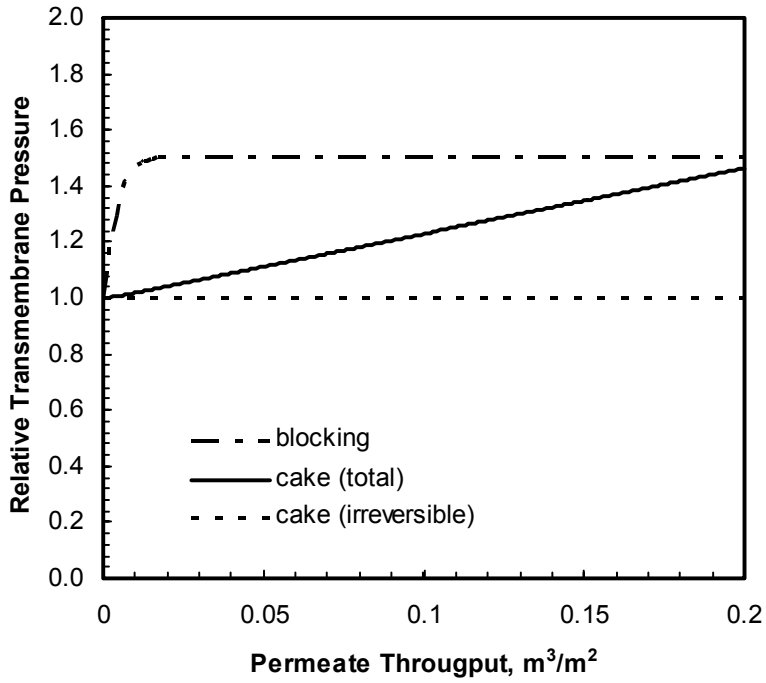

Figure 2-7. Increase of Relative Transmembrane Pressure due to Blocking or Cake Layer Formation as a Function of Permeate Throughput. Depositional attachment probability, $\alpha_{pm} = 1$, and coagulational attachment probability, $\alpha_{pp} = 0$.

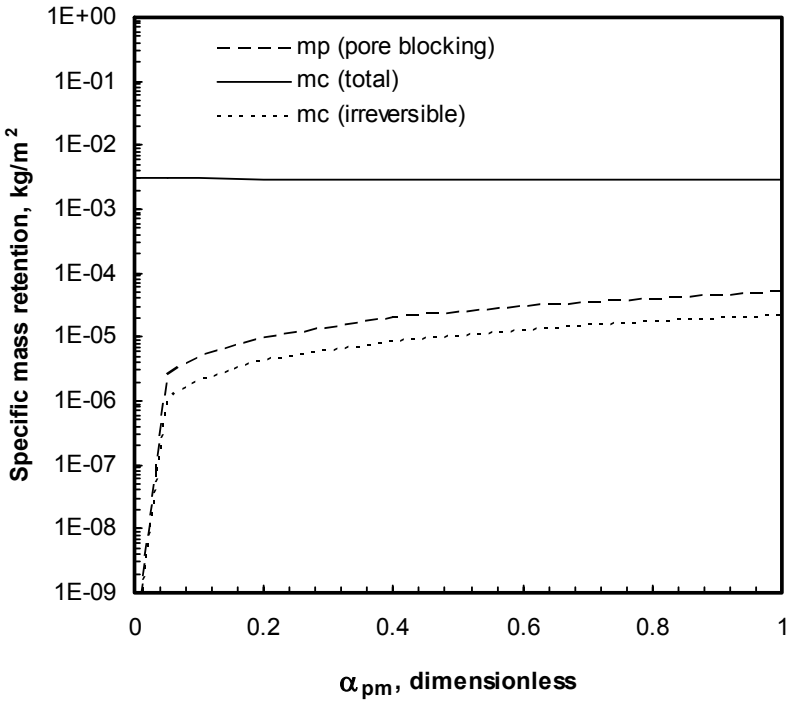

Figure 2-8. Specific Mass of Particles Contributing to Different Types of Fouling as a Function of Depositional Attachment Probability, α_{pm}. The coagulational attachment probability, α_{pp}, is set to zero in the calculation. The permeate throughput, $V_s = 0.15$ m^3/m^2.

Figure 2-8 presents the variation of the specific mass of particles ($V_s = 0.15$ m^3/m^2) contributing to pore bocking or cake layer formation when the depositional attachment probability is increasing but the coagulational attachment probability remain zero. It is shown that the mass of particles contributing to total cake layer formation is almost constant, regardless of the changes of the attachment probability. In comparison, the masses of particles for pore blocking and irreversible cake formation increase simultaneously with the increasing α_{pm}, rapidly when $\alpha_{pm} < 0.1$, but slowly after that. Overall, the mass of particle for pore blocking accounts for a maximum of one percent of the total mass delivered to the membrane. On the other hand, the resulting increase of the relative transmembrane pressure is shown in Figure 2-9. The fouling due to pore blocking increases dramatically as α_{pm} increases, and there is no sharp increase when α_{pm}

< 0.1 as observed in Figure 2-8. Comparatively, the total and hydraulically irreversible fouling caused by cake layer formation is more or less unchanged. Therefore, the total surface fouling (pore blocking plus cake layer formation) increases monotonously with increasing α_{pm} as illustrated in Figure 2-10, almost exclusively due to the increase of the fouling by pore blocking. When α_{pm} reaches unity, approximately half of the total fouling becomes hydraulically irreversible.

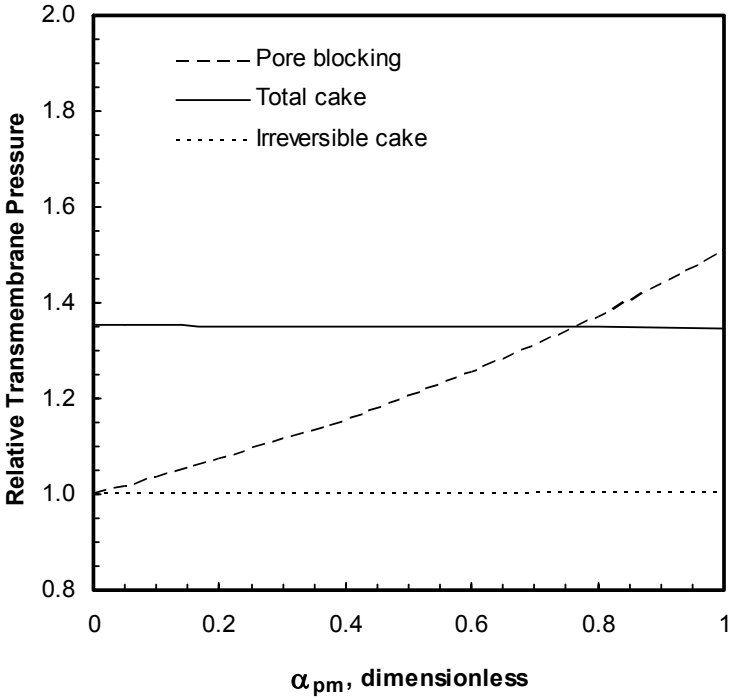

Figure 2-9. Increase of Relative Transmembrane Pressure due to Different Types of Fouling as a Function of Depositional Attachment Probability, α_{pm}. The coagulational attachment probability, α_{pp}, is set to zero in the calculation. The permeate throughput, V_s = 0.15 m^3/m^2.

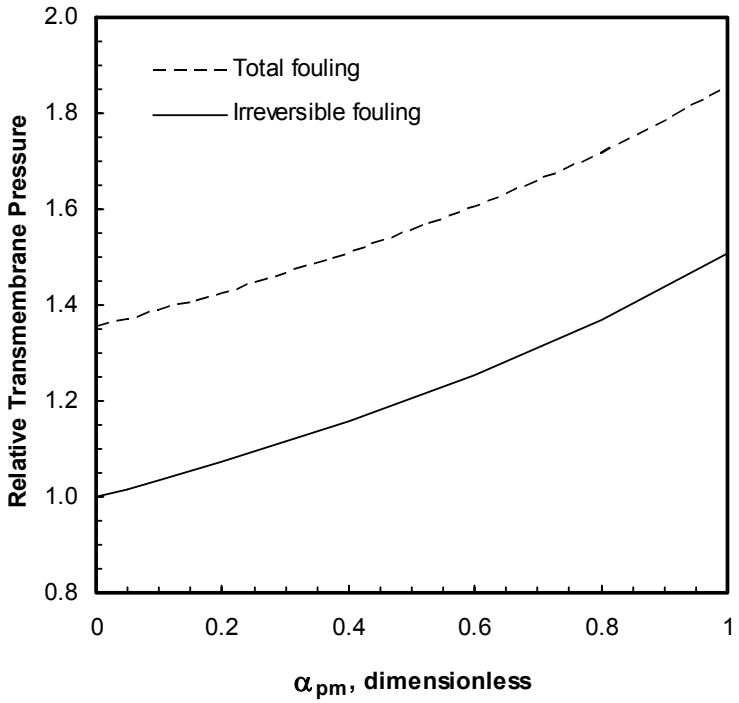

Figure 2-10. Increase of Total and Hydraulically Irreversible Fouling as a Function of Depositional Attachment Probability, α_{pm}. The coagulational attachment probability, α_{pp}, is set to zero in the calculation. The permeate throughput, $V_s = 0.15$ m^3/m^2.

The impacts of coagulational attachment probability on the fouling are simulated under the condition that the depositional attachment probability remains unity. The corresponding variation of the specific mass of particles contributing to pore blocking, total cake layer formation, and hydraulically irreversible cake formation are presented in Figure 2-11. As shown in the figure, the mass of particles for blocking decreases slightly as α_{pp} increases, coincident with a substantial increase of the mass of particles in the irreversible cake layer. It should be pointed out, however, that the increase in the irreversible cake layer is predominantly a result of the enhanced particle-particle attachment, rather than the decrease in the particle attachment to membrane pores. This is further manifested by the changes in the corresponding types of fouling as presented in Figure 2-12. This figure demonstrates that the increase in the relative transmembrane

pressure due to pore blocking is reduced significantly from approximately 1.5 to 1.1 when α_{pp} increases from zero to unity, while that due to the hydraulically irreversible cake increases from approximately 1.0 to 1.35. In contrast, the total fouling by cake formation is constant as expected although the irreversible part increases. The predicted overall increases of the relative transmembrane pressure before and after hydraulic backwashing are shown in Figure 2-13. Interestingly, the total fouling decreases due to the enhancement of particle-particle attachment, but the hydraulically irreversible fouling fluctuates only slightly. Completely irreversible fouling occurs when both α_{pm} and α_{pp} reach unity.

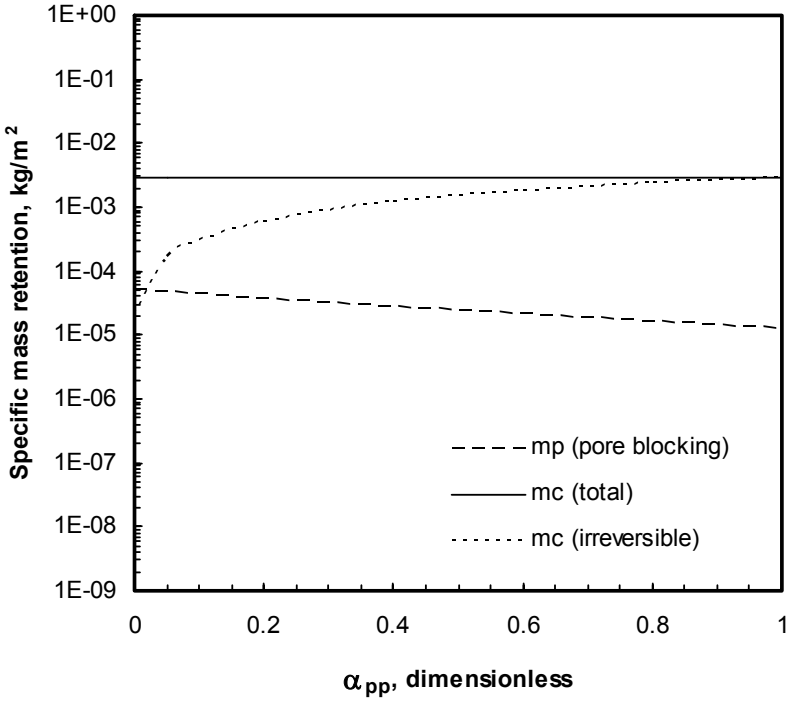

Figure 2-11. Specific Mass of Particles Contributing to Different Types of Fouling as a Function of Coagulational Attachment Probability, α_{pp}. The depositional attachment probability, α_{pm}, is set to unity in the calculation. The permeate throughput, $V_s = 0.15$ m^3/m^2.

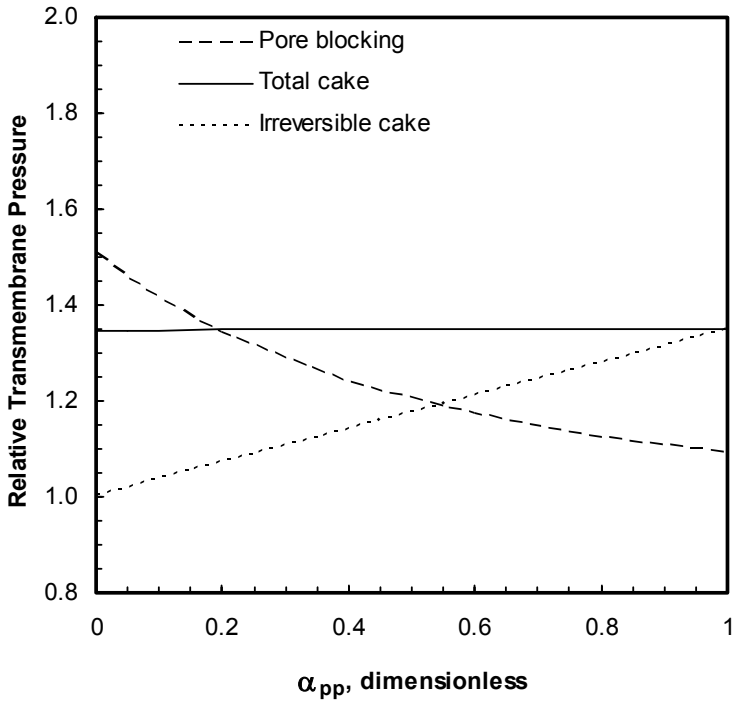

Figure 2-12. Increase of Relative Transmembrane Pressure due to Different Types of Fouling (V_s = 0.15 m^3/m^2) as a Function of Coagulational Attachment Probability, α_{pp}. The depositional attachment probability, α_{pm}, is set to unity in the calculation.

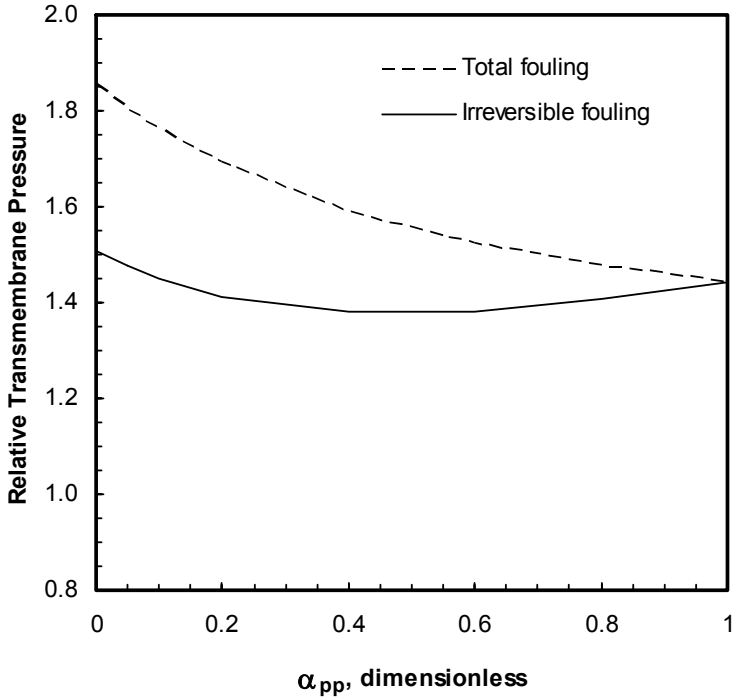

Figure 2-13. Variations of Total and Hydraulically Irreversible Fouling (V_s = 0.15 m^3/m^2) as a Function of Coagulational Attachment Probability, α_{pp}. The depositional attachment probability, α_{pm}, is set to unity in the calculation.

2.4.3 Fouling by Small Particles with Significant Pore Constriction

The fouling of a model membrane by 20 nm particles ($a = 1\times10^{-8}$ m) is calculated using the model with varying depositional attachment probabilities. As discussed previously, the coagulational attachment probability is consistently set to be zero, which means that no particle-particle attachment is favored. As shown in Figure 2-14, the specific mass of particles contributing to pore blocking, m_p, or irreversible cake formation, m_c (irreversible), is less than one percent of that contributing to all cake formation, m_c (total). Therefore, most of the small particles rejected by the membrane are in the cake layer and in contact with other particles, similar to large particles elucidated in previous section. Moreover, m_p and m_c (irreversible) do increase slowly with increasing α_{pm}. The slow increase in m_p, however, leads to rapid increase of the relative transmembrane pressure (see Figure 2-15). The pressure increases from zero to ten fold as α_{pm} increases from 0.05 to 0.9, much greater than the fouling by large particles (see Figure 2-12). In consequence, the total and the hydraulically irreversible fouling increase simultaneously as shown in Figure 2-16. It should be pointed out that a condition of $\alpha_{pm} = 1$ is not used in the simulation because the relative pressure quickly goes up to infinity in this case. This may be explained by an overestimation of the blocking efficiency of small particles on the membrane surface. In fact, there will always be inter-particle spaces that allow water to flow through. Therefore, the actual loss of membrane pore area in Eqn (63) should be less than σm_p. We do not attempt to solve this problem herein because more advanced mathematical tools are required.

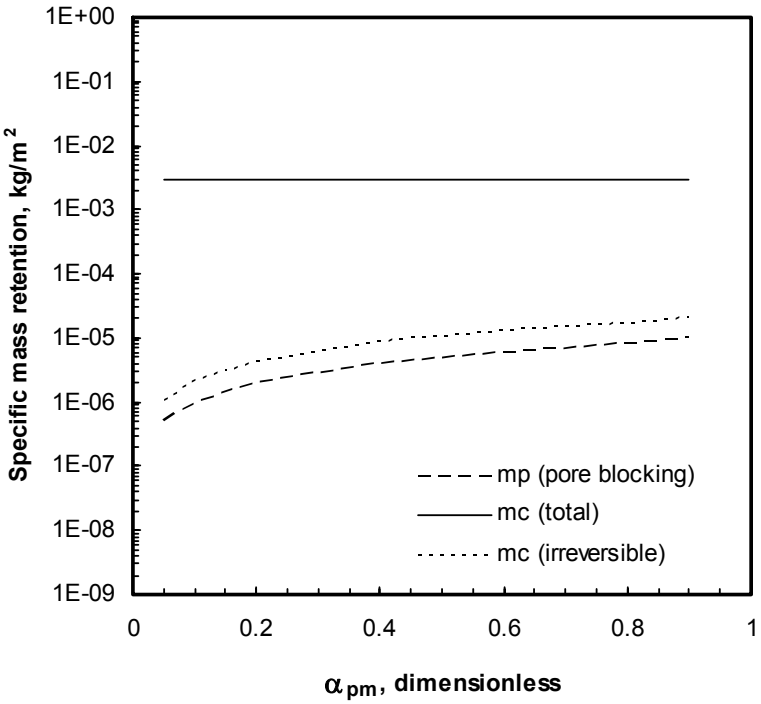

Figure 2-14. Specific Mass of Particles Contributing to Different Types of Surface Fouling as a Function of Depositional Attachment Probability, α_{pm}, for Small Particles with Substantial Pore Constriction. The coagulational attachment probability, α_{pp}, is set to zero in the calculation. The permeate throughput, $V_s = 0.15$ m^3/m^2.

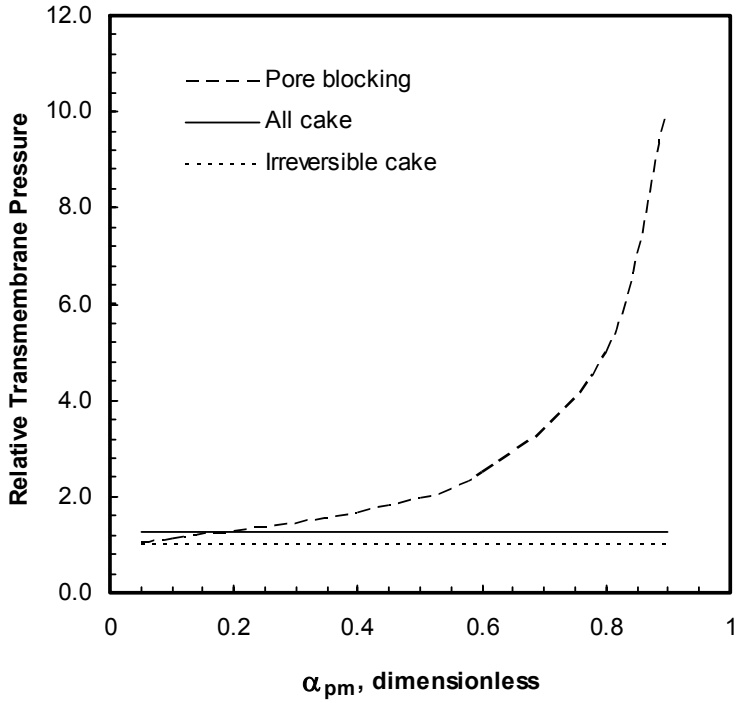

Figure 2-15. Increase of Relative Transmembrane Pressure due to Different Types of Fouling (V_s = 0.15 m^3/m^2) as a Function of Depositional Attachment Probability, α_{pm}. The coagulational attachment probability, α_{pp}, is set to zero in the calculation.

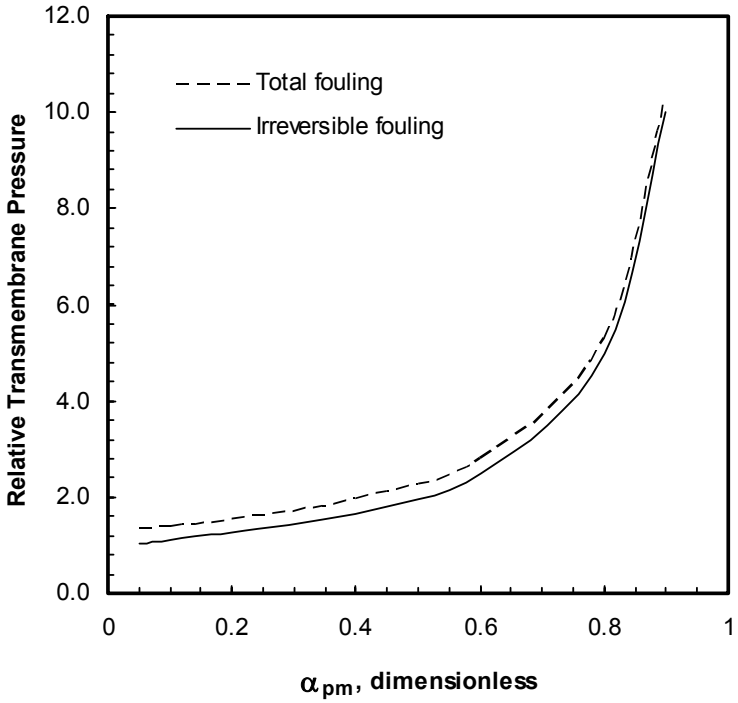

Figure 2-16. Variations of Total and Hydraulically Irreversible Fouling (V_s = 0.15 m^3/m^2) as a Function of Depositional Attachment Probability, α_{pm}. The coagulational attachment probability, α_{pp}, is set to zero in the calculation.

2.4.4 Fouling by Small Particles without Significant Pore Constriction

Eqn (62) is used in the estimation of the fouling caused by those particles that are too small to constrict the pore substantially. However, it is recognized there are two prerequisites in applying this equation: one is the sufficiency of pore wall area to be covered by a given mass of particles, and the other is the magnitude of α_{pm} for depositional attachment. The latter has been discussed in previous section (see Figure 2-5), and α_{pm} values in the range of 0.1 to 1 are found to be a valid condition. The former determines the maximum amount of particles that can attach to pore walls before breakthrough occurs. It can be easily estimated using the concept of σ and the results are illustrated in Figure 2-17. Also shown in the figure is the corresponding maximum

increase of the relative transmembrane pressure that can be caused by those attached particles. The results demonstrate that the maximum mass increases linearly with increasing particle radius. If particle radius is approximately 1 nm (close to some humic substances), the maximum mass of these "particles" will be slightly less than 2×10^{-3} kg/m^2, and the maximum pressure after fouling will be 1.03, a value negligible in practice.

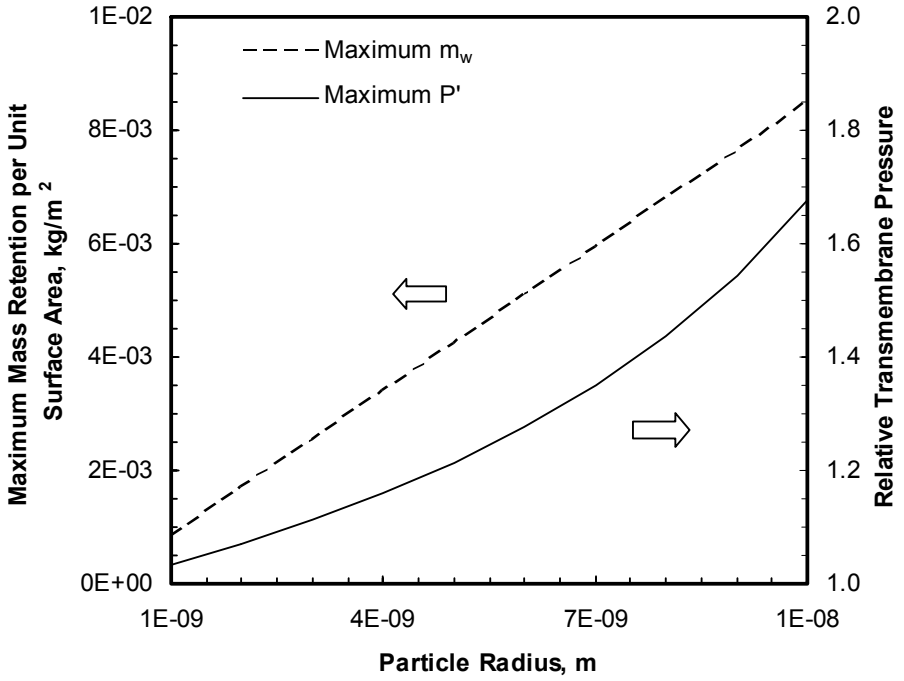

Figure 2-17. Estimated Maximum Specific Weight of Particles Attaching to Membrane Pore Walls and Their Impacts to the Relative Transmembrane Pressure with Varying Particle Size.

Certainly, this is on the condition that these tiny materials do not form multi-layers in membrane pores. In comparison, particles with a radius of 10 nm can attach to pore walls at a specific mass of 8.5×10^{-3} kg/m^2, which leads to a maximum relative pressure of approximately 1.7. This is much greater than that of 1 nm particles. However, the magnitude of fouling is still far less than the case of fouling by the same particles with substantial pore constriction as shown in Figure 2-15. The difference in the possible

extent of fouling indicates the efficiency of surface pore blocking in all types of membrane fouling.

According to Eqn (62), the increase of relative transmembrane pressure is not explicitly dependent on particle size. Therefore, the following discussions are in general applicable to particles with all sizes after taking into account the maximum conditions presented in Figure 2-17.

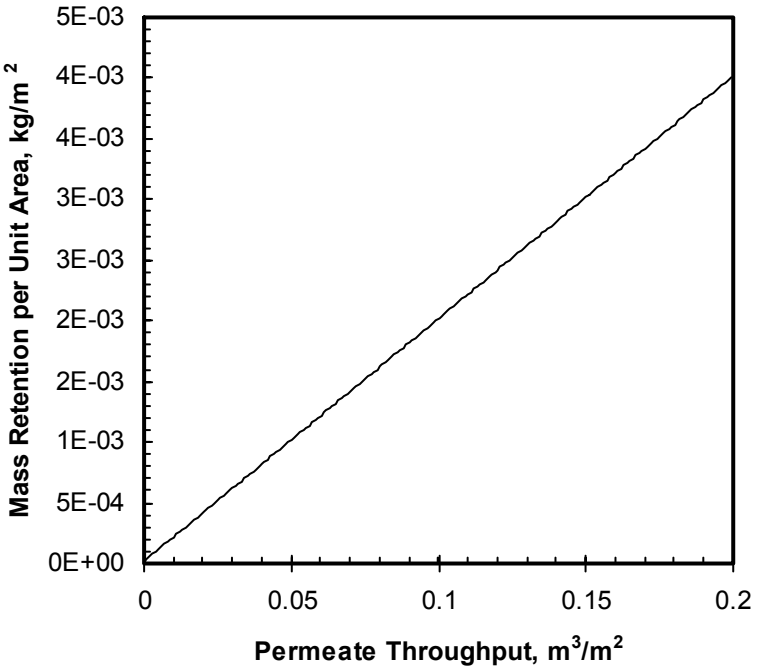

Figure 2-18. Increases of the Specific Mass of Particles on Membrane Pore Walls with the Increasing Permeate Throughput for Small Particles without Substantial Pore Constriction. The depositional attachment probability is in a range of 0.1 ~ 1.

Figure 2-18 shows the specific mass of particles attaching to pore walls with increasing permeate throughput. It is found that the increase of the specific mass is proportional to the increase of the permeate throughput, which results from the simplification made previously and is reasonable under the preset conditions. The corresponding increase of the relative transmembrane pressure with permeate throughput

is illustrated in Figure 2-19. The shape of relative transmembrane pressure curve shows a slightly concave down pattern. Nevertheless, the relative pressure can increase to a maximum of approximately 1.15 at a permeate throughput of 0.15 m^3/m^2 if pore plugging is the primary fouling mechanism.

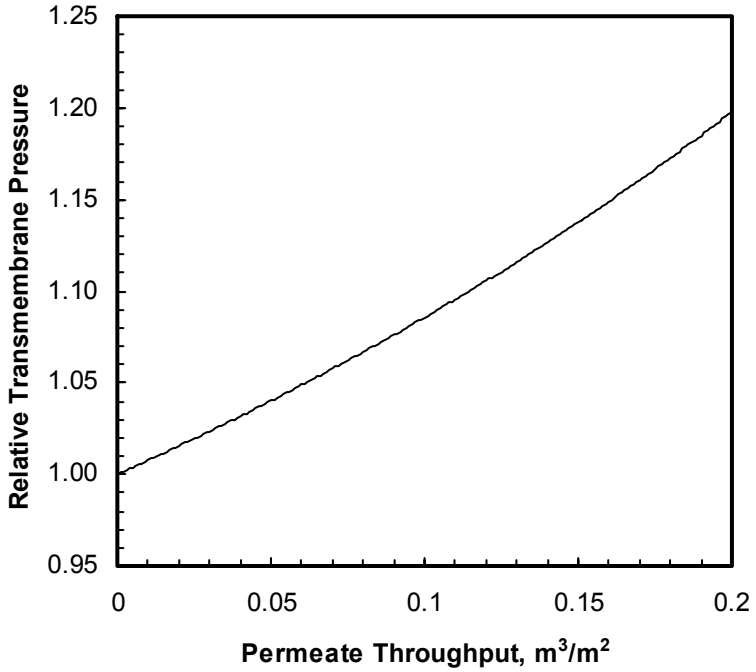

Figure 2-19. Increases of the Relative Transmembrane Pressure with Increasing Permeate Throughput for Small Particles without Substantial Pore Constriction. The depositional attachment probability is in a range of 0.1 ~ 1.

2.5 DISCUSSION

2.5.1 Effects of Particle Size

As elucidated in the model development and simulation, the effects of particle size on the fouling of microfiltration membranes are manifested in three related aspects. First, it determines whether the fouling can be dominated by surface fouling ($a > D_m/2$) or internal pore plugging ($a < D_m/6$). It is also one of the governing factors for the occurrence of surface fouling by particles with sizes of $D_m/2 > a > D_m/6$. Second, it

affects the extent of fouling once particles are unstable. When $a > D_m/2$, this size effect is reflected by the correctional factor of $(D_m^2/4a^2)$ used in Eqn (55). For particles smaller than $D_m/6$, particle size can determine the maximum fouling by pore plugging as shown in Figure 2-17. Overall, particles in a size range of $D_m/2 \geq a > D_m/6$ can potentially cause the greatest extent of fouling due to their efficiency in pore blocking. Finally, particle size may affect the attachment probabilities as well. This effect is usually considered in theoretical interpretation of surface interactions.

The size effects predicted by the model is different from those found in earlier studies on cross-flow MF [67]. For cross-flow MF, particle size strongly affects their transport, especially so-called shear-induced transport, in MF of micron sized particles. In contrast, the size effects for the dead-end filtration of submicron sized particles, the scenario discussed in this model, are primarily results of varying efficiencies for pore blockage.

2.5.2 Effects of Depositional Attachment Probability

The abovementioned size effects are dependent on the physiochemical or chemical conditions for particle attachment. The simulation results presented in the previous section indicate that the depositional attachment probability is likely to be the governing factor in the fouling of microfiltration membranes. For the fouling caused by particles with sizes of $a > D_m/2$, the fouling is the maximal when α_{pm} reaches unity (see Figure 2-10). As for pore blocking or plugging caused by smaller particles, membrane fouling only occurs when favorable particle-membrane attachment exists; otherwise, particles will penetrate through the membrane pores without causing any fouling. From

this standpoint, it is reasonable to state that the size of particles is in general an important but secondary factor in membrane fouling.

2.5.3 Effects of Coagulational Attachment Probability

The effects of coagulational (particle-particle) attachment on fouling are estimated for particles larger than the membrane pore size using the model. Two major effects are noticed herein. One is the competition between particle-particle and particle-membrane attachment, which results in the decrease of the total fouling because more particles are intercepted by attached particles and unable to reach membrane pores (see Figure 2-11). The other coincident effect is the increase of the hydraulic irreversibility of the fouling, i.e., a greater fraction of the fouling becomes irreversible as α_{pp} increases (see Figure 2-13).

2.5.4 Hydraulic Reversibility of Membrane Fouling

The hydraulic reversibility of membrane fouling is addressed in the model in a primitive way. A basic assumption made is that only the fouling caused by physiochemically attached particles is hydraulically irreversible, no matter on membrane surfaces or inside pores. This assumption gives us the opportunity to evaluate this important issue using only two parameters, i.e., attachment probabilities. This is compared to the use of a separate peptization coefficient for particle reentrainment by Polyakov [68] in his model for hollow fiber membrane filtration. The results imply that one possible approach to reduce hydraulic irreversible fouling is to reduce the attachment probabilities, especially the depositional attachment probability. This is, once again,

related to the origin of different types of surface interactions, which, unfortunately, has yet to be well understood to date as discussed in Chapter 1 and in Polyakov's model [68] as well.

It should be pointed out that the hydraulic reversibility of fouling is related not only to the strength of the attachment, but also the magnitude of hydrodynamic forces that can be applied during hydraulic backwashing. Practically, there is a trend to reduce the hydrodynamic forces applied in backwashing in order to extend the lifetime of membranes used in large scale systems. Therefore, it would be more plausible to improve the reversibility of fouling by means of reducing the attachment.

Another related question is the effect of hydrodynamic drag forces on the strength of physiochemical attachment. Although previous studies [69] have demonstrated that particle attachment increases with increasing permeate fluxes, the relationship between the hydraulic reversibility of fouling and the hydrodynamic drag is still unclear, both theoretically and experimentally. It is speculated, however, that this hydrodynamic effect depends on the existence of repulsive interactions between particles or between particles and membrane surfaces. If there are strong repulsive surface interactions, increasing the hydrodynamic drag may be helpful in overcoming the repulsive energy barrier, and the particles become more likely to reach the deep energy well (if it is substantial).

2.6 CONCLUSION

A mathematical model for the fouling of porous membranes by monodispersed particles was developed in this chapter on the basis of an analysis of particle collision and attachment in membrane filtration for particle removal and the classical Hermia model

for the loss of membrane permeability. The occurrences of pore blocking, pore plugging/constriction, and cake layer formation are interpreted for particles with different sizes and physiochemical stabilities.

The model simulation results reveal that physiochemical, especially the depositional stabilities of aqueous particles play the primary role in determining the occurrence and extent of membrane fouling. Hydraulically irreversible fouling only happens in the presence of physiochemically destabilized particles. Of all three major types of fouling, surface pore blocking causes the fastest loss of membrane permeability, and is solely the result of the favorable attachment of particles on the entrance of membrane pores.

The size of particles plays an important, but secondary role in membrane fouling. In the presence of favorable particle-membrane attachment, particles with radii of 1/6 to 1/2 of the diameter of membrane pores are the most effective in blocking membrane pores and causing fouling. Particles larger or smaller than this size range cause less fouling even under the same physiochemical conditions.

Those modeling results draw our attention to the relative importance of particle size and physiochemical stability in membrane fouling. An experimental investigation was therefore necessary to validate this simple but relevant relationship. This was achieved by performing colloidal fouling of a MF membrane using monodispersed latex particles with known sizes and controlled physiochemical stabilities. The results are presented in next chapter.

Chapter Three

MODEL VALIDATION USING SYNTHETIC COLLOIDAL PARTICLES

3.1 INTRODUCTION

In the previous chapter, a mathematical model was developed on the basis of particle transport and attachments during MF processes. The model simulation results indicated that the physiochemical stabilities of aquatic particles and the resulting particle attachments play the primary roles in membrane fouling. In general, membrane fouling increases as the probability of particle-membrane attachment increases, but decreases as the probability of particle-particle attachment increases. Therefore, there is a competition between the two types of particle attachments on the magnitude of membrane fouling. Meanwhile, the magnitude of membrane fouling caused by unstable particles is also affected by particle sizes due to the existence of different fouling mechanisms. The fouling is the greatest when the radius of the particles is within a range of 1/6 to 1/2 of the diameter of the membrane pores, given favorable chemical conditions. The simulation results can be illustrated qualitatively with two schematic figures.

Figure 3-1 shows the fouling of a MF membrane by colloidal particles larger than its pore size. Apparently, particles cannot penetrate into membrane pores as a result of size exclusion. A particle (1) is delivered to a membrane pore by the permeation flow. Lacking favorable attachment conditions, this particle stays at a certain distance from the pore entrance if the hydrodynamic drag force exerted on the particle by the permeate flow cannot overcome the interaction energy barrier between the particle and the membrane. This particle becomes a member of the cake layer, and can be flushed away from the membrane surface by the reversed hydrodynamic drag during hydraulic backwashing of

the membrane. Therefore, the fouling caused by this particle is hydraulically reversible. On the other hand, if this particle is indeed unstable with respect to deposition, the pore blockage will be more effective and less likely to be hydraulically reversible. In comparison, the second particle (2) is intercepted by the solid surface and becomes part of the cake layer as it does not directly reduce the area of the pore entrance beneath.

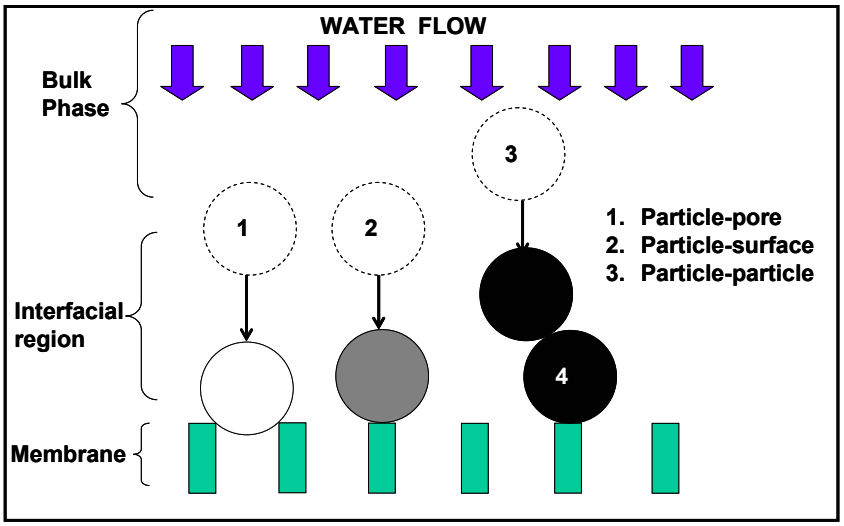

Figure 3-1. A Diagram of MF Membrane Fouling by Colloidal Particles Larger than the Membrane Pore Size. The white circle (1) represents a particle stable with respect to both coagulation and deposition, the grey circle (2) represents a particle unstable in deposition but stable in coagulation, and the black circles (3 and 4) represent particles unstable in both coagulation and deposition.

However, it is likely to remain on the membrane surface during hydraulic backwashing in that favorable conditions exist for particle-membrane attachment. Another result of the deposition of the second particle is that membrane pores below it are now covered by the projected area of the particle and no longer accessible to other incoming particles, thereby being excluded from pore blockage. (Recall the use of a correction factor, $D_m^2/4a^2$, for pore blocking efficiency in the mathematical model). Meanwhile, steady particle-particle attachment is observed between the third (3) and the fourth (4) particles as both particles are unstable with respect to coagulation. The fourth particle is also attached to the

membrane surface as is the second particle. Due to the difference in coagulational stability, this particle (4) becomes an effective collector to capture incoming particles that pass around it. The captured particle (3) then participates in the formation of a cake layer, rather than blocking other pores despite the possible presence of favorable particle-membrane attachment. This is where the aforementioned competition between particle-membrane and particle-particle attachments originates. (Recall the use of a coefficient, $4^{\alpha_{pp}}$, in the model to qualitatively describe this effect.) On the other hand, particle 4 is more likely to remain in the cake layer during hydraulic backwash in the presence of favorable particle-particle attachment. In other words, the fouling under conditions that particles are unstable in both coagulation and deposition is the most likely to be hydraulically irreversible in all fouling scenarios when the fouling is caused by large particles. In contrast, a cake layer can also be formed by particles that are only unstable in deposition, but this cake layer is readily removable by hydraulic backwashing since the particle-particle attachment is not favorable. Overall, it is expected that the hydraulic reversibility of the fouling will decrease as the particle stability decreases.

Figure 3-2 illustrates the fouling of a MF membrane caused by colloidal particles smaller than its pore size. When the membrane is clean, the absence of a physical sieving effect gives the first particle (1) opportunity to penetrate through the membrane pore. If the particle-membrane attachment is unfavorable, this particle directly goes through the membrane and is not captured by the membrane. Comparatively, the third particle (3) that is unstable with respect to deposition attaches to the internal wall of membrane pores and is removed by the membrane. According to the model calculation, this particle is unlikely travel in the pore deeper than its diameter. Therefore, it is captured close to the

opening of the pore. The attachment of this particle results in the constriction of the membrane pores. This in turn decreases the hydraulic permeability of the membrane. Another effect of pore constriction is shown with the fifth particle (5). In this case, the penetration of the sixth particle (6) through the membrane is prohibited because the physical size of the pore is now less than that of the particle, i.e., the occurrence of physical sieving effect. This happens when the radius of the particle is in a critical range of 1/6 to 1/2 of pore diameter. Meanwhile, the second (2) and the fourth (4) particles collide with the solid surface outside the membrane, similar to the large particles.

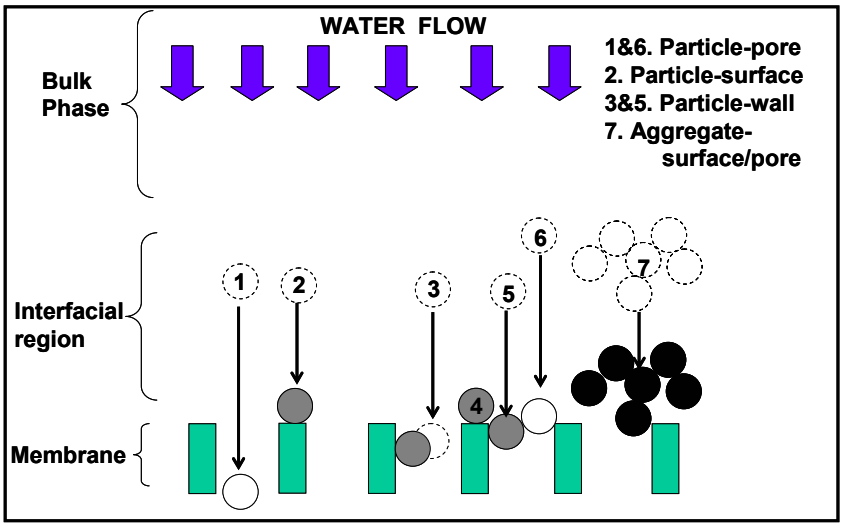

Figure 3-2. A Diagram of MF Membrane Fouling by Colloidal Particles Smaller than the Membrane Pore Size. The white circles (1 & 6) represent particles stable with respect to both coagulation and deposition, the grey circles (2-6) represent particles unstable in deposition but stable in coagulation, and the black circles (7) represent particles unstable in both coagulation and deposition.

It is noteworthy, however, that the fourth particle (4) is less effective than a large one (see Figure 3-1) in preventing surrounding pores from being blocked. Consequently, small particles cause more fouling than large particles when the fouling happens completely on the external surfaces of the membrane. Also, the surface fouling caused by unstable

small particles is more hydraulically irreversible than that by large particles due to the dominance of particle-membrane attachment. Finally, when the small particles become unstable with respect to coagulation, their rates of perikinetic coagulation are $(d_{large}/d_{small})^2$ times faster than the large particles at the same mass concentrations [66]. Here, d_{large} and d_{small} are the diameter of the large and the small particles, respectively. Therefore, destabilized small particles are more likely to form aggregates before they reach the membrane surface than the large ones. This scenario is presented as a cluster of particles (7). This aggregate of multiple particles contributes to the formation of a highly porous cake layer that can be highly permeable to water flows. In consequence, the fouling caused by small particles that are unstable in coagulation may or may not be important depending on the permeability of the aggregates, although their attachment on the membrane surface is irreversible.

3.2 MATERIALS AND METHODS

3.2.1 Model Particles and Natural Organic Matter

The model colloidal particles used in the study were purchased from Interfacial Dynamics Corporation (IDC). Some characteristics of these particles are presented in Table 3-1. These particles are free of surfactant. The original latex suspensions received were diluted into ultrapure waters to prepare stock suspensions at a concentration of 200 mg/L. The ultrapure water was genetrated by a Milli-Q® reagent water system that used distilled RO water as the feedwater.

Table 3-1. Some Characteristics of the Polystyrene Latex Particles Used in the Study as Reported by the Manufacturer.

Size (nm)	Batch Number	Chemical Composition	Charge Density ($\mu C/cm^2$)	Stock Concentration (g/100mL)
19 ± 3	1973	Polystyrene sulfate	2.4	8.0
93 ± 5	1371,2	Polystyrene sulfate	2.2	8.0

The natural water containing the model natural organic matter (NOM) was collected from the Great Dismal Swamp Wildlife Refuge in southeastern Virginia, USA, in September, 2001. Details of this water and NOM sample can be found elsewhere [15]. Some known characteristics of the model NOM are introduced in Chapter 4. The collected water sample has a NOM concentration of approximately 100 mg C/L as dissolved organic carbon (DOC), and therefore, no extraction or concentration of the NOM was performed. The only major pretreatment used in the study was the prefiltration of the water sample using 1.2 μm glass fiber filters (Whatman, GF/C) to remove coarse materials in the water. The prefiltered water was diluted about 100 fold to reach a dissolved organic carbon (DOC) concentration of approximately 1 mg C/L for use in the colloidal fouling study.

3.2.2 Other Chemicals

Reagent grade calcium chloride ($CaCl_2$) was dissolved in ultrapure water to prepare a stock solution of 1 M. An appropriate volume of the stock solution was added into model waters to reach desired calcium concentrations. Sodium bicarbonate ($NaHCO_3$, reagent grade) was also dissolved to prepare a stock solution of 0.1 M. The solution was diluted 1000 fold in model waters to reach a concentration of 0.0001 M. $NaHCO_3$ was used herein as a proton buffer to control pH.

3.2.3 Microfiltration Membrane

The MF membrane used in the study was a commercial hollow fiber membrane supplied by US Filter/Memcor. This membrane is made of polyvinylidene fluoride (PVDF) as specified by the manufacturer. An analysis of the membrane surface composition using X-ray photon spectroscopy (XPS) confirmed the predominance of the structure of $C_2H_2F_2$, but also revealed the presence of a minor fraction of impurities containing oxygen on membrane samples that were not treated using nonpolar solvent. The source of the impurities was unclear. Moreover, the nominal pore size of the membrane was reported to be 100 nm based on bubble point test as reported by the manufacturer. A microsphere rejection test using various sizes of latex particles (IDC) indicated that the mean size of the membrane pores is approximately 58 nm, which is between the size of the large (ca. 93 nm) and small (ca. 19 nm) latex particles used to challenge this membrane. The morphology of the membrane was investigated using a scanning electron microscope (JEOL 6700F). All membrane samples for SEM imaging were dried in air and then precoated with a thin layer (1~2 nm) of platinum. The cross-sectional image of the membrane was obtained by immersing the dry membrane fibers in liquid nitrogen for a short period of time, and then cutting them with a stainless steel blade.

Prior to a fouling experiment, the membrane fibers were ported into a module consisting of four 20 cm long fibers using epoxy glue. The ported module was kept in the atmosphere at room temperature overnight to allow the glue to reach its maximum strength. The module was then wetted using a mixture of one volume of isopropanol (ACS reagent grade) and two volume of ultrapure water in filtration mode for an hour.

The membrane module was cleaned prior to use by filtering 2 L of ultrapure water in 24 hours. A new module was prepared and used in each fouling experiment.

3.2.4 Bench-Scale Microfiltration Unit

The precleaned PVDF membrane module was installed onto a bench-scale microfiltration unit. As shown in Figure 3-3, the unit consisted of a peristaltic pump (Cole Parmer, Masterflex precision pump), a raw water column (Pyrex graded glass cylinder, 100 mL) with membrane module submerged, a digital compound pressure gauge (Cecomp Electronics, DGP100B+/-15PSIG-5), a UV-Vis spectrophotometer (Shimadzu, UV 160), and a top loading electronic balance (Mettler Toledo, PJ6000). The balance (Mettler Toledo, PG3001-S) was used for measuring the cumulative permeate weight. The pressure gauge was used for measuring the hydraulic pressure in the permeate line.

The unit can be operated in two basic modes: filtration and backwash. In the filtration mode, the pump worked as a suction pump and drew the water from the outside to the inside of the membrane fibers at a constant flowrate, and the permeate flowed through a flowthrough cell in the UV-Vis spectrophotometer while the absorbance at a wavelength of 546 nm (for 93 nm latex particles) or 254 nm (for 19 nm latex particles) was recorded continuously during the filtration. In the backwashing mode, the direction of the pump was reversed; the permeate was withdrawn from the permeate container and pumped through the membrane fibers from inside to outside. The permeate and the backwashing fluxes were controlled at approximately 90 L/m^2-hr (LMH) or 53 gfd (gal/ft^2-day) in all fouling experiments conducted. The use of the same flux for filtration and backwashing simplified the operation of the system. The author has also found in

another study that backwashing flux had little impact to the hydraulic reversibility of fouling observed with submerged, outside-in hollow fiber membranes used in water treatment [70].

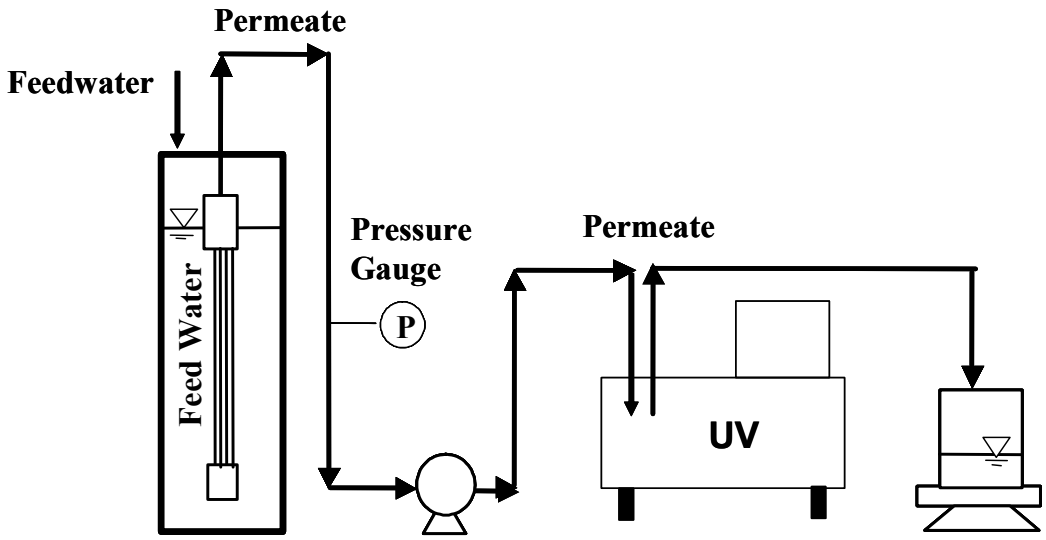

Figure 3-3. A Schematic Diagram of the Bench-Scale Submerged, Continuous Microfiltration Unit. UV represents the UV-visual spectrophotometer used to measure permeate UV absorbance.

3.2.5 Determination of Coagulational Stability

Coagulational stability of the model latex particles was determined under a variety of calcium concentrations using three complimentary techniques: 1) jar tests, 2) electrophoretic light scattering, and 3) light extinction kinetics of latex suspensions. During those tests, the stock latex suspensions were diluted into 20 mg/L using ultrapure water, and mixed with 0.0001 M $NaHCO_3$ as proton buffer. In some waters, NOM was added in the means mentioned previously.

Jar Test

Six 250 mL beakers were first prepared, each containing 150 mL of a 19 nm latex suspension at concentration of 2 mg/L. These beakers were then placed onto a jar test

apparatus, and mixed at 100 rpm. Next, different volumes of the $CaCl_2$ stock solution were added into each beaker to reach the desired calcium concentration. The suspension was continuously mixed at 100 rpm for 2 minutes. Subsequently, the suspensions were kept quiescently for 24 to 36 hours. An aliquot of each suspension was taken at a series of time intervals to measure the turbidity using a bench turbidimeter (Hach 2100A).

Electrophoretic Mobility

The electrophoretic mobility of 93 nm latex suspensions at a particle concentration of 20 mg/L with different concentrations of $CaCl_2$ and/or NOM was measured using a Zetaplus apparatus (Brookhaven Inc.) that employs a light scattering technique. Latex and other chemicals were mixed in the same sequence as used in the jar tests. The variations of electrophoretic mobility are indicative of the changes of the electric potential at the shear plane of the particles. Due to the extremely low signal strength, this technique was not applicable to 19 nm latex suspensions.

Light Extinction Kinetics

This technique has been previously used by Tiller and O'Melia to study the aggregation kinetics of hematite particles [71]. In this study, a 93 nm latex suspension at a concentration of 20 mg/L was prepared with the addition of 0.0001 M $NaHCO_3$ solution to control the pH. Perikinetic flocculation took place in a 1 cm long cuvette. First, an aliquot of 0.3 mL Dismal Swamp water was transferred into the cuvette if necessary to reach a DOC concentration of approximately 1.0 mg C/L. 3 mL of the latex suspension was added subsequently. The contact time between the NOM and the latex

was not controlled, but typically less than one minute. Next, the cuvette was placed into the sample holder of a UV-Vis spectrophotometer (Shimadzu, UV-160) with ultrapure water as the reference. A certain volume of $CaCl_2$ stock solution (1 M) was added into the sample cuvette afterwards and mixed rapidly using a cuvette stirrer, and a time course scanning was initiated immediately at a wavelength of 546 nm. The scanning lasted from 60 seconds to 2 hours, depending on how fast the coagulation happened. The initial rate of the flocculation was determined from the slope of the time-dependent signal (the intensity of light extinction) curve at zero time. The maximum initial rate obtained in the absence of NOM was used as the reference level where the $\alpha_{experiment}$ was set to be unity. This was observed at a calcium concentration of approximately 0.091 M. The rates obtained under other conditions were normalized to this value to obtain $\alpha_{experiment}$ values.

3.2.6 Determination of Depositional Stability

Commercial PVDF powders (Atofina/Arkema, Kynar 461) were used as a surrogate material to study the depositional stability of latex particles on PVDF surfaces. This type of Kynar samples was chosen because it has been commonly used in the manufacture of membranes, according to the manufacturer. A SEM analysis indicated that the powders are mostly uniform sized particles with diameters around 0.4 μm. They form micron sized clusters in air and water. The surface compositions of the powders were analyzed using XPS, which confirmed the predominance of $C_2H_2F_2$ on the surface of the powders.

Prior to the deposition experiment, a series of 20 mg/L of 93 nm latex suspensions were prepared by the means used in the jar tests, each containing desired concentrations

of $CaCl_2$. PVDF powders were added next into these suspensions at a solid concentration of 2.5 g/L. The suspensions of PVDF and latex particles, as well as reference latex suspensions without PVDF powder, were mixed using a rotating disk mixer for 20 hours at room temperature. After that, all mixtures were filtered through 0.45 μm microfiltration membranes (Millipore, HA). The turbidity of the filtrates was measured using the bench turbidimeter.

3.2.7 Fouling Experiment Protocol

All latex suspensions used in the fouling experiments were prepared as described previously. The operating protocol for the fouling experiments is shown in Figure 3-4.

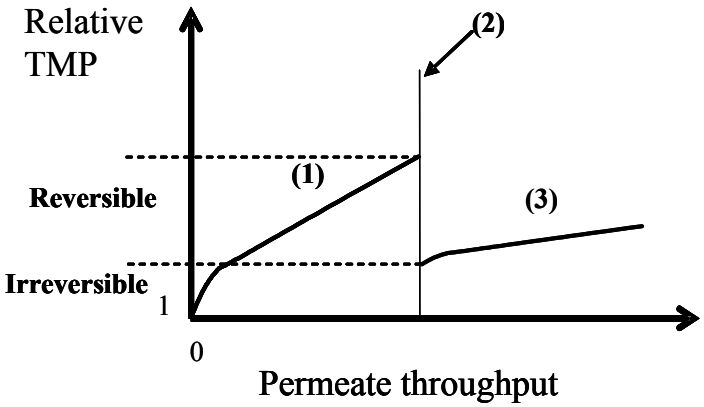

Figure 3-4. Major Steps in the Fouling Experiment. The increase of relative transmembrane pressure (TMP) is expressed as a function of permeate throughput (permeate volume per unit membrane surface area). Steps 1 to 3 represent filtration of raw water, hydraulic backwashing, and filtration of the permeate, respectively.

After a clean membrane module was mounted onto the bench scale microfiltration unit, ultrapure water was filtered first to determine the transmembrane pressure (TMP) of the clean membrane. The permeate UV absorbance (λ = 254 nm for 19 nm latex and 546 nm for 93 nm latex) was also checked to ensure the absence of background interference.

Next, the raw water column was filled with the model water to be tested. The permeate pump was then started to filter the water at the desired constant flux. The increase of TMP was recorded as the membranes were fouled by latex particles. The pump was stopped when the permeate volume reached 250 mL, which is equivalent to a permeate throughput of 150 L/m^2. A permeate backwashing was initiated immediately for 1 minute at the same flux. The mixtures of the model water and the backwash water in the raw water column were poured into a glass beaker and weighed. An aliquot of the water was taken for UV measurement at the aforementioned wavelength. The empty column was subsequently filled with the permeate collected in the previous filtration step. A second filtration step was then performed until 50 mL (30 L/m^2 of throughput) of water was filtered. The TMP was recorded during this period of time. As shown in Figure 3-4, the total fouling was defined as the increase of TMP in the end of the raw water filtration (the reversible plus the irreversible), while the hydraulically irreversible fouling (HIF) was determined as the increase of the TMP immediately after the permeate backwash.

3.3 RESULTS

3.3.1 Coagulational Stability

The coagulational stability of 19 nm latex particles was strongly affected by the addition of $CaCl_2$. As shown in Figure 3-5, the turbidity of the latex suspensions in the absence of NOM increased when calcium concentrations exceeded 0.001 M, indicating the formation of latex aggregates. In comparison (see Figure 3-6), the presence of 5 mg C/L NOM did not change the calcium concentration above which the aggregation

occurred. However, the increase in the turbidity of the latex suspensions was greater than in the absence of NOM when the calcium concentration was higher than 0.001 M.

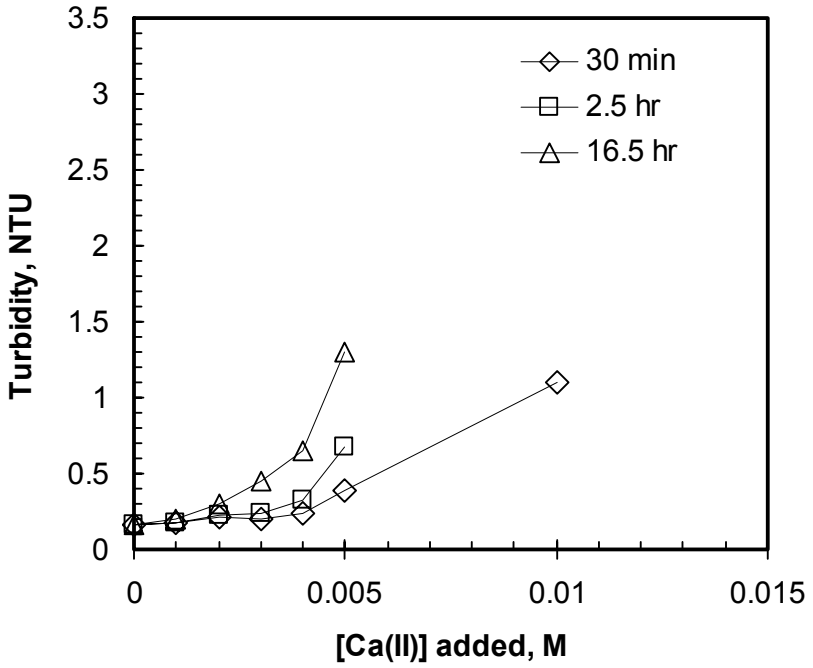

Figure 3-5. Coagulation of 19 nm Latex Particles at Various Ca(II) Concentrations. Model waters contained 20 mg/L of 19 nm polystyrene sulfate latex particles, 0.0001 M $NaHCO_3$, and various concentrations of $CaCl_2$. pH = 6.9 ~ 7.0.

The coagulational stability of 93 nm latex particles was also subject to changes in calcium concentration. Figure 3-7 shows the decrease (less negative) of the electrophoretic mobility (EPM) of 93 nm latex particles with increasing calcium concentration; the presence of NOM resulted in greater decreases in EPM when [Ca(II)] was between 0.005 and 0.030 M. The NOM effect was less extensive when [Ca(II)] was above this range. The particles were still fairly negatively charged (negative EPM) with 0.001 M $CaCl_2$ added, regardless of the presence of NOM. This was consistent with the jar test results with 19 nm latex particles, which was reasonable considering their similar surface properties.

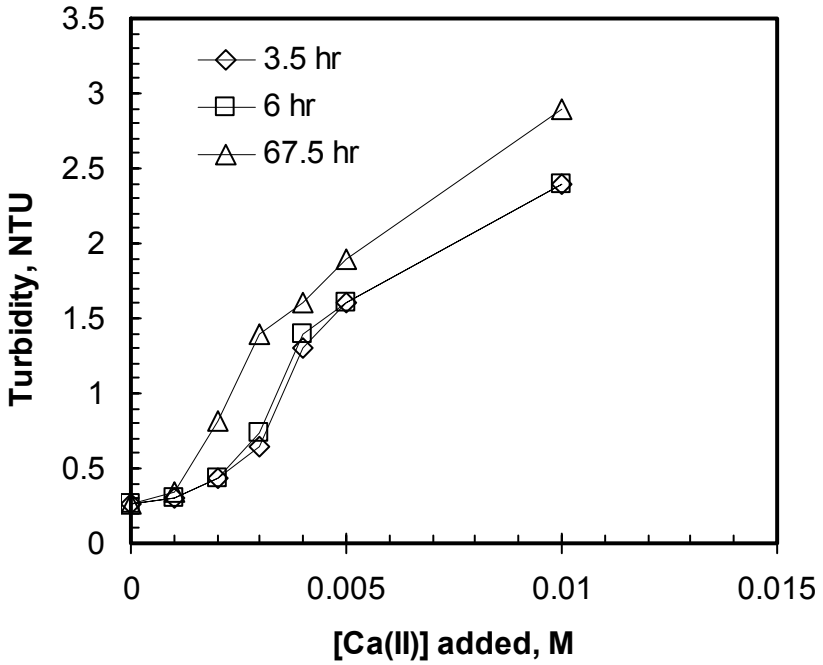

Figure 3-6. Coagulation of 19 nm Latex Particles at Various Ca(II) Concentrations in the Presence of NOM. Model waters contained 20 mg/L of 19 nm polystyrene sulfate latex particles, 5 mg C/L Dismal Swamp water NOM, 0.0001 M $NaHCO_3$, and different concentrationss of $CaCl_2$. pH = 6.9 ~ 7.0.

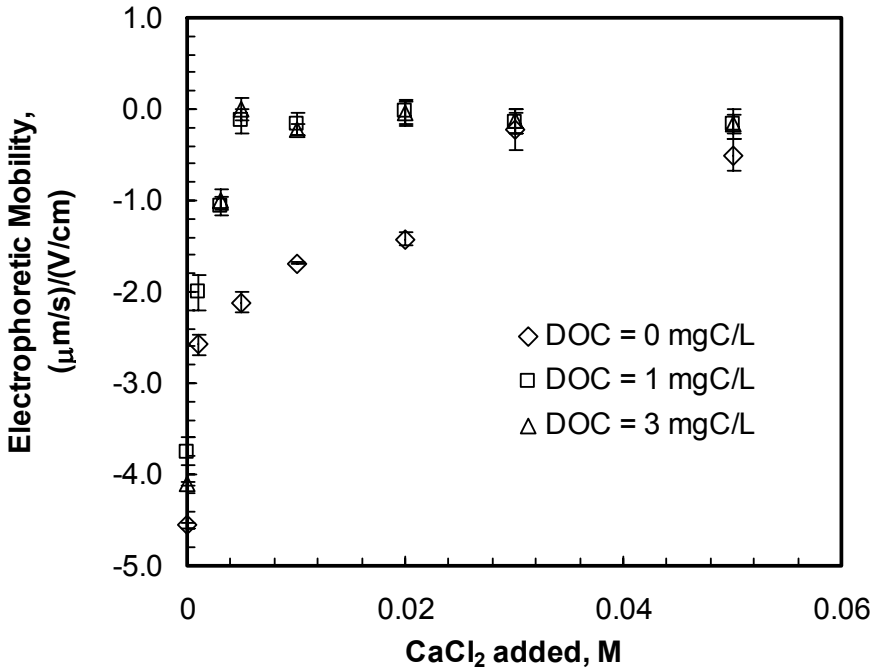

Figure 3-7. Variation of the Electrophoretic Mobility of Latex Particles as a Function of Ca(II) Concentration. Model waters contained 20 mg/L of 93 nm latex particles, 0.0001 M $NaHCO_3$, and NOM and $CaCl_2$ at indicated concentrations. The pH was buffered at 6.9 ~ 7.0 in the absence of NOM, and 6.3 ~ 6.9 in the presence of NOM. Error bars indicate the standard deviations calculated based on 4~5 measurements.

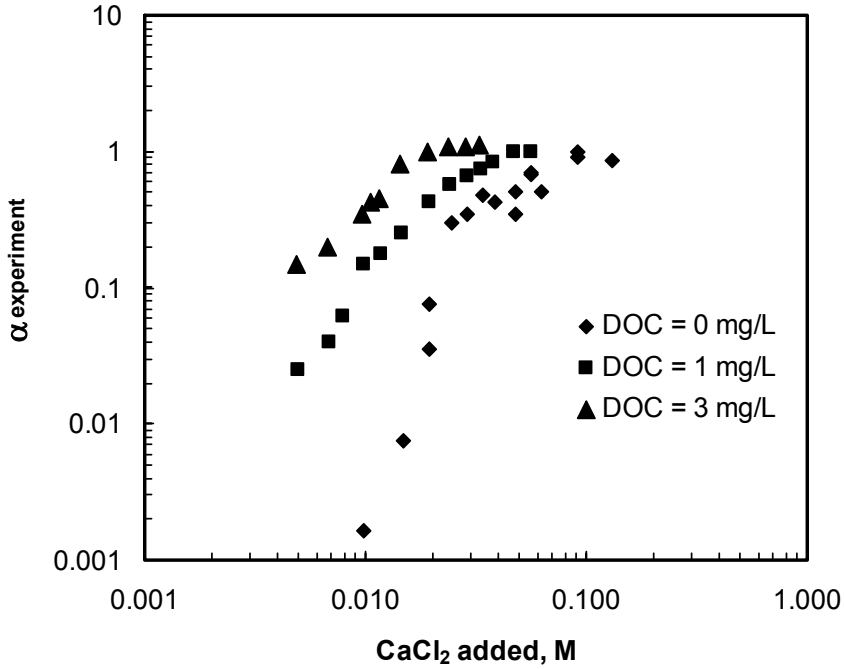

Figure 3-8. Variations of Experimental α Values as a Function of Ca(II) Concentration. The values were determined from the perikinetic flocculation of 93 nm latex particles. pH was not measured, but is expected to be in a range of 6.0 ~ 7.0 based on the results obtained under similar conditions.

The perikinetic flocculation results with 93 nm latex particles are illustrated in Figure 3-8. As seen in the figure, the experimentally determined sticking probability varied dramatically with the addition of $CaCl_2$. In the absence of NOM, α became close to unity when [Ca(II)] was above 0.091 M, approximately 0.002 when [Ca(II)] was 0.010 M, and undetectable when [Ca(II)] was lower than 0.010 M. In contrast, the addition of merely 1 mg C/L of NOM accelerated the coagulation substantially. Even when [Ca(II)] was as low as 0.005 M, α increased to approximately 0.025 from being non-detectable. In fact, the particles became completely destabilized when [Ca(II)] reached 0.05 M (DOC = 1 mg C/L) or 0.02 M (DOC = 3 mg C/L). Overall, the latex particles used in the study were stable with respect to coagulation when [Ca(II)] was not greater than 0.001 M, and became unstable when [Ca(II)] reached 0.010 M, regardless of the presence of NOM.

3.3.2 Depositional Stability

The addition of $CaCl_2$ also impacted the depositional stability of latex particles on PVDF surfaces. Figure 3-9 summarizes relevant experimental results. As seen in the figure, the filtered turbidity of the water samples did not decrease significantly in the absence of calcium, even in the presence of PVDF powders. This suggests that the particles were stable with respect to deposition and therefore were unable to attach to relatively large PVDF powders that can be rejected by the 0.45 μm MF membrane. The addition of 0.001 M $CaCl_2$, in comparison, reduced the depositional stability of latex particles and caused them to attach to PVDF powders. This resulted in a substantial decrease of the filtered turbidity from approximately 34 NTU to 7 NTU. In the meantime, the coagulational stability of latex particles remained unchanged; therefore, the filtered turbidity of the reference latex suspension without PVDF powders was still close to that without calcium.

Furthermore, the coexistence of 1 mg C/L NOM with 0.001 M $CaCl_2$ appeared to stabilize the latex particles with respect to deposition, as the filtered turbidity went back to approximately 22 NTU from the level of 7 NTU observed in the absence of NOM. On the other hand, it was also observed that the filtered turbidity became less than 2 NTU once the concentration of calcium was greater than 0.010 M. This indicates that the latex particles were destabilized at high calcium concentrations. They formed aggregates with sizes larger than the membrane pore size and were consequently rejected by the membrane. Although the hydrodynamic conditions were different, this trend in general agrees with the results obtained in the coagulational stability studies introduced previously.

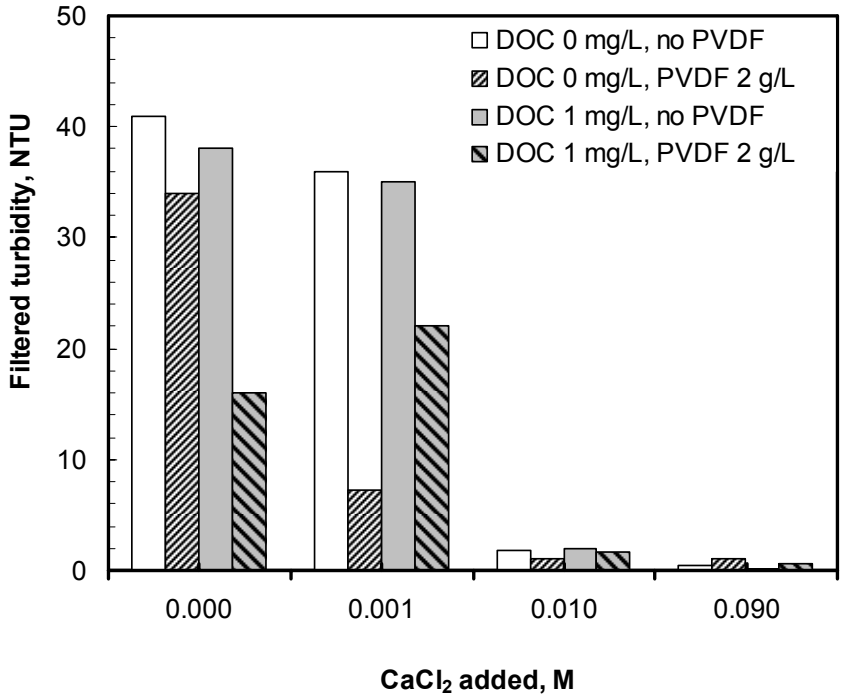

Figure 3-9. Variation of Filtered Turbidity as a Result of Latex Particle Attachment at Different Calcium Concentrations. All model waters contained 20 mg/L of 93 nm polystyrene latex particles and 0.0001 M $NaHCO_3$ as pH buffer. PVDF content, if added, was 2.5 g/L pH was in a range of 6.3 ~ 7.0.

Another effect of NOM noticed in the experiment was the change of the cake structure formed by PVDF powders on the HA membranes. As shown in Figure 3-9, the presence of 1 mg C/L of NOM strengthened the removal of latex particles by the PVDF cake layer on the top of the HA membranes, causing the filtrate turbidity to decrease from 40 NTU to 15 NTU. This effect appeared to be mitigated when $CaCl_2$ was added.

Based on the particle stability studies, model particles with desired physical sizes and physiochemical stabilities were found under corresponding solution chemical conditions (see Table 3-2). Therefore, the fouling of a PVDF membrane by these particles with different stabilities can be assessed individually and then compared to that predicted by the model.

Table 3-2. Various Groups of Colloidal Particles with Different Properties: Theoretical and Experimental Conditions.

Size[1]		Depositional Stability in the Model	Coagulational Stability in the Model	Chemical Conditions in Fouling Experiments[2]
Model	Experimental			
Large	93 nm	Stable	Stable	[Ca(II)] = 0 M
Large	93 nm	Unstable	Stable	[Ca(II)] = 0.001 M
Large	93 nm	Unstable	Unstable	[Ca(II)] = 0.010 M
Small	19 nm	Stable	Stable	[Ca(II)] = 0 M
Small	19 nm	Unstable	Stable	[Ca(II)] = 0.001 M
Small	19 nm	Unstable	Unstable	[Ca(II)] = 0.010 M

Note: [1] The particle was considered large or small based on its relative size to the membrane pore size. [2] Chemical conditions used in fouling experiments were determined independently, and DOC = 0 in all cases.

3.3.3 Membrane Fouling by Large Particles

Based on the results of model simulations, the fouling of MF membranes by particles larger than membrane pore size is predicted to be dominated by two major mechanisms: pore blocking and cake layer formation. For unstable particles, the fouling is the greater when pore blocking dominates and less when cake layer formation is enhanced by the presence of favorable particle-particle attachment. For stable particles, the only possible fouling mechanism is cake layer formation, and the fouling is fully hydraulically reversible.

The experimental results on the fouling of the membrane by 93 nm latex particles are presented in Figure 3-10. In the figure, all three runs showed a slightly faster increase in relative transmembrane pressure (TMP) as the first 10 L/m^2 of raw water was filtered. After that, the relative TMP increased linearly as a function of permeate throughput. According to the model, this indicates that the fouling was preceded with pore blocking and then shifted to cake layer formation as the number density of open pores to be blocked decreased. More importantly, in the absence of $CaCl_2$, the particles were still stable with respect to both coagulation and deposition; under these conditions, the membrane was fouled at the slowest rate and predominantly by cake layer formation

because of the absence of favorable particle-membrane attachment. For the same reason, the fouling that accumulated in the end of the first filtration step was easily removed by the subsequent hydraulic backwash.

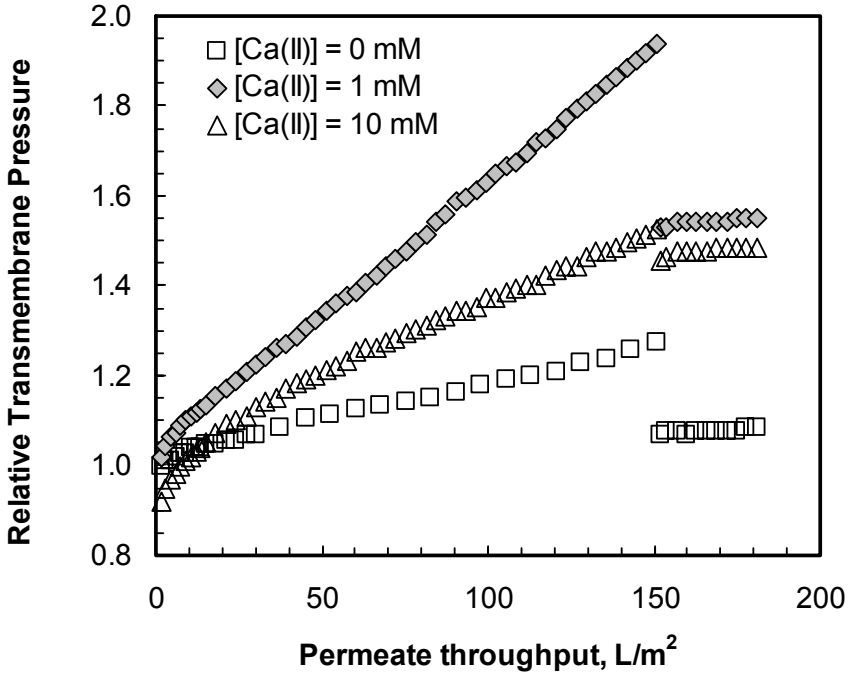

Figure 3-10. Fouling of a PVDF Microfiltration Membrane by 93 nm Latex Suspensions with Different Concentrations of $CaCl_2$. All model waters contained 20 mg/L of 93 nm latex particles, 0.0001 M $NaHCO_3$, and different concentrations of $CaCl_2$ as indicated. Suspension pH was approximately 6.5 to 7.0.

As the calcium concentration was increased to 0.001 M, latex particles were destabilized with respect to deposition. They became more effective in attaching to the membrane surface and blocking membrane pores, thereby fouling the membrane at a rate four times faster than that by the stable particles. In this case, the fouling was found less hydraulically reversible as half of the increase in the relative TMP remained after the backwash. This removable or hydraulically reversible fraction of fouling was contributed by particles being attached to other particles in the cake layer. Since particle-particle attachment was still unfavorable at this calcium concentration as found in the coagulation study, hydraulic backwashing was effective in removing these particles. Once the

calcium concentration increased to 0.010 M, latex particles became unstable with respect to both deposition and coagulation. Consequently, not only particle-membrane, but also particle-particle attachment was favorable. In this case, particles that have already attached to membrane surfaces can behave as individual collectors to capture incoming particles and reduce the amount of particles that can arrive at the membrane surface. As a result, more latex particles were attached to other particles and less can participate in the blocking of membrane pores. This trend observed experimentally is consistent with the model-predicted competitive effects of particle-membrane and particle-particle attachments on membrane fouling. Moreover, the model predicted that the existence of favorable attachments between all related surfaces leads to a fouled layer that was difficult to remove by hydraulic backwash. This was exactly what happened in the corresponding fouling experiment (see Figure 3-10).

The removal of 93 nm latex particles, on the other hand, was found to be independent of the calcium concentration (see Figure 3-11). This was anticipated as the particle size was close to the upper limit of the pore size distribution of the MF membrane. As expected, latex particles can still be removed by size exclusion even in the absence of any favorable physiochemical attachment. Meanwhile, the TMP measured at the beginning of the run with a calcium concentration of 10 mM was approximately 10 percent lower than that measured with ultrapure water. Thus, the starting point for the relative TMP in Figure 3-10 was lower than unity. The reason for this is unclear, but it doesn't affect the general trend observed in the variation of membrane fouling.

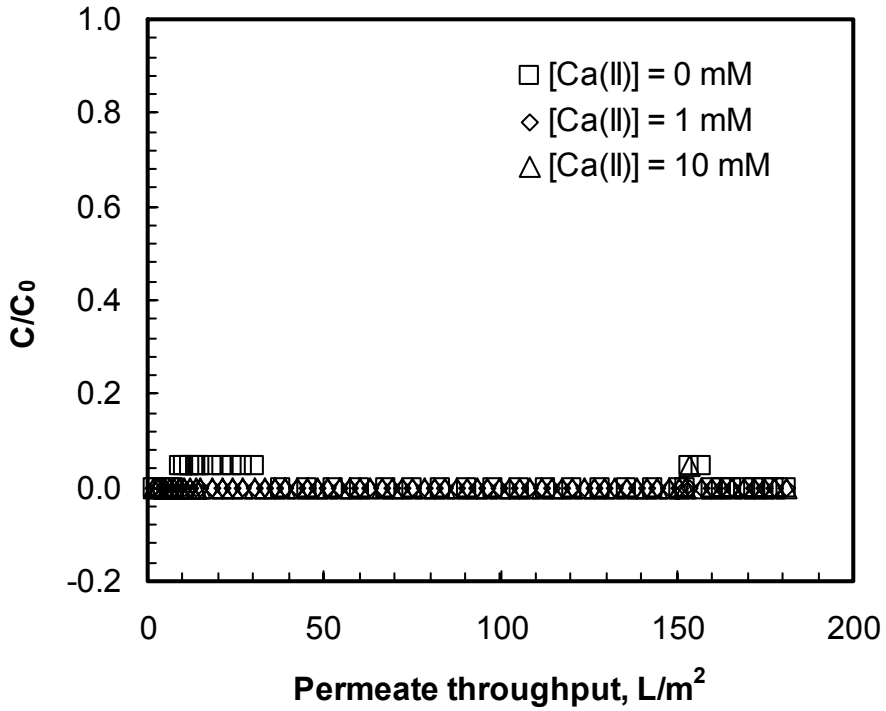

Figure 3-11. Rejection of 93 nm Polystyrene Latex Particles by a PVDF Microfiltration Membrane at Different Calcium Concentrations. Model water chemistry was as described in Figure 3-10.

3.3.4 Membrane Fouling by Small Particles

Based on model simulation, the fouling of the MF membrane by 19 nm latex particles is predicted to be strongly dependent on particle stabilities. For stable particles, fouling is unlikely to happen since small particles can penetrate through membrane pores. For particles unstable in deposition, severe fouling can occur as a result of pore blocking. It is noted that 19 nm latex particles have radius of 9.5 nm, which is a sixth of the average size of the membrane pores (58 nm), just in the lower range of the critical particles sizes predicted by the model. For particles unstable in coagulation, large aggregates will be formed rapidly as discussed in Chapter Two. In this case, the major fouling mechanism is cake layer formation caused by these aggregates. The cake layer is likely to be fairly permeable since latex particles are rigid and hydrophobic and cannot form gel-like layers.

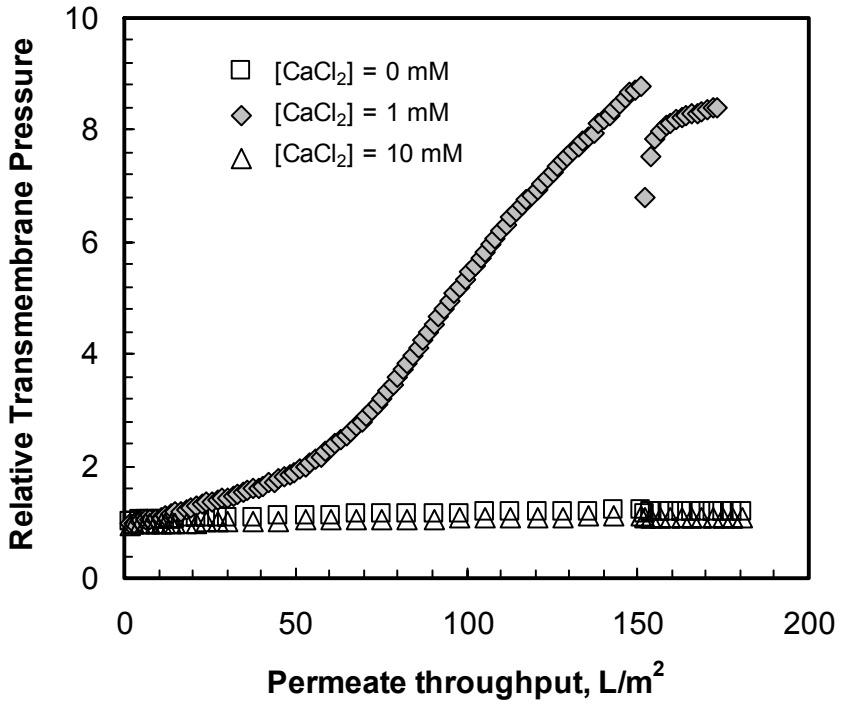

Figure 3-12. Fouling of a PVDF Microfiltration Membrane by 19 nm Polystyrene Latex Particles with Various Concentrations of $CaCl_2$. All model waters contained 20 mg/L of 19 nm latex particles, 0.0001 M $NaHCO_3$, and different concentrations of $CaCl_2$ as indicated. Suspension pH was approximately 6.5 to 7.0

The experimental results agree reasonably well with the model predictions. In the absence of $CaCl_2$, the particles were stable with respect to both coagulation and deposition. Consequently, the majority of the particles (ca. 90 percent) passed through the PVDF membrane since they were smaller than most of the membrane pores (see Figure 3-13). Correspondingly, the fouling developed very slowly (see Figure 3-12). As $CaCl_2$ was added at a concentration of 0.001 M, particles became unstable with respect to deposition, i.e., particle-membrane attachment was favorable. When the first 40 L/m^2 of raw water was filtered, particles in the water attached to the internal surfaces of the membrane, causing internal plugging of the membrane pores. As shown in Figure 3-12, this was observed as a steady increase of the relative TMP in this stage. In the meantime, the particle concentration in the permeate increased as the internal membrane surfaces

available for deposition decreased (remember particle-particle attachment was still unfavorable).

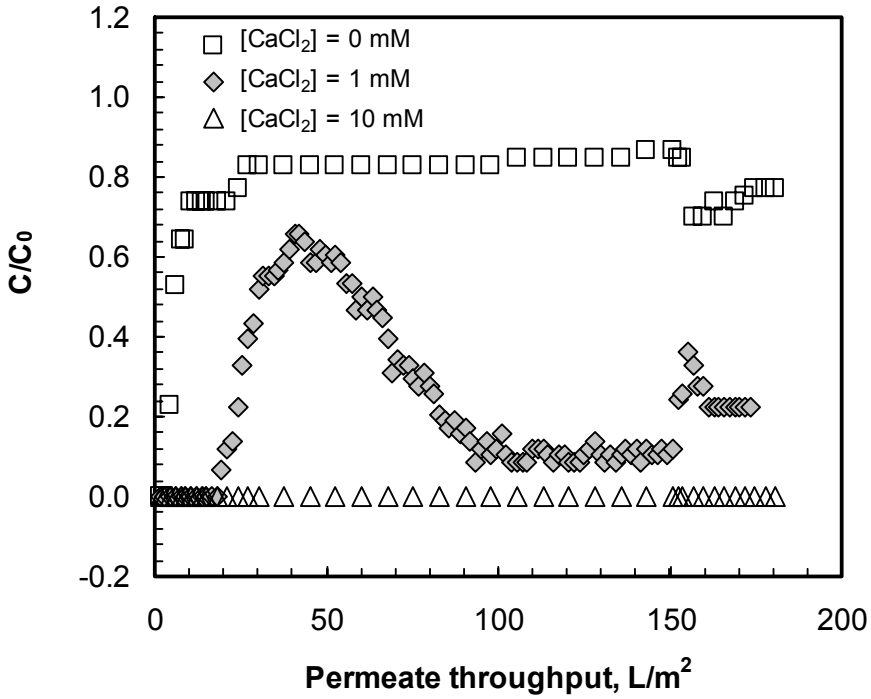

Figure 3-13. Rejection of 19 nm Polystyrene Latex Particles by a PVDF Microfiltration Membrane at Different Calcium Concentrations. Model water chemistry was as described in Figure 3-12

The attachment of small particles on membrane pore walls led to constriction of the membrane pores on the outside membrane surface. Therefore, the fouling shifted from internal pore plugging to surface pore blocking; a rapid increase of the relative TMP occurred in the range of the permeate throughput from approximately 40 to 100 L/m^2 (see Figure 3-12). Simultaneously, the constriction of pores increased the rejection efficiency of the membrane to these small particles. As shown in Figure 3-13, the particle concentration in the permeate decreased from approximately 70 percent to a mere 10 percent. Finally, the formation of cake layers followed the pore blocking stage. The increase of relative TMP began to decrease after a permeate throughput of 100 L/m^2 as

shown in Figure 3-12; the particle concentration in the permeate remained at approximately 10 percent of that in the raw water (see Figure 3-13). Because the attachment between these small particles was unfavorable at this calcium concentration, hydraulic backwashing reduced the fouling somewhat as shown in Figure 3-12. However, most of the fouling was hydraulically irreversible as most particles were in contact with the membrane surfaces, inside or outside, under favorable attachment conditions.

The increase of [$CaCl_2$] to 0.010 M made the small particles unstable with respect to coagulation. Unlike the large 93 nm latex particles, the half time for the perikinetic coagulation of 19 nm latex particles was approximately 120 times shorter than 93 nm latex particles, given the same mass concentration and chemical conditions. As a result, the coagulation of 19 nm latex particles happened almost instantaneously when 0.010 M of $CaCl_2$ was added into the suspension, which is compared to a predicted half time of approximately 4 second, estimated using the perikinetic coagulation equation (assuming a collision efficiency of 0.001). The size of the aggregates was not measured in the study, but was estimated to be at least in 200 μm (the lowest visible size for naked eyes). The subsequent filtration of the aggregate suspension caused little fouling on the PVDF membrane (see Figure 3-12); the particle concentration in the permeate was also consistently zero (see Figure 3-13), indicating a complete rejection of the large flocs by the membrane.

3.3.5 SEM Images of Clean and Fouled Standard PVDF Membranes

The membranes fouled by 19 and 93 nm latex particles at a calcium concentration of 0.001 M were characterized using SEM, together with a clean membrane as a

reference. Figure 3-14 shows the cross-sectional and the outer surface views of the membrane before colloidal fouling. The presence of heterogeneous three dimensional porous structures can be observed in both images. After the filtration of 93 nm latex particles, the outer surface of the membrane was covered by a loose layer of latex as shown in Figure 3-15. Individual particles can be clearly seen in the layer. On the other hand, no penetration of the 93 nm latex particle inside the membrane can be found after the inspection of the cross-section of the membrane, suggesting the predominance of surface fouling (blocking and/or cake formation) in this case. This result was consistent with previous discussions in this chapter and in Chapter 2. In comparison, Figure 3-16 shows the fouling of the same membrane caused by 19 nm latex particles. In addition to the presence of the outside layers, some cluster-like latex particles were also observed in the cross-sectional image, indicating the penetration and deposition of small particles inside the membrane. Further inspection of the entire cross-section of the fouled membrane (images not shown herein) showed that the internal deposition of small particles occurred throughout the entire depth of the membrane except for the very inner layer. The particles found inside the membrane existed either as individual particles or cluster-like structures. It is unclear whether these clusters were formed in the filtration or prior to it. These particles should be responsible for the fouling by pore plugging and constriction described previously.

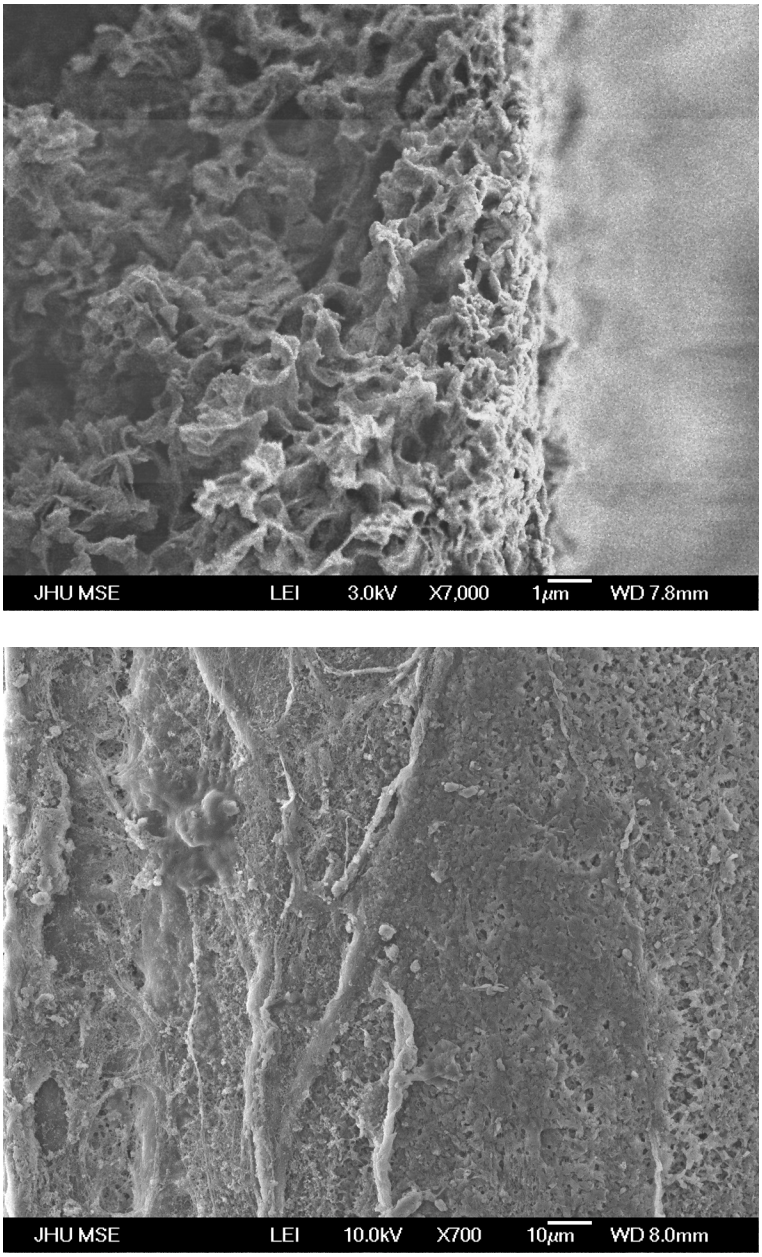

Figure 3-14. Scanning Electron Micrographs of a Clean PVDF Microfiltration Membrane. The upper and the lower images are cross-sectional and outer surface views of the membrane prior to fouling, respectively.

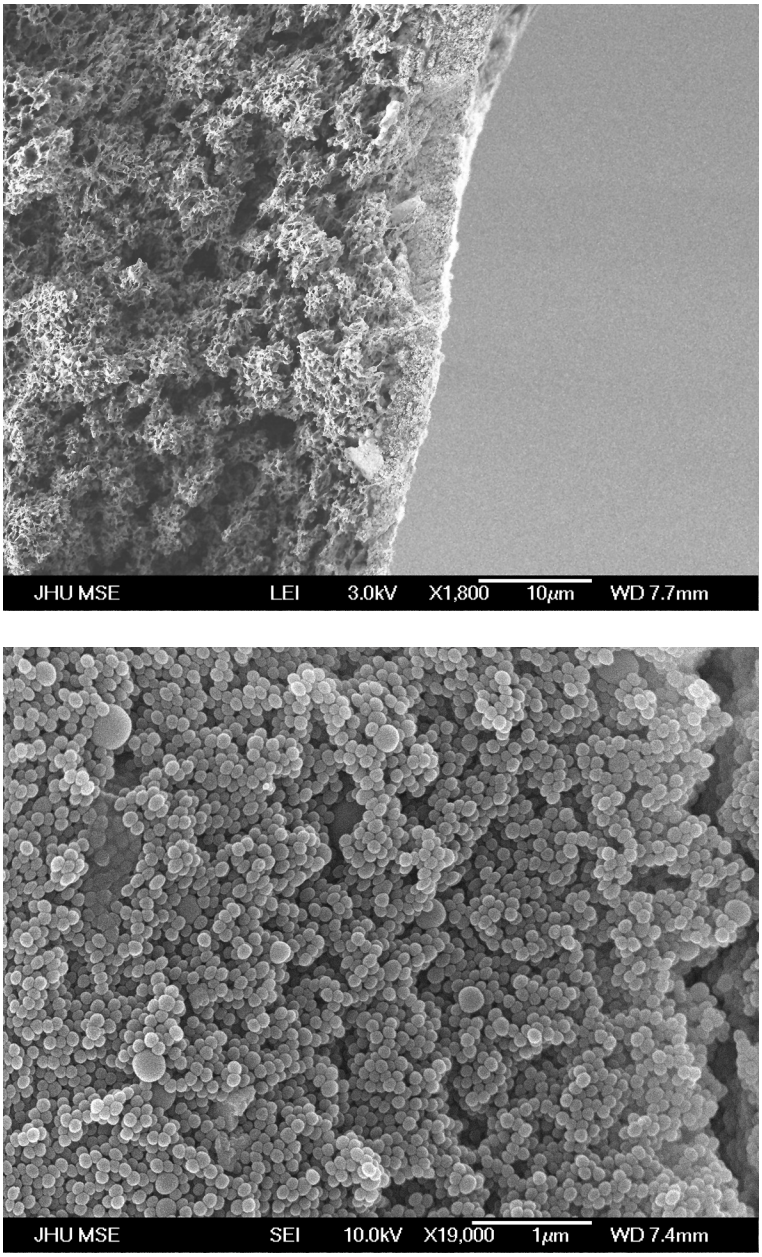

Figure 3-15. Scanning Electron Micrographs of a PVDF Microfiltration Membrane Fouled by 93 nm Latex Particles in the Presence of 0.001 M $CaCl_2$. The upper and lower images are cross-sectional and outer surface views of the membrane, respectively. The layer of spherical latex particles can be seen covering the outer surface of the membrane.

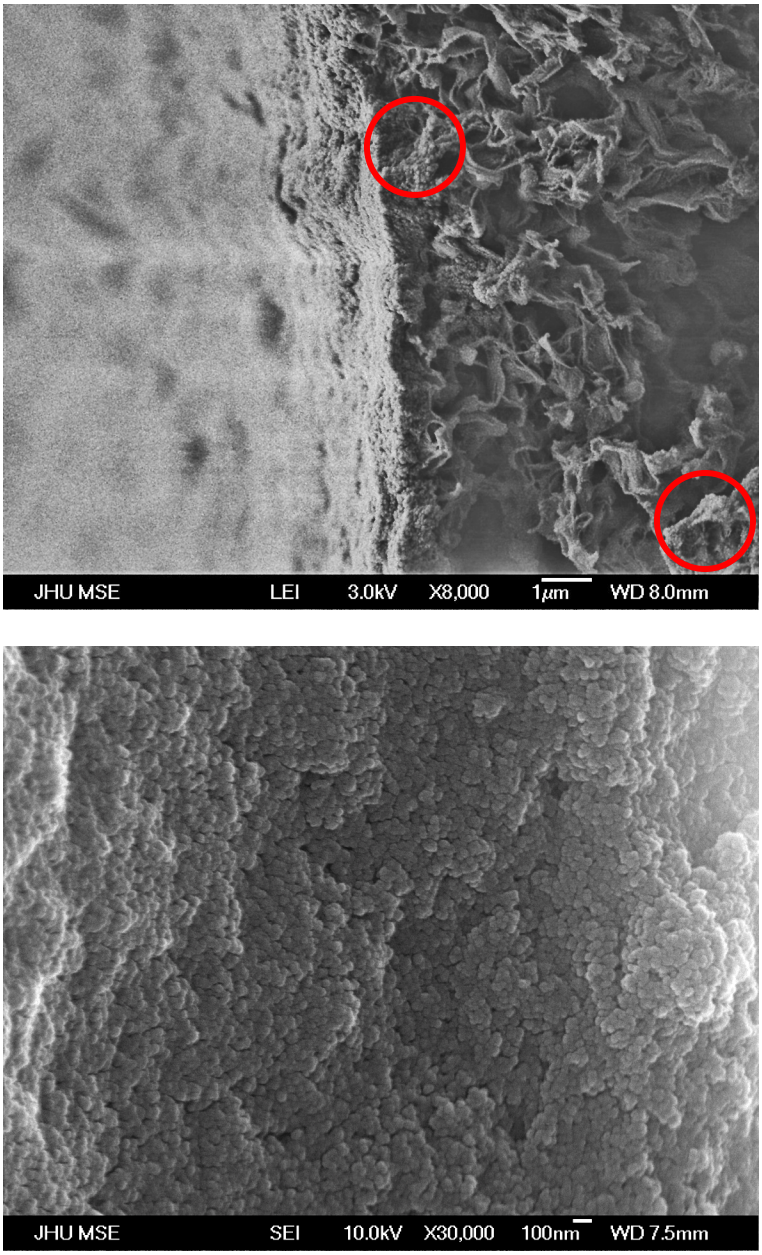

Figure 3-16. Scanning Electron Micrographs of a PVDF Microfiltration Membrane Fouled by 19 nm Latex Particles in the Presence of 0.001 M $CaCl_2$. The cross-sectional image (upper) shows the presence of latex particles on both the outside and the inside surfaces of the membrane (e.g., in the region within the cycle). The surface image (lower) demonstrates a dense layer of latex particles on the outside surface of the membrane.

Another interesting phenomenon observed was the presence of multiple layers of latex particles, mostly in some large (in the order of 10 μm or above) depressed areas on the external surface of the membrane. This happened with both 19 and 93 nm latex

particles although the membranes were hydraulically backwashed prior to SEM imaging. The inefficacy of hydraulic backwashing in removing the particles in contact with other particles in the absence of favorable particle-particle attachment was probably a result of the uneven distribution of the backwashing flow through the commercial MF membrane that has non-homogeneous porous structures. This should not, however, impact the predicted relationship between membrane fouling and particle attachment since the fouling caused by such thin cake layers is unimportant compared to that by pore blocking.

3.3.6 Quantitative Relationship between Rejection and Fouling

The total mass of latex particles that could be rejected in these experiments is equivalent to 5 mg if the rejection efficiency was 100 percent. Table 3-3 summarizes the experimental results of the quantitative relationship between the mass of latex being removed throughout a run and the amount of fouling observed under different chemical conditions. As shown in the table, the severest fouling occurred when the particles were small and unstable with respect to deposition (19 nm, 0.001 M $CaCl_2$) although the mass of particles rejected was less than many other runs. This is consistent with the predicted efficacy of particles with radii of 1/6~1/2 of membrane pore size in membrane fouling. On the other hand, the competition between particle-particle and particle-membrane attachments proposed in the conceptual model was clearly demonstrated for particles with each size. For example, the removal efficiency for the 93 nm latex particles was independent of the chemical conditions due to the physical sieving effect. The resulting total fouling, however, was the worst when only particle-membrane attachment was favorable (Ca(II) = 0.001 M), and decreased when particle-particle attachment was also

favored. As for the hydraulically irreversible fouling, the effects of the physiochemical attachment appeared not only in the extent of fouling, but also the mass of 93 nm particles retained by the membrane after hydraulic backwash. More particles were retained when the physiochemical stabilities of the particles shifted from stable, depositionally unstable, to coagulationally unstable. Similarly trends were observed with 19 nm latex particles in regard to the changes of both total and hydraulically irreversible fouling. The nonlinear correlation between membrane fouling and particle removal (as a result of the coexistence of different types of attachments and fouling mechanisms) is consistent with the model prediction, and different from the simple linear assumption used in other models such as the original Hermia model.

Table 3-3. Latex Rejection and Membrane Fouling under Different Chemical Conditions.

Chemical Conditions	Corresponding Attachment Conditions	Total Fouling		Hydraulically Irreversible Fouling	
		Mass Removed, mg	Relative TMP	Mass Retained, mg	Relative TMP
19 nm, no Ca(II)	low α_{pm} and α_{pp}	0.83	1.21	0.28	1.16
19 nm, 0.001 M Ca(II)	high α_{pm}, low α_{pp}	3.88	8.78	3.54	8.18
19 nm, 0.010 M Ca(II)	high α_{pm} and α_{pp}	4.91	1.11	4.85	1.08
19 nm, 0.001 M Ca(II), 1 mg C/L NOM	low α_{pm} and α_{pp}	1.51	1.83	1.34	1.94
19 nm, 0.001 M Ca(II), modified membrane	low α_{pm} and α_{pp}	4.83	1.78	4.34	1.67
93 nm, no Ca(II)	low α_{pm} and α_{pp}	5.00	1.28	0.83	1.07
93 nm, 0.001 M Ca(II)	high α_{pm}, low α_{pp}	5.00	1.94	2.32	1.53
93 nm, 0.010 M Ca(II)	high α_{pm} and α_{pp}	5.00	1.51	4.95	1.44
93 nm, 0.001 M Ca(II), 1 mg C/L NOM	low α_{pm} and α_{pp}	5.00	2.22	1.76	1.67

It should be reiterated herein that the decrease of fouling when particle-particle attachment was favorable resulted from the fact that the cake layers formed by polystyrene latex particles are relatively permeable. Hydrophilic colloidal materials, such

as alginate, can form less permeable gel-like cakes on membrane surfaces in the presence of favorable inter-molecular interactions. In this case, the "increase-then-decrease" pattern of changes of fouling extent may be replaced with a monotonous increase as the attachment conditions vary.

3.3.7 NOM Effects

Since the presence of NOM can reduce the attachments of latex particles on PVDF surfaces (see Figure 3-9), it was expected that the extent of fouling would change accordingly. This was confirmed with the fouling experimental results presented Table 3-3. As shown in the table, the total mass of 19 nm latex particles removed by the membrane decreased from 3.88 to 1.51 mg during filtration, and the mass retained by the membrane decreased from 3.54 to 1.34 mg after the backwash, when 1 mg C/L of NOM was added in the presence of 0.001 M $CaCl_2$. Both the total and the hydraulically irreversible fouling decreased by more than 75 percent as a result. The extent to which the fouling decreased was more than that of rejection, suggesting the disappearance of the pore constriction effects and their relevance in the fouling by small particles. In contrast, the fouling by large particles (93 nm) was changed less extensively in the presence of NOM, partially because the overall extent of fouling caused by large particles was much less than that by small particles when particle-membrane attachment was favorable. Nevertheless, the amount of large particles remaining on the membranes after backwashing decreased significantly from 2.32 to 1.76 mg in the presence of NOM (see Table 3-3), consistent with the decrease of particle-membrane attachment discussed previously.

3.3.8 Impact of Membrane Properties

To further understand the mechanisms of colloidal fouling, a modified PVDF membrane was also tested with 19 nm latex particles in the presence of 0.001 M $CaCl_2$, the condition under which the severest fouling was observed with the standard PVDF membrane. The permeate flux and the backwashing flux were the same as in the fouling experiments using the standard PVDF membrane. The modified PVDF membranes had a tighter surface pore structure compared to the standard membrane.

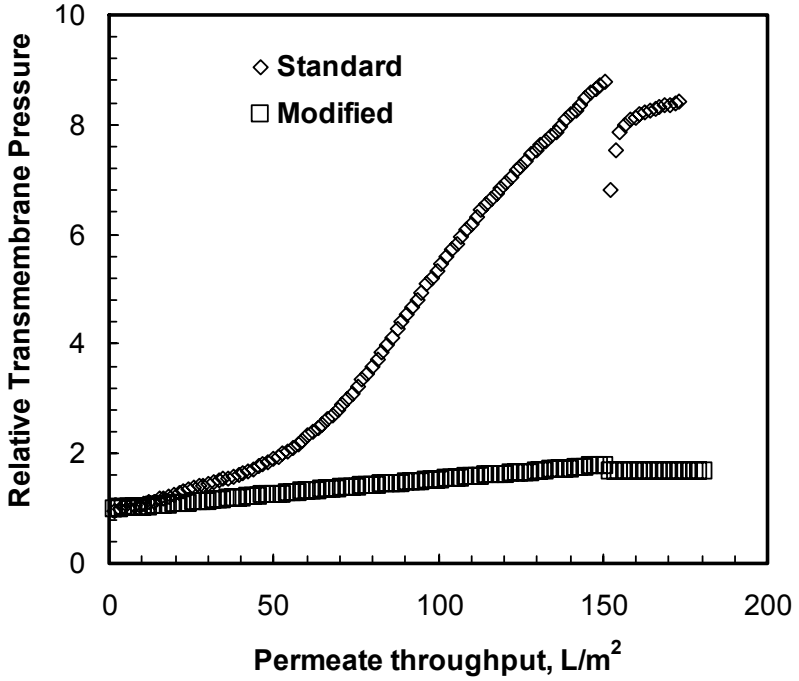

Figure 3-17. Comparison of the fouling of the standard PVDF membrane and a modified PVDF Membrane by 19 nm Latex Particles in the Presence of 0.001 M $CaCl_2$. The model water contained 20 mg/L of 19 nm polystyrene sulfate latex particles, 0.0001 M $NaHCO_3$, and 0.001 M $CaCl_2$. pH = 7.0.

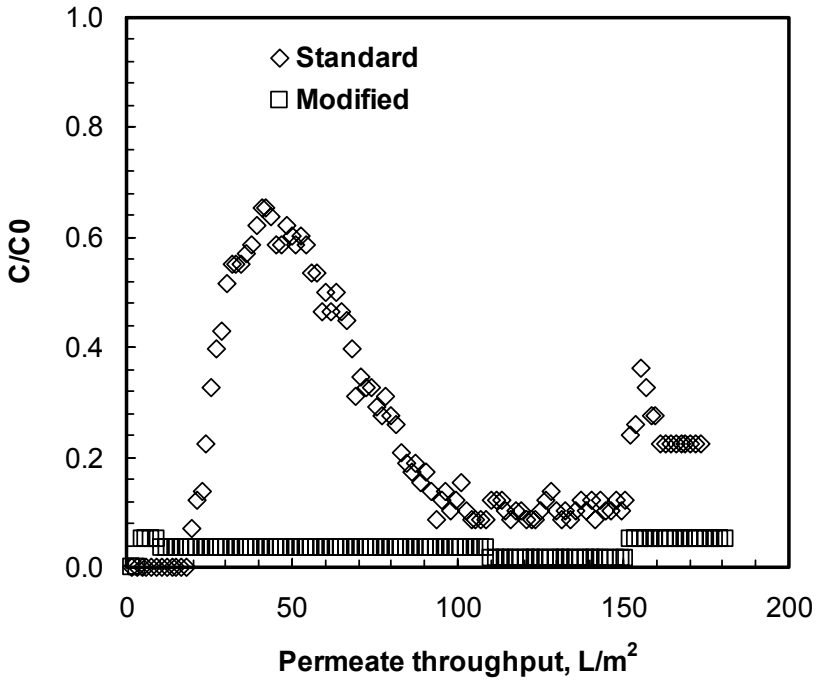

Figure 3-18. Comparison of the Nomalized Concentration of 19 nm Latex Particles in the Permeate after Filtration Using the Modified and the Standard PVDF Membrane. Model waters contained 20 mg/L of 19 nm polystyrene sulfate latex particles, 0.0001 M $NaHCO_3$, and 0.001 M $CaCl_2$.

As shown in Figure 3-17 and Table 3-3, the same particle suspension caused a much slower increase of relative TMP on the modified PVDF membrane, 78 percent versus 878 percent on the standard PVDF membrane at a permeate throughput of 150 L/m^2. Despite some proprietary changes to the chemical composition, the surface pores of the modified membrane are also much smaller and tighter than the standard PVDF membrane as inspected under the SEM. Therefore, the fouling occurred primarily on the outside surface of the membrane as shown in the SEM image (Figure 3-19). This dominance of size exclusion effect also enhanced the removal of 19 nm latex particles by the modified membrane. As shown in Figure 3-18, complete removal of the particles was observed throughout the filtration run, unlike that with the standard membrane.

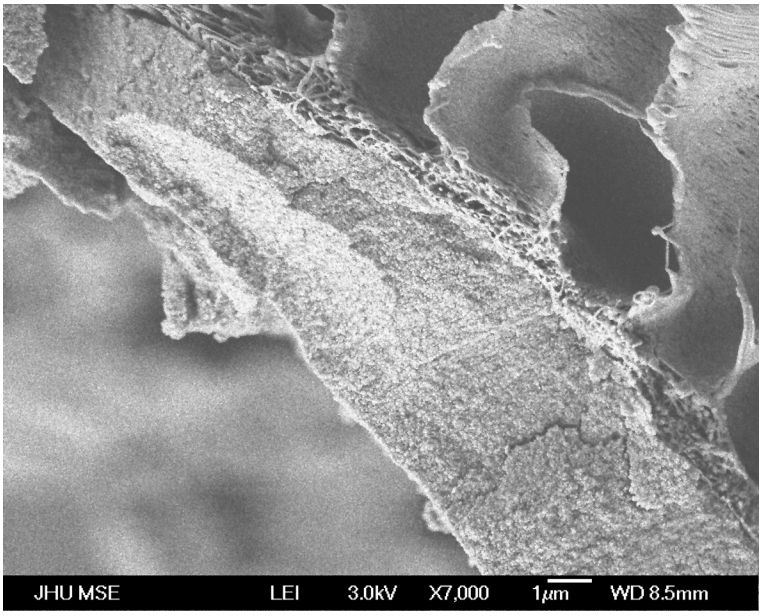

Figure 3-19. Scanning Electron Micrograph of a Modified PVDF Membrane Fouled by 19 nm Latex Particles in the Presence of 0.001 M $CaCl_2$. A layer of latex particles was seen outside the tight membrane surface layer (in the middle), and the support layer of the membrane with macroscopic pores was also shown on the upper right part of the image.

An interesting question can be raised immediately in this regard. Was the observed decrease in membrane fouling primarily a result of the decrease in membrane pore size or by a decrease in particle-membrane attachment. This question is difficult to answer without detailed information on the modified membrane. However, it is speculated that the decrease in membrane pore size played a role in the reduction of membrane fouling. In other words, the 19 nm latex particles now became "large" particles relative to the pore size of the modified membrane, and behaved in a way similar to the 93 nm latex particles in the fouling of the standard membrane that has an average pore diameter of 58 nm.

3.4 CONCLUSION

The motive of the study was to test the relationships between physiochemical stabilities of colloidal particles and membrane fouling predicted by the model developed in Chapter 2. This model was tested experimentally in two sequential steps: determination of particle stabilities and fouling tests, using polystyrene sulfate latex particles and a standard PVDF MF membrane. The effects of particle size were tested by choosing particles with sizes smaller and larger than the average pore size of the membrane. Although theoretical predication of the "stickness" of colloidal particles is difficult as a result of poor understanding of its nature, the experimentally observed relationship between the extent of fouling and the variation of coagulational and depositional attachments did match qualitatively what was expected theoretically. Meanwhile, calcium ions were found to be a suitable chemical in controlling the depositional and coagulational stabilities of the latex particles.

The results clearly demonstrated the distinctive presence of coagulational and depositional attachments in MF fouling processes. It was found that the extent of colloidal fouling and its hydraulic reversibility were primarily dependent on what types of particle attachments dominated under given conditions. The fouling was the severest when the depositional attachment was dominant, and decreased when the coagulational (particle-particle) attachment became important. In comparison, the relative size of the particles to membrane pores played secondary but important roles in the fouling process. Overall, the fouling by particles with radius of a sixth of membrane pore size and sticky to the membrane surface was the most problematic in all conditions investigated. This is consistent with the model prediction. The implication of this finding in the fouling of MF

membranes by different components of a natural organic matter (NOM) will be elucidated in next chapter.

Additionally, the presence of aquatic natural organic matter strongly reduced the attachment of latex particles on the PVDF surfaces tested, which was coincident with a significant decrease of the extent of fouling caused by small particles. The NOM effect was less extensive for large particles because the impact of depositional attachment became less significant as a result of reduced collision probability between particles and the bare membrane surface. A similar decrease in fouling occurred when the particle-membrane attachment was minimized by replacing the MF membrane with a modified membrane that has smaller surface pores. In this case, small 19 nm latex particles were rejected completely on the surface of the membrane and no longer caused internal fouling of the membrane. The extent of fouling decreased by four fold as a result.

Different from other studies reported, such as [41], [72] and [73], the chemical attachment coefficients were qualitatively assessed in this study, rather than being used as purely fitting parameters, or somewhat "arbitrary" application of surface interaction calculations. Thus, the correlation between MF membrane fouling and chemical attachment found a realistic foundation. However, quantitative assessment of chemical attachments in membrane filtration is still difficult to real systems. This is shown in the NOM fouling study discussed next.

Chapter Four

MODEL APPLICATION TO NOM FOULING

4.1 INTRODUCTION

The model developed in Chapter 2 has been validated using monodisperse polystyrene latex particles in Chapter 3. The relative importance of particle size and physiochemical stabilities/attachments in colloidal fouling of a MF membrane was manifested experimentally. In this chapter, the applicability of the model to NOM fouling is investigated using experimental data.

4.2 MATERIALS AND METHODS

4.2.1 Major Properties of the Model NOM

The source of NOM, Dismal Swamp water, was taken from the Great Dismal Swamp, Southern Virginia, USA, in November 2001. It was transported to The Johns Hopkins University and stored in an environmental chamber at low temperature and in a dark environment after being saturated with purified nitrogen gas. The water sample was filtered through a binder-free glass fiber filter (Whatman GF/C) with a pore size rating of 1.2 μm prior to use. The prefiltered water has a NOM concentration of approximately 100 mg C/L as dissolved organic carbon (DOC). The specific UV absorbance (SUVA) is approximately 4.5, which is in the typical range for pedogenic NOM. An XAD resin fractionation of the water was conducted by the University of Colorado at Boulder (UC), which found that the water is comprised primarily of hydrophobic NOM fractions (64.3 percent). It also consists of 21.0 percent of a transphilic fraction and 14.7 percent of a

hydrophilic fraction. A fluorescence spectrometry analysis of the NOM sample further found that the NOM in the water has a spectrum (see Figure 4-1) close to humic substances [74].

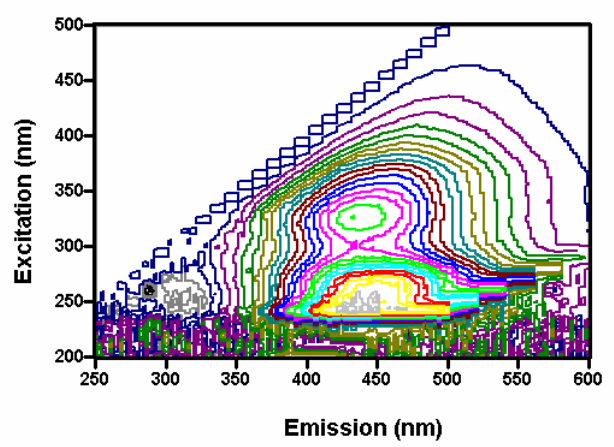

Figure 4-1. Excitation emission fluorescence spectrum of Dismal Swamp water NOM. The peak region appeared in the range of 300 – 350 nm (excitation) and 420 – 460 nm (emission), typical for humic substances. *Courtesy of Lee and Amy*.

A pyrolysis GC/MS analysis conducted at the University of Poitier revealed the dominant presence of hydroxyl and aromatic structures in Dismal Swamp water NOM (DSW NOM). The hydroxyl moieties can be present either as phenol groups or part of carboxyl groups. These functional groups make NOM negatively charged in a broad pH range. An acid-base titration of undiluted Dismal Swamp water conducted by Spinette [75] confirmed the presence of negative charges on this NOM sample (see Figure 4-2), consistent with the previous findings of Dempsey and O'Melia [15].

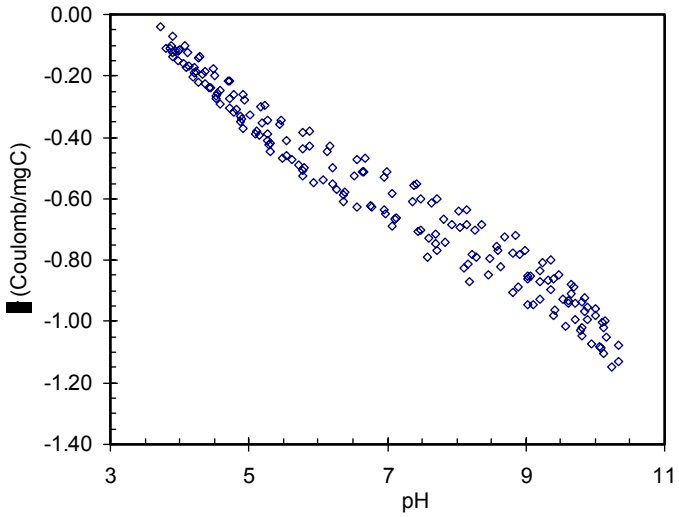

Figure 4-2. Acid base titration of Dismal Swamp water NOM. The water contained 100 mg C/L DOC, 1.4×10^{-4} M Ca(II), and 0.01 M NaCl. The scattered data were obtained in several rounds of titration and back titration using the same water sample. *Courtesy of Rodrigue Spinette*.

With the presence of these ionizable functional groups on DSW NOM, both the intramolecular and intermolecular electrostatic interactions of NOM can be altered by varying solution chemical conditions, e.g., solution pH, ionic strength, or calcium concentration. In a preliminary study using an atomic force microscope (AFM), Gorham and Fairbrother [76] investigated the morphology of DSW NOM that was deposited on the smooth surface of graphite at different pHs. As shown in Figure 4-3, it was found that the NOM deposit is packed in a denser layer at a pH of 3.7 than at 6.1, indicative of weaker repulsions between NOM molecules at the low pH. The presence of the functional groups may affect the reactions of DSW NOM with cations in the aqueous phase as well. For instance, Shin *et al.* [77] studied the coagulation of DSW NOM by alum, and found that the alum demand has a pronounced stoichiometric relationship with NOM concentration.

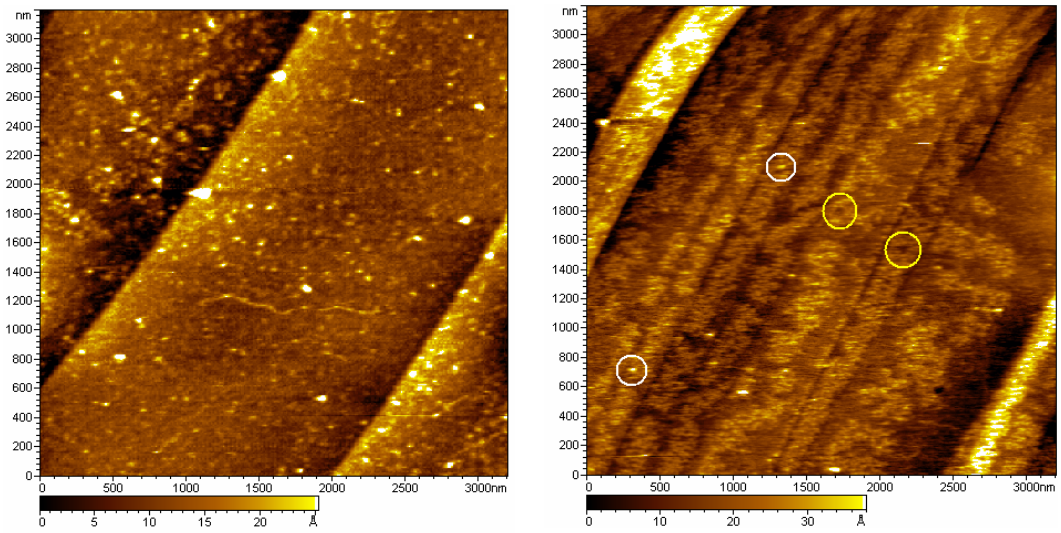

Figure 4-3. Atomic force microscopic (AFM) imaging of Dismal Swamp water NOM deposit on graphite surface at pHs of 6.1 (left) and 3.7 (right). The scale bars represent the height of the points from the base. The lighter color dots indicate the presence of NOM deposits on graphite. The cycles on the right figure highlight the presence of "peaks" and "holes" on the NOM aggregates. *Courtesy of Gorham and Fairbrother.*

In order to apply the mathematical model presented in Chapter 2 to NOM fouling, not only the "stickiness", but also the size of DSW NOM entities has to be estimated. The latter is more difficult for NOM than for synthetic colloidal particles. Previous studies have found that aquatic NOM, including pedogenic NOM from other sources, are usually fairly polydisperse, and the presence of large species with molecular weights above 10 kD is often observed [78, 79]. Similar techniques have also been applied to the characterization of DSW NOM during this study. As shown in Figure 4-4, size exclusion chromatography (SEC) conducted at the University of Colorado demonstrated that most DSW organics (after being prefiltered by 0.2 μm nylon membranes) have a molecular weight of approximately 3 kD compared to a series of polyethylene glycol (PEG, a uncharged polymer) standards. Meanwhile, another minor peak appeared at a molecular weight of approximately 30 kD. This peak was only detected by the DOC detector, not by the UV detector, indicating the lack of chromophores on the NOM structures. The

presence and the fate of this peak needs to be checked in future studies because the importance of different NOM fractions on fouling has been noticed in other studies [26, 70, 78].

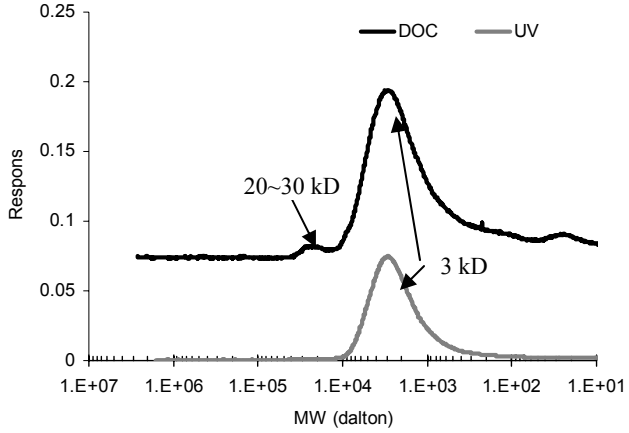

Figure 4-4. SEC chromatograph of Dismal Swamp water NOM. The responses of the instrument for DOC and UV are plotted as functions of equivalent MW of PEGs. The water sample contained 4.89 mg C/L Dismal Swamp water NOM, 1 mM NaCl, and 0.1 mM $NaHCO_3$. The pH and ionic strength were controlled at 7 and 0.0011, respectively. *Courtesy of Lee and Amy* (unpublished data).

Since it is the hydrodynamic radii of NOM species (not their molecular weights) that determine their physical exclusions by a membrane, a conversion can be approximated using a simple empirical equation [80]:

$$\overline{r_h} \text{ (in nm)} \approx \overline{M}^{1/2} \text{ (in kD)}$$

where $\overline{r_h}$ and $\overline{M}$ are the average hydrodynamic radius and molecular weight of PEG particles. Thus, the equivalent hydrodynamic radii of the 20~30 kD and 2~3 kD peaks are approximately 5 and 1.6 nm, respectively.

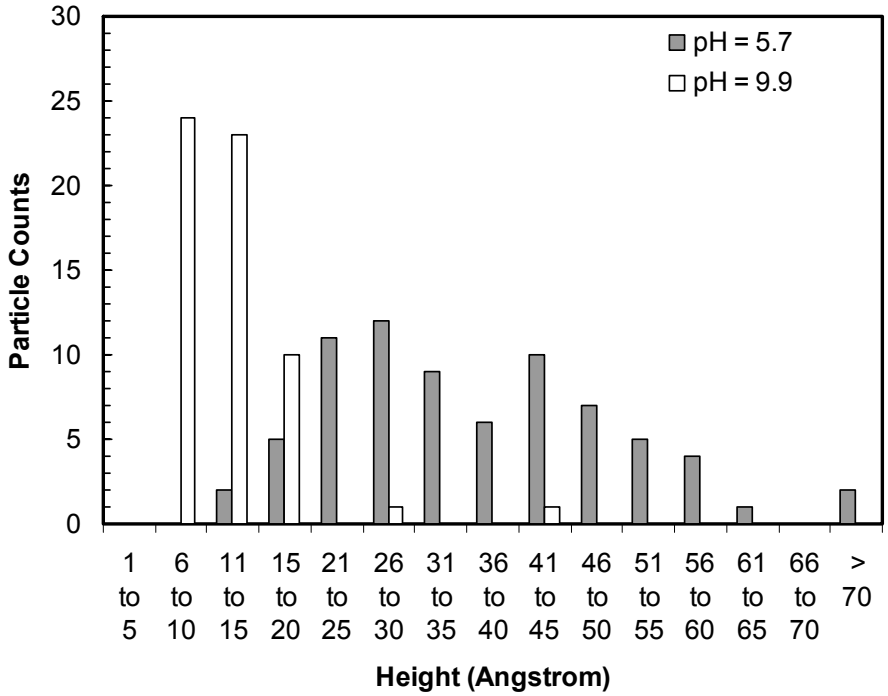

Figure 4-5. Comparison of number of particles with different sizes/heights within an area of 100 nm ×100 nm (pH = 9.9) or 50 nm × 100 nm (pH = 5.7) at two pHs, measured using an atomic force microscope. Water samples were prepared by adjusting the pH of prefiltered Dismal Swamp water using NaOH solution. Ionic strength of the water was not controlled. *Courtesy of Gorham and Fairbrother*

Additional information on the size of DSW NOM was also obtained by analyzing the AFM images of NOM entities at the interface of PVDF and aqueous solutions. The advantage of the AFM technique is the possibility of in-situ measurement of NOM sizes at solid/water interfaces although only NOM "particles" that are sorbed at the solid/water interfaces can be imaged. Figure 4-5 illustrates the results of "particle" counts within different height ranges based on images obtained at different solution pH as shown in Figure 4-2. Interestingly, it is demonstrated that the size of NOM entities increased with decreasing pHs. This trend appeared to differ from the expectation that the size of negatively charged polyelectrolytes should decrease with decreasing pHs as a result of diminishing intramolecular electrostatic repulsion. However, this general rule describes

the variation of polyelectrolyte conformation in the bulk aqueous phase, rather than at solid/water interfaces. The conformation and configuration of negatively charged NOM entities should be more complicated at interfaces, as pointed out in other studies [19, 81]. Rigorous consideration of this problem is beyond the scope of the study. Overall, the AFM images suggest that DSW NOM consists of a particular fraction whose sizes (or heights), or those of their agglomerates, are variable in a broad range from below 1 nm to above 7 nm depending on solution chemistry.

4.2.2 Model Water Composition

Model waters used in the study consisted of 5 mg C/L DSW NOM and other electrolytes. Three boundary conditions were investigated separately: low ionic strength, moderate ionic strength and/or calcium concentration, and high calcium concentration. For low and moderate ionic strengths, the effects of solution pH were also studied. The details of model water compositions are presented in Table 4-1.

Table 4-1. Raw water compositions and characteristics used in the fouling study

Run No.	DOC, mg C/L	pH	Ionic Strength[1]	$[CaCl_2]$ added, M	$[NaHCO_3]$, M
1	5	8.2	0.0001 (NaOH)	0	0
2	5	7.5	0.00001 (Na_2CO_3)	0	0
3	5	4.0	0.003 (HCl)	0	0
4	5	7.0	0.003 (NaCl)	0	0.0001
5	5	11.0	0.003 (NaOH)	0	0
6	5	7.0	0.003 ($CaCl_2$)	0.001	0
7	5	7.0	0.03 ($CaCl_2$)	0.01	0
8[2]	5	6.9	0.0001 ($NaHCO_3$)	0	0.0001
9[2]	5	7.0	0.003 (NaCl)	0	0.0001

Note: [1] the chemicals in the parenthesis were added in each run to reach the desired ionic strength as presented in the table. [2] Runs 8 and 9 were two runs in sequence, i.e., the permeate from Run 8 was used as the raw water for Run 9 after adjusting the solution chemistry.

4.2.3 NOM Adsorption on Surrogate PVDF Surfaces

Similar to the latex particles, adsorption of DSW NOM entities on the surrogate PVDF powders was conducted using the approach presented in Chapter 3. The variation of UV_{254} absorbance was measured using a UV-Vis spectrophotometer (Shimadzu UV-160) as an indicator of NOM adsorption.

4.2.4 NOM Aggregation/Precipitation

The aggregation/precipitation of NOM induced by $CaCl_2$ was studied using the standard jar test procedures as described in Chapter 3. Different volumes of 1 M $CaCl_2$ stock solution were added into each jar to obtain the desired calcium concentration. The increase of turbidity in each jar was measured after a series of time durations using a bench-top turbidimeter (Hach, 2100A).

4.2.5 Membrane Filtration Setup and Protocol

Membrane fouling experiments were conducted using the same filtration apparatus used in colloidal fouling study. The same operating protocol was followed. Both total and hydraulically irreversible foulings were determined from each run. An exception was Run 8, in which extended filtration was performed without intermittent hydraulic backwash. The purpose was to collect sufficient permeate samples to be used as the raw water for Run 9. The ionic strength of the permeate was adjusted to 0.003 by adding 1 M NaCl stock solution and equilibrating overnight before Run 9.

4.2.6 Environmental Scanning Electron Microscopy (E-SEM)

The field emission scanning electron microscopy (FESEM) employed in the colloidal fouling study was performed under high vacuum (less than 10^{-6} torr) and with dry samples, which is inappropriate for the characterization of organic foulants in a hydrated condition [82]. Therefore, an environmental SEM (FEI Quanta FEG 200) was used to characterize the NOM entities accumulated on membrane internal and external surfaces when NOM fouling occurred. This instrument is equipped with a water-cooled Peltier stage that allows the imaging to be performed constantly at low temperatures. The principles of E-SEM have been reported elsewhere [83].

The fouled membrane samples were prepared in-situ about 10 minutes prior to the imaging. Then, the fibers were taken out of the feedwater column and cut into approximately 5 mm long pieces immediately for the imaging of membrane external surfaces using a stainless steel razor blade. Meanwhile, the membrane samples for cross-sectional imaging were obtained by carefully cutting the fiber at a location next to the open end of the membrane module. The cutting location had been partially glued with epoxy glue during module fabrication in order to minimize the collapse of membrane fibers in cutting. An example of the cross-sectional cut is shown in Figure 4-6.

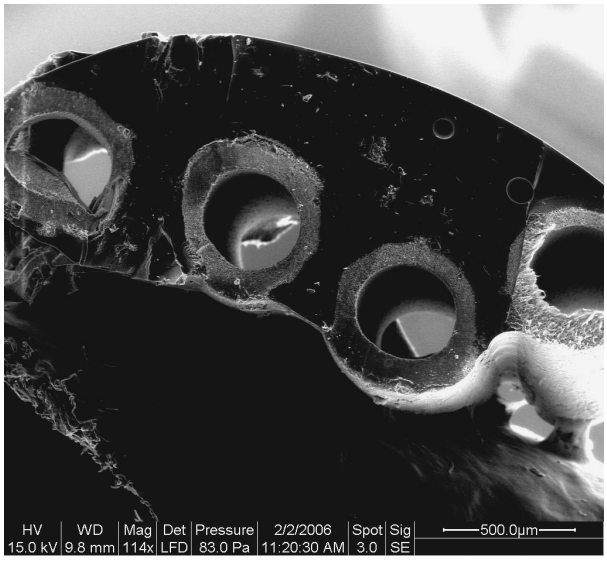

Figure 4-6. An environmental SEM image of the cross-sectional areas of membrane fibers attached on the microscopic stage. The membrane fibers show gray color, while the stage and the epoxy glue used in membrane potting show black.

The prepared membrane samples were carefully placed on the Peltier stage right after cutting with the surface to be imaged facing up. It was found that double-sided conductive glue tapes should not be used in this case, unlike the FESEM used in the colloidal fouling study. Small droplets of deionized water were added around the fibers to help to maintain the moisture of the samples. Next, the imaging was performed at 5 °C and pressures of around 1 torr (or 133 Pa). Since the saturated vapor pressure for water is 872 Pa at this temperature, the relative humidity in the microscope chamber was approximately 15 percent. This meant that water in the solid sample would vaporize under such an operating condition. Experimentally, the impact was partially overcome by adding extra water surrounding the sample and shortening the imaging time. The exact operating pressure was varied slightly during the imaging in order to optimize the imaging quality as indicated in individual images. However, it was found that the maximum magnification could not exceed approximately 30,000 regardless of the

adjustments; the image became difficult to interpret above this level. This limits the minimum size of particles to be observed to approximately 20 nm.

4.3 RESULTS

4.3.1 NOM Adsorption on PVDF Surfaces

The adsorption of DSW NOM on PVDF powders was found dependent on calcium concentration and solution pH as shown in Figure 4-7. In the absence of $CaCl_2$, the addition of PVDF powders from 0 to 25 g/L only caused the normalized UV_{254} to vary in a narrow range of 0.94 to 0.99. This suggested that the adsorption of NOM on PVDF is minor if the solution pH is neutral. However, if $CaCl_2$ was added into the system at a concentration of merely 1 mM, the adsorption of NOM on PVDF became substantial as the normalized UV_{254} decreased gradually from 0.94 to 0.73 with increasing PVDF concentration. Once 3 mM $CaCl_2$ was added into the system, the normalized UV_{254} of the filtrates further decreased to a minimum of 0.69, slightly lower than that with 1 mM $CaCl_2$. More dramatic decrease was observed at a pH of 4 and in the absence of $CaCl_2$. In this case, the normalized UV_{254} decreased from 0.83 to 0.59 as the PVDF concentration increased from 0 to 25 g/L.

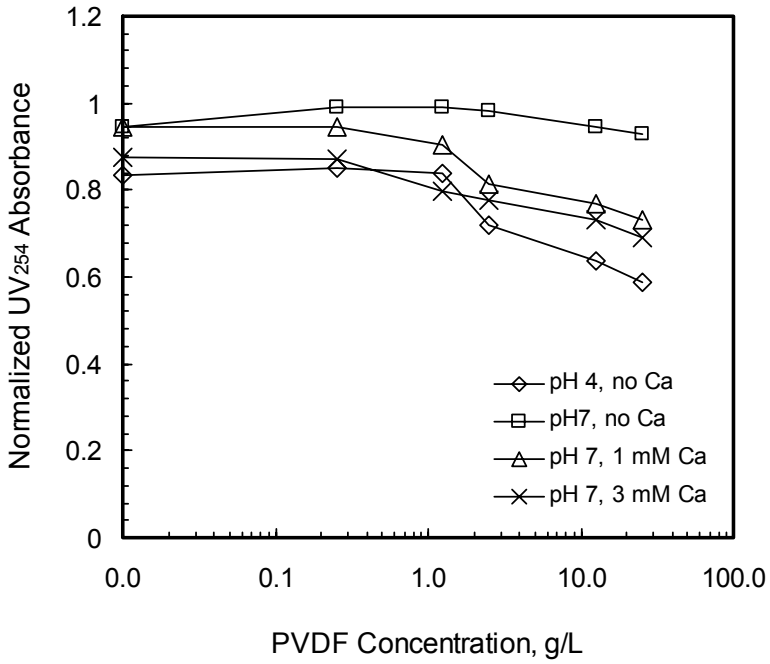

Figure 4-7. Variations of solution UV_{254} absorbance with increasing PVDF dose under various chemical conditions.

The decrease of UV_{254} determined in the adsorption experiment was likely to be a combination of aggregation/filtration (with the 0.45 μm HA membranes) and adsorption, rather than adsorption alone. This was manifested by the variation of the normalized UV_{254} absorbance at the PVDF concentration of zero, which was a measure of the aggregation/filtration effect. According to the data shown in Figure 4-7, the aggregation/filtration effect was significant at a pH of 4 and at a pH of 7 in the presence of 3 mM $CaCl_2$. In comparison, this effect was less extensive at a pH of 7 with 0 and 1 mM $CaCl_2$. This observed calcium dependence was similar to the adsorption of polystyrene latex particles on PVDF powders discussed in Chapter 3. For both types of adsorption experiments, the attachment/adsorption of aquatic materials to PVDF always appeared to occur at calcium concentrations lower than that for "particle-particle" aggregation.

Because PVDF powders are hydrophobic and immiscible with water, a substantial amount of dry powder existed at the end of adsorption experiment when PVDF doses were greater than 1 g/L. Therefore, it is meaningless to calculate the uptake of organic materials per unit mass of powder added into the solution and fit the results to theoretical adsorption isotherms.

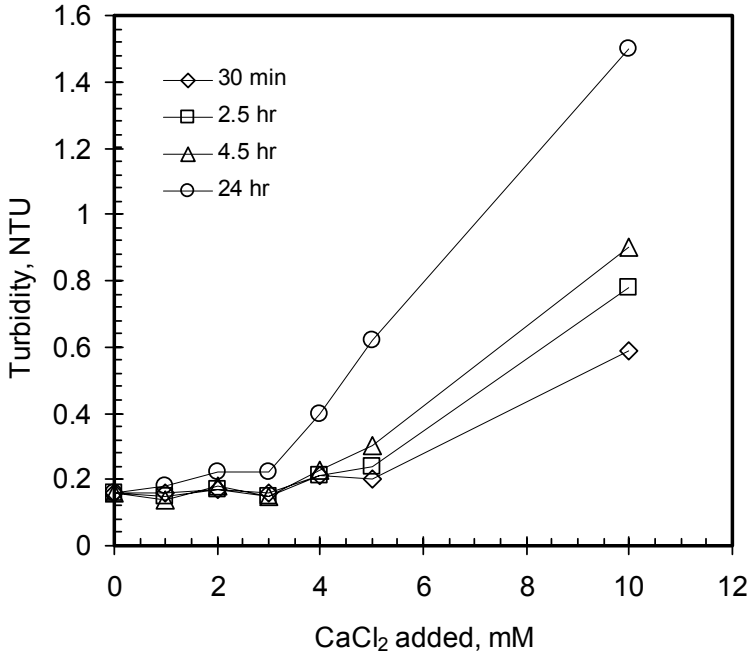

Figure 4-8. Variations of turbidity as a function of $CaCl_2$ concentration and aggregation time. The raw water contained 5 mg/L DSW NOM and 0.0001 M $NaHCO_3$; solution pH was approximately 6.2~6.9.

4.3.2 NOM Aggregation/Precipitation

The jar test results manifested the dependence of NOM aggregation on calcium concentration. The increase of NOM solution turbidity was observed with increasing $CaCl_2$ concentration as shown in Figure 4-8. When the $CaCl_2$ concentration was not greater than 0.003 M, the increase in turbidity was insignificant even after 24 hours reaction. Above this concentration, the increase in turbidity became dramatic and was

greater as more $CaCl_2$ was added or the reaction time was longer. The maximum increase in turbidity (from approximately 0.15 to 1.5 NTU) occurred when 0.01 M $CaCl_2$ was added and the reaction time reached 24 hours. Overall, the "critical" concentration of $CaCl_2$ for the aggregation/precipitation of DSW NOM existed in a range of 0.003 to 0.004 M, which was consistent with the results obtained in the adsorption experiment as depicted previously. Consequently, calcium concentrations of 0.001 and 0.01 M were chosen as two representative conditions in the NOM fouling experiments as elucidated later. The impact of calcium ions on the stability of NOM fractions suggests the possible reduction of intermolecular/inter-particle electrostatic repulsive interactions as a result of the reaction between calcium and NOM.

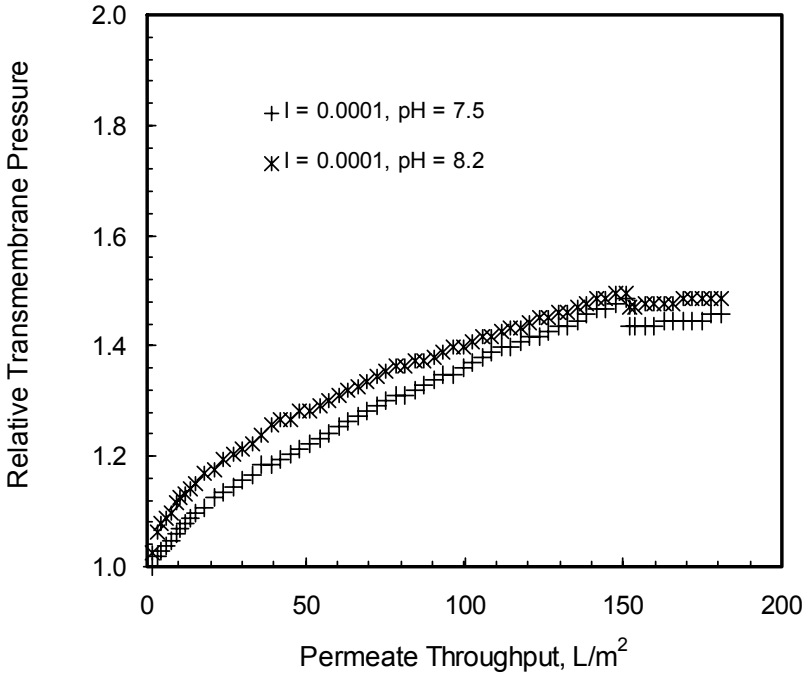

Figure 4-9. Increase of the relative transmembrane pressure as a function of permeate throughput at low ionic strength.

4.3.3 NOM Fouling at Low Ionic Strength

Membrane fouling by DSW NOM was observed at low ionic strength and without the addition of $CaCl_2$. As shown in Figure 4-9, the fouling began with a rapid increase of the relative transmembrane pressure (TMP) in the first 20 L/m^2 throughput, and then gradually decelerated. After 50 L/m^2, the increase of relative TMP became almost linearly proportional to the increasing permeate throughput. The TMP increased by a total of 0.50 in the end of the first filtration step (150 L/m^2). Immediately after the hydraulic backwash, the TMP decreased slightly to 1.47, suggesting that the majority of the fouling was hydraulically irreversible.

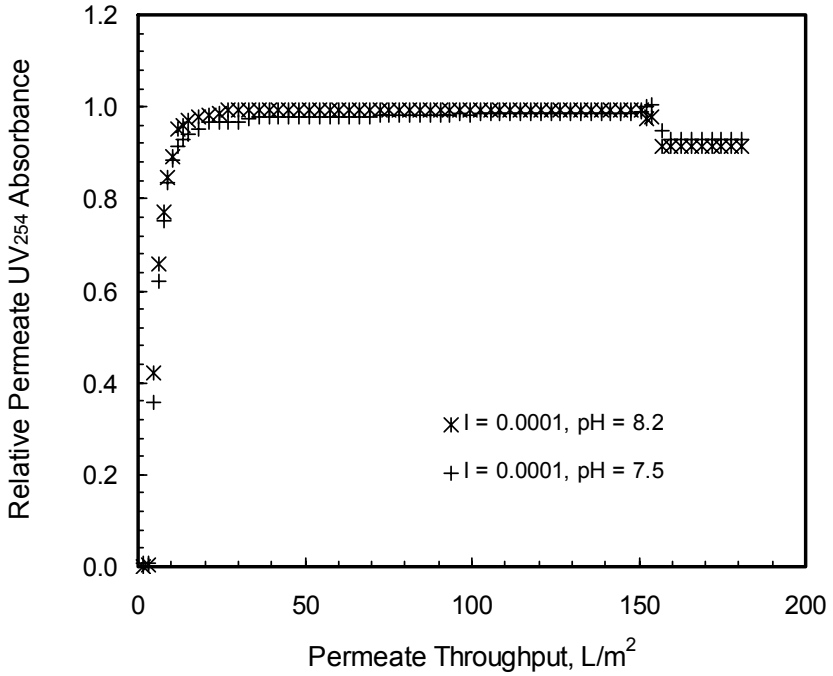

Figure 4-10. Variations of the relative permeate UV_{254} absorbance as a function of permeate throughput under low ionic strength conditions.

The relative permeate UV_{254} absorbance showed an interesting trend as illustrated in Figure 4-10. The values of relative permeate UV_{254} absorbance increased rapidly in the first 13 L/m^2 and then reached approximately unity in 20 L/m^2. There was no apparent decrease of UV_{254} absorbance after that although membrane fouling continued as shown in Figure 4-9. This indicated that the fouling under this particular condition, especially after the first 20 minutes, was not caused by aquatic materials that are major contributors of UV_{254} absorbance.

4.3.4 NOM Fouling at Moderate Ionic Strength

A series of experiments was conducted at an ionic strength of 0.003 with varying pHs and calcium concentrations. The fouling results are presented in Figure 4-11. As shown in the figure, the greatest fouling happened at a pH of 4, in which the normalized TMP increased by 70 percent. Intermediate fouling were observed in runs conducted at a pH of 7, both with and without calcium. The least fouling occurred at a pH of 11.2. A closer look of the fouling curves, however, reveals that the fouling that occurred at pHs of 4 and 7 had different profiles. Membrane fouling proceeded at a fairly stable rate throughout the first filtration step at a pH of 4, while at pH 7 it experienced a faster increase at the first 20 L/m^2 and then slowed down to a stable but lower rate after 50 L/m^2. The latter was comparable to the fouling observed at lower ionic strength as introduced previously. Similar comparison can be made between the two runs conducted with and without calcium and at the same pH of 7. A steady increase of TMP was found throughout the first filtration step in the presence of 0.001 M calcium, which was in contrast to the run without calcium. Finally, the run conducted at a pH of 11.2 also

showed a faster increase of TMP at the beginning and a switch to a slower but steady increase afterwards.

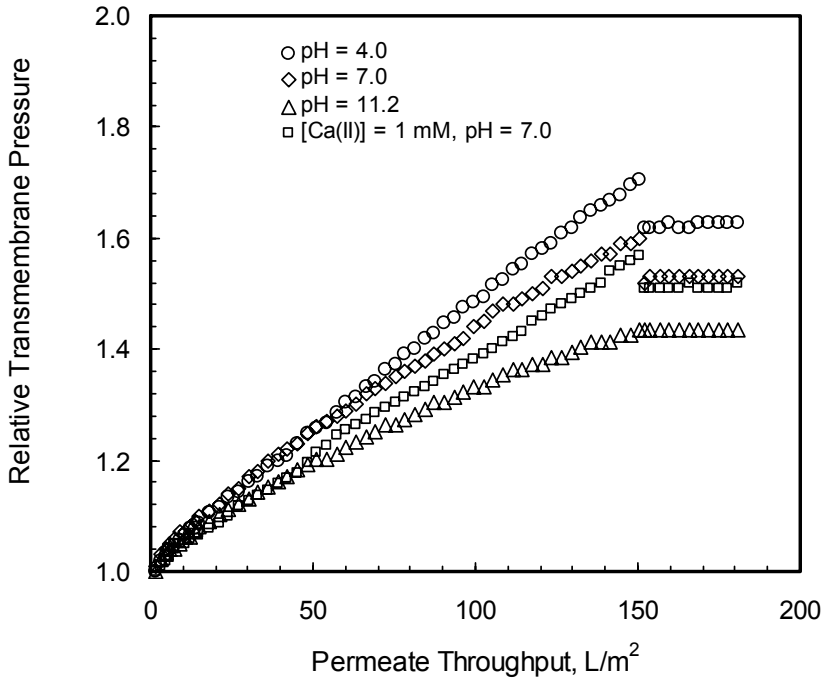

Figure 4-11. Increase of relative transmembrane pressure as a function of permeate throughput under moderate ionic strength conditions (I = 0.003).

The decrease of the permeate UV_{254} absorbance under corresponding conditions followed individual patterns as shown in Figure 4-12. At a pH of 11.2, the relative permeate UV_{254} absorbance increased rapidly to approximately 0.91 within the first 13 L/m^2, which was similar to what was observed at the low ionic strength (see Figure 4-10). However, it remained at 0.94 to 0.96 thereafter, rather than unity as observed in the latter case. This result indicates that a small amount of contributors to UV_{254} absorbance in the feedwater NOM were removed continuously throughout the first filtration step. The rejection of this fraction was to a certain extent enhanced as pH decreased or 0.001 M $CaCl_2$ was added. The difference was insignificant when the feedwater pH decreased

from 11.2 to 7.0 although the relative UV_{254} absorbance at pH 7.0 increased slightly more from 0.88 after the first 13 L/m^2 to 0.99 in the end of the first filtration step.

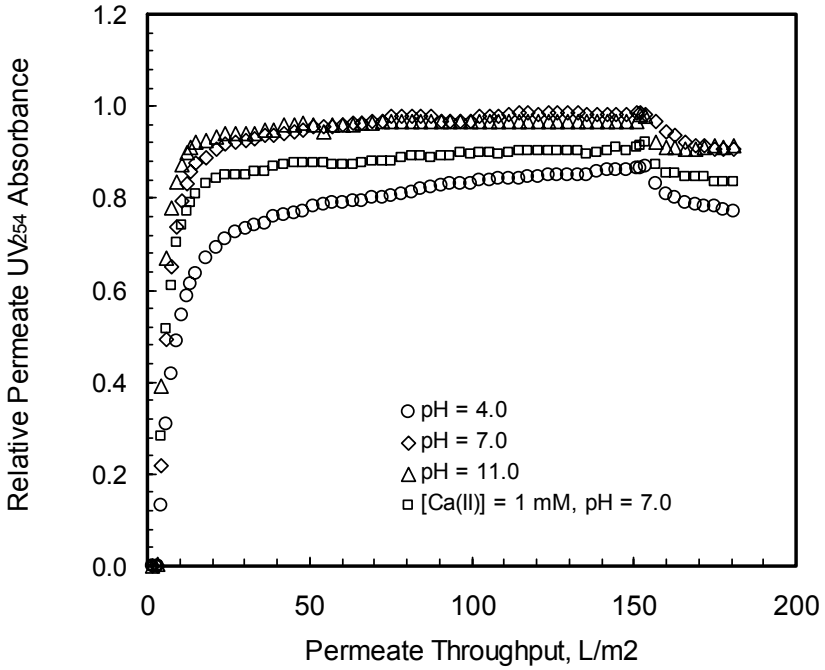

Figure 4-12. Variations of the relative permeate UV_{254} absorbance as a function of permeate throughput under moderate ionic strength conditions (I = 0.003).

Once the feedwater pH decreased to 4.0, the relative UV_{254} absorbance was consistently lower than other pHs, and kept increasing from 0.61 at 13 L/m^2 to 0.87 at the end. In comparison, the presence of 0.001 M $CaCl_2$ had distinctive but less extensive impacts on the decrease of the permeate UV_{254} absorbance. In this case, the permeate UV_{254} absorbance varied from relative values of 0.79 at 13 L/m^2 to 0.91 at the end. Overall, the greater decrease of the permeate UV_{254} absorbance at lower pH or in the presence of low concentration of calcium agreed with the results obtained in the independent adsorption experiments (see Figure 4-7), suggesting that adsorption may be the dominant mechanism for the rejection of UV_{254}-related organic materials.

The hydraulic reversibility of fouling at the moderate ionic strength was consistently greater than that observed at low ionic strength except for pH 11.2 as shown in Figure 4-11. More than 10 percent of the increase in relative TMP was reduced after hydraulic backwash in these cases. On the other hand, the fouling became completely irreversible at a pH of 11.2. The general trend in the increasing of fouling reversibility at moderate ionic strength was coincident with the increase in the retention of UV_{254} absorbance. It is speculated that the enhanced adsorption of fulvic acids can reduce the attachment of some NOM moieties to the membrane surface and make the fouling more reversible.

4.3.5 NOM Fouling at High Calcium Concentration

The addition of 0.01 M $CaCl_2$ into feedwater caused the aggregation of some organic materials in DSW as found in the jar tests (see Figure 4-8). The formation of new organic particles with suitable size resulted in an increase of fouling as shown in Figure 4-13 compared to that at low calcium concentration. These particles were also destabilized with respect to both coagulation and deposition (or adsorption), thereby causing hydraulically irreversible fouling. At a calcium concentration of 0.01 M, the relative permeate UV_{254} absorbance increased to approximately 0.77, and then stabilized in a range of 0.77 to 0.79. In contrast, at a calcium concentration of 0.001 M, the value increased rapidly to approximately 0.85 within the first 20 L/m^2 of permeate throughput, and then continued to increase slowly to 0.92 at 150 L/m^2. Overall, more UV_{254}-related NOM was removed by the membrane at the calcium concentration of 0.01 M.

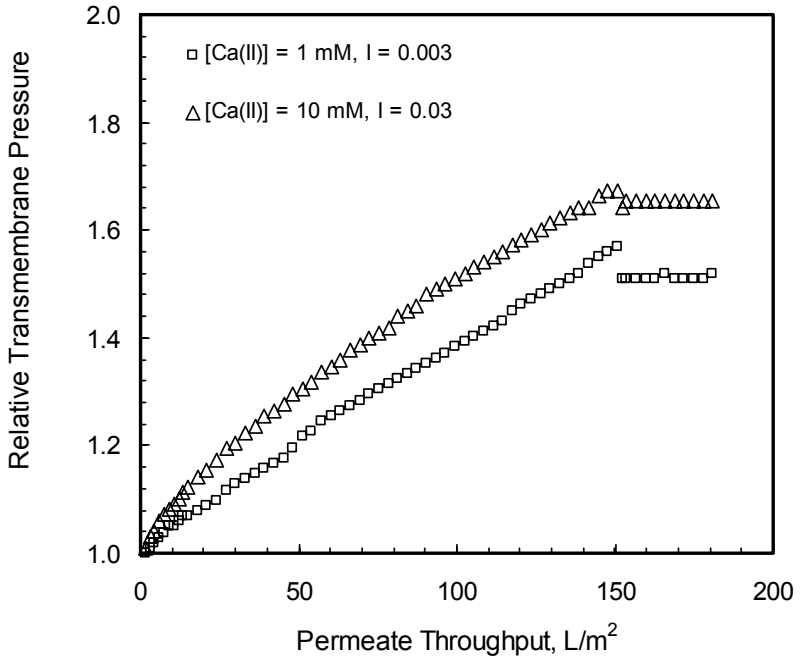

Figure 4-13. Increase of the relative transmembrane pressure as a function of permeate throughput at low and high calcium concentrations. pH = 7.0.

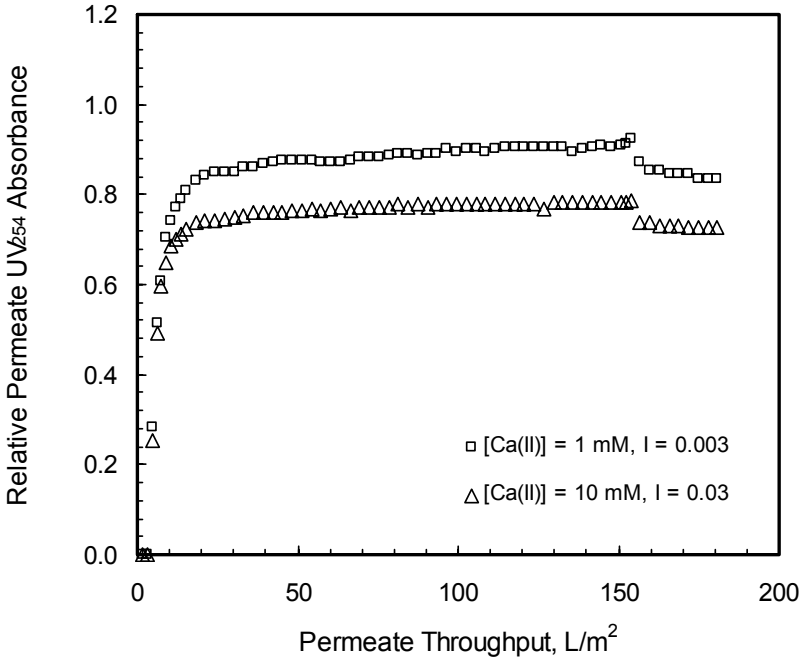

Figure 4-14. Variations of the relative permeate UV_{254} absorbance as a function of permeate throughput at low and high calcium concentrations. pH = 7.0.

4.3.6 Permeate Filtration and Fouling

The subsequent fouling of membranes by the permeate after hydraulic cleaning was explored by conducting another filtration step subsequent to the first one using the same membrane (Runs 1-7), and by performing separate runs in sequence under different chemical conditions (i.e., Runs 8 and 9).

As shown in previous figures, subsequent filtration of the permeate using the same membrane did not cause further increase in TMP, regardless of the chemical conditions used. This result was very important because it suggests that: 1) the removal of fouling materials should be almost complete when the feedwater was filtered in the first time; and 2) it was this/these particular fraction(s) of NOM that caused the fouling. According to Yuan and Zydney [84], the variations of solution chemistry determined occurrence of NOM aggregation, thereby altering the size distribution of aquatic NOM. This affected the amount of NOM that can be removed by different MF membranes used in their study and the extent of total fouling in consequence.

In contrast to the observation made in Runs 1-7, additional fouling was observed in Run 9 using the permeate collected in Run 8 after increasing its ionic strength to 0.003; as shown in Figure 4-15. This was coincident with the additional removal of UV_{254} as presented in Figure 4-16. This result suggests that the increase in ionic strength further destabilized some NOM moieties in the permeate of Run 8, which became effective foulants to the PVDF membrane in Run 9.

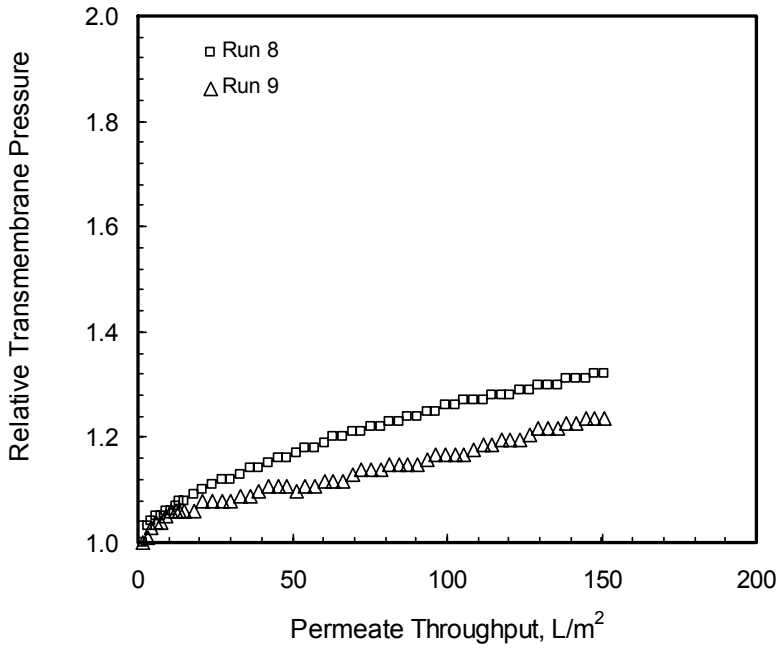

Figure 4-15. Increase of the relative transmembrane pressure as a function of permeate throughput at increasing ionic strengths. The feedwater for Run 9 was the permeate collected from Run 8, and NaCl was then added to a desired ionic strength of 0.003. Feedwater pHs were controlled at approximately 6.9~7.0.

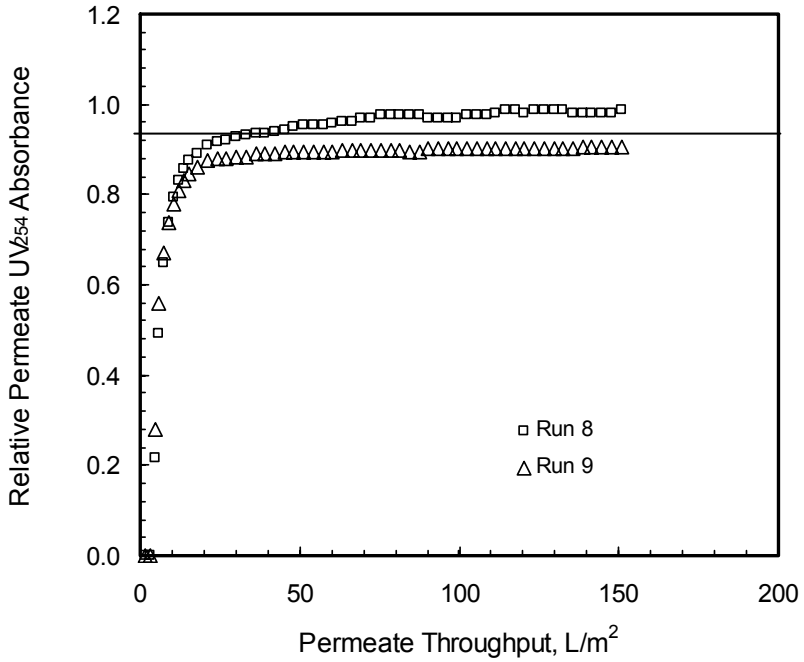

Figure 4-16. Variations of the relative permeate UV_{254} absorbance as a function of permeate throughput at increasing ionic strengths. The feedwater for Run 9 was the permeate collected from Run 8 and had an initial UV_{254} absorbance of 0.93 relative to that of the Run 8 feedwater as indicated by the horizontal line. Feedwater pHs were controlled at 6.9~7.0.

4.3.7 Environmental SEM Images

Environmental SEM provided direct observation of the fouled membranes under two extreme conditions, i.e., low ionic strength and no calcium versus high calcium concentrations. Figure 4-17 shows the overview of a membrane fouled by DSW NOM at an ionic strength of approximately 0.0001 and neutral pH. The 3-D porous structure of the membrane was maintained although the relative TMP increased by 43 percent. Meanwhile, some cloud-like fluffy materials were observed in some valleys on the membrane surface (the white areas shown in Figure 4-17). A closer look of this area reveals the presence of not only the cloudy materials, but also some fine particles (see Figure 4-18). Cross-sectional images of the membrane appeared to be similar to that observed in the fouling by the 19 nm latex particles. As shown in Figure 4-19, some fine particles were observed throughout the internal surface of the membrane. The mean size of these fine particles was measured as 80 ± 41 nm. Due to the restriction on the resolution of E-SEM, particles smaller than 17 nm (1 pixel in Figure 4-19) were invisible. Since fulvic acids are usually less than 3 nm in diameter [14], these particles observed herein should not be fulvic acids, but other substances. Overall, these images indicate that NOM fouling at low ionic strength was probably dominated by blocking of membrane pores (both internal and external) by these fine particles. On the other hand, those fluffy materials in the valley areas were perhaps less important in this case as they existed only on limited areas of the membrane surface.

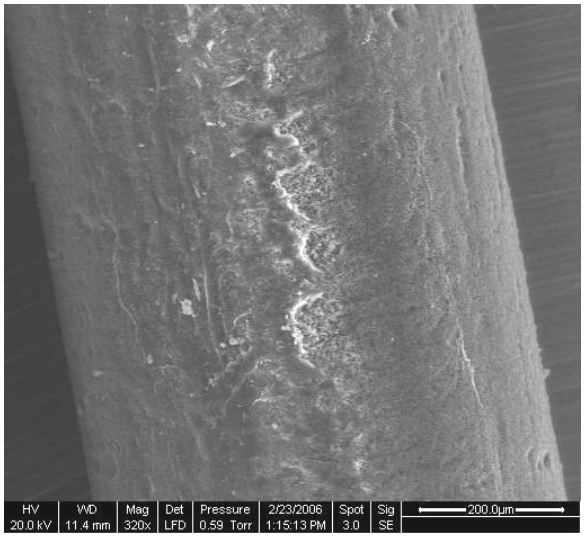

Figure 4-17. E-SEM image of the outside surface of a PVDF membrane fouled by DSW NOM. The feed water contained 20 mg C/L NOM and 10^{-4} M $NaHCO_3$. The permeate throughput was 25 L/m^2. Feedwater pH was approximately 6.5.

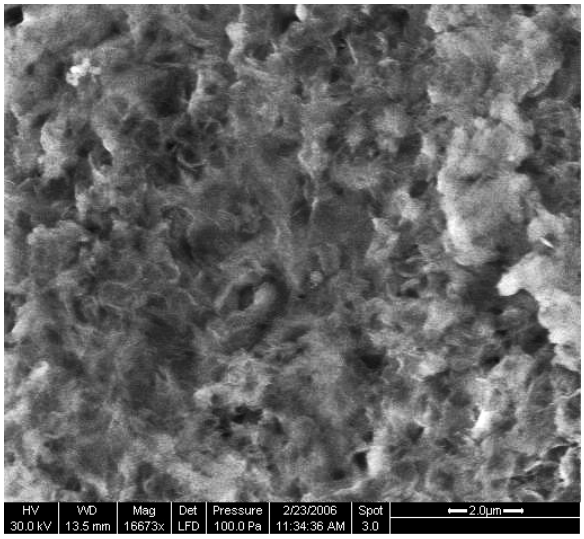

Figure 4-18. E-SEM image of the PVDF membrane surface in the valley region. Experimental conditions were as described in Figure 4-17.

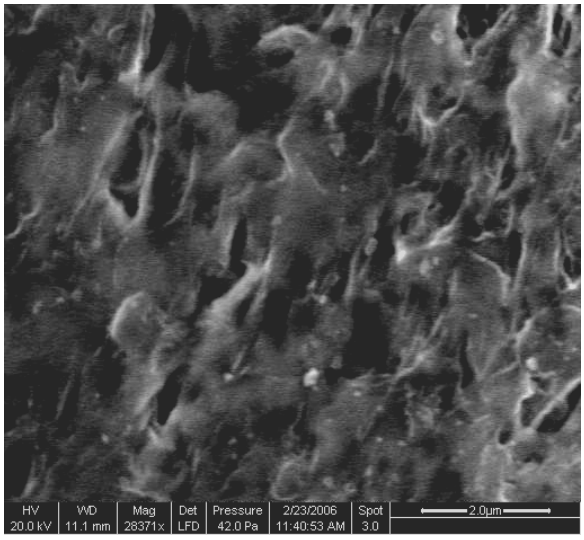

Figure 4-19. E-SEM image of the cross-section of a fouled PVDF membrane. Experimental conditions were as described in Figure 4-17.

The membrane fouled by NOM in the presence of 0.01 M $CaCl_2$ looked totally different from the previous one although the normalized TMP increased by 37 percent, only slightly less than that observed at low ionic strength. Figures 4-20 and 4-21 show the outside surface of the membrane under the E-SEM. A broad area of membrane surface was covered by both micron-sized particles (see Figure 4-20) and thin and cloudy materials (Figure 4-21). The presence of such a covering layer was more distinctive in the cross-sectional view of the membrane. As shown in Figure 4-22, a thin layer of organic materials existed outside the membrane. Part of the cake layer collapsed and fell to the middle of the cross-section, which was expected to be a result of the cutting during the sample preparation. The thickness of this layer was estimated as approximately 5 μm based on this image.

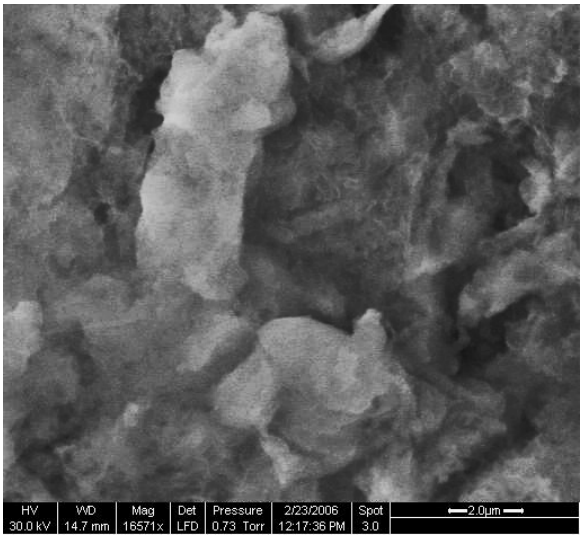

Figure 4-20. E-SEM image of micron-sized NOM aggregates accumulated on the outside surface of a fouled PVDF membrane. The feed water contained 20 mg C/L NOM and 0.01 M $CaCl_2$. The permeate throughput was 25 L/m^2. Feedwater pH was approximately 6.1.

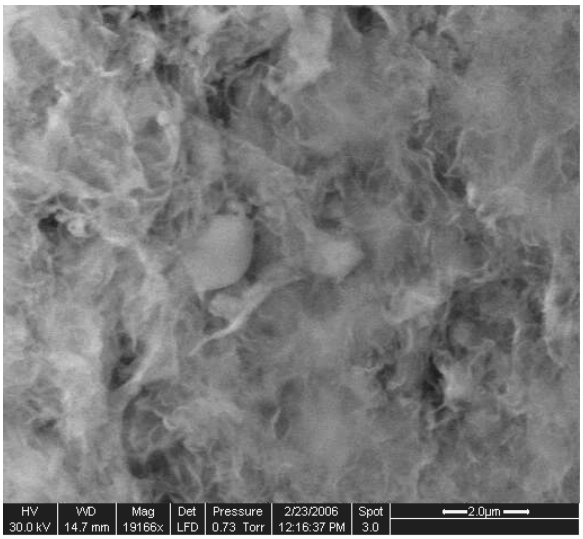

Figure 4-21. E-SEM image of fluffy NOM accumulated above membrane pores on the outside surface of a fouled PVDF membrane. The experimental conditions were as described in Figure 4-20.

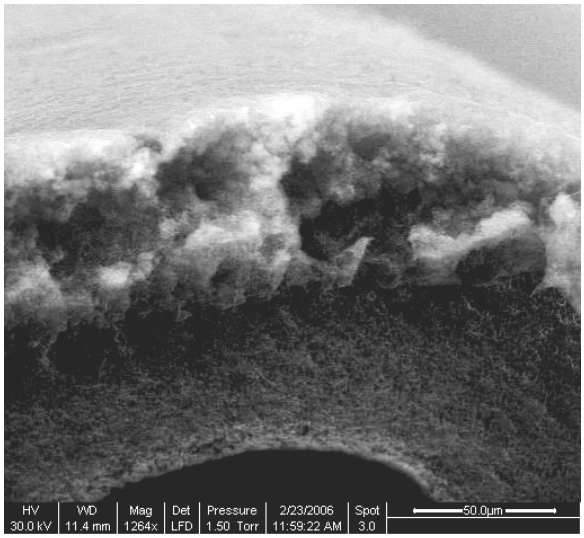

Figure 4-22. E-SEM image of a cross-sectional view of the cake layer on the outside surface of a fouled PVDF membrane, formed presumably by NOM aggregates. The experimental conditions were as described in Figure 4-20.

A closer look at the layer is shown in Figure 4-23. It seemed to be loose and textured, rather than dense and uniform. This probably explained the relatively slow increase in TMP during the filtration. The possible presence of fine particles under this layer was investigated as well. It was found that, unlike at low ionic strength, the pores beneath the covering layer appeared to be "clean" (see Figure 4-24). This was similar to what was observed in the fouling caused by 93 nm latex particles. Therefore, these images suggest that the fouling in the presence of 0.01 M $CaCl_2$ was probably caused by the aggregates of fine particles. The formation of aggregates was consistent with the increase of solution turbidity observed in the jar tests as depicted previously (see Figure 4-8). The size of these aggregates was larger than the largest dimension of the membrane pores, thereby causing membrane fouling by building cake layers on membrane outside surfaces.

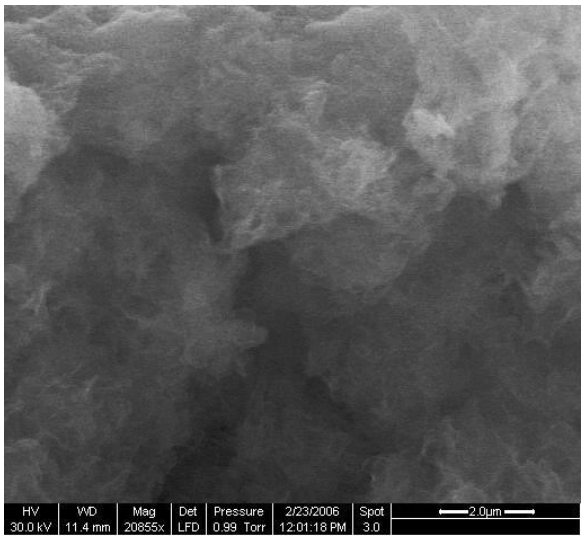

Figure 4-23. E-SEM image of the cake layer formed outside the membrane external surface. The experimental conditions were as described in Figure 4-20.

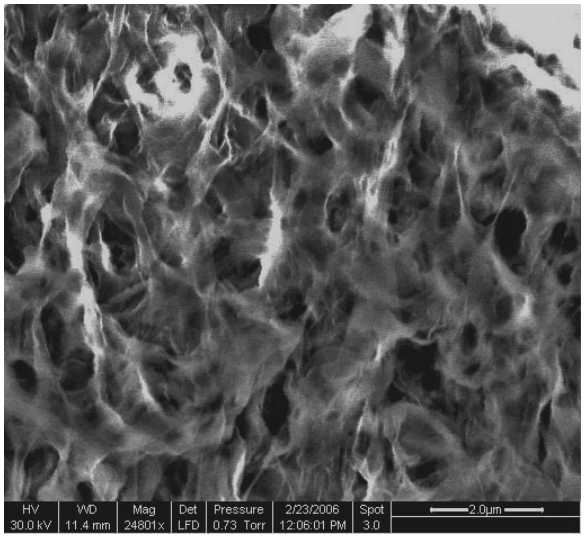

Figure 4-24. E-SEM image of the cross-sectional view of a fouled membrane beneath the NOM cake layer shown previously. The experimental conditions were as described in Figure 4-20.

4.4 DISCUSSION

4.4.1 Different Roles of NOM Components in Membrane Fouling

The information obtained experimentally suggests the presence of three major components that are relevant to the fouling of MF membranes. Component A is organic

colloidal particles as seen in the E-SEM images for low ionic strength experiments. These particles are smaller than the coarse materials retained by the GF/C glassfiber prefilter, but larger than the other two components. Their sizes (80 ± 41 nm) are close to (some even larger than) the pore size rating of the MF membrane (100 nm). Therefore, they are partially subject to removal by MF membranes through size exclusion effects. Their chemical properties are unclear, but their physiochemical properties appear to be stable with respect to coagulation but unstable with respect to deposition/adsorption by PVDF surfaces. The origin of their affinity to PVDF surfaces was unclear in the absence of enough information about their chemical compositions. They have little contribution to the measurement of UV_{254} absorbance; thus their removal by the membrane was not reflected in the measurement of UV_{254}. Due to these properties, Component A is perhaps the dominant NOM responsible for the fouling of the PVDF membranes under low ionic strength, and at high pH, moderate ionic strength. It should be important under other chemical conditions. This view is consistent with the fouling observation in which, under different chemical conditions, the relative TMP only varied in a narrow range of 1.40 to 1.70. On the other hand, the affinity of this component to polymeric surfaces may affect their detection by the SEC-DOC/UV analysis. Strong binding of this component to the nylon prefilter may lead to their removal by the prefilter, and their attachment to the gel permeation column may substantially delay their elution as well. This could have made this fraction undetectable or its size underestimated by SEC. Koh *et al.* [85] also found that a 0.2 μm polypropylene (PP) membrane can adsorb a small fraction of a lake water NOM at a nominal uptake of about 14 mg DOC adsorbed per gram of PP membrane. The remaining NOM fraction showed little fouling potential on a 20 kD

polyethersulfone (PES) membrane. These results are consistent with the view that the NOM fraction critical to membrane fouling is adsorptive to polymeric membranes.

The second NOM component (Component B) is in a broad size range of a few nanometers to microns. Materials in the lower end of this component were viewed under the AFM (see Figure 4-3). At low ionic strength, a majority of them are smaller than 10 nm, and therefore were not observed under E-SEM, but probably accounted for the high molecular weight peak (20~30 kD) shown in the SEC results (Figure 4-6). Chemically, this component of NOM is responsible for part of the measured UV_{254} absorbance, and is detectable by UV spectrophotometry. These NOM moieties are likely to possess functional groups that are reactive with proton or calcium ions in water; therefore, their stability is subject to change with the variations of solution pH and calcium concentrations. They undergo association or dispersion once those conditions change. As solution pH decreases to the acidic range or the ionic strength increases to 0.003, this component of NOM forms (larger) aggregates/agglomerates. This process causes the shift of the particle size distribution. This was measured as the increase of the number of large particles by AFM (see Figure 4-5), and the increase in solution turbidity observed in the jar test (see Figure 4-8). In this respect, the increase in calcium concentration resulted in the formation of the micron-sized flocs that were viewable by E-SEM (e.g., Figure 4-20), while the decrease in pH seemed to form submicron-sized aggregates that are smaller than the nominal membrane pore size. In regard to the attachment of these NOM moieties on membrane surfaces, the ionic strength of the solutions appeared to be important, besides pH and calcium concentration. The increase of ionic strength to 0.003 is sufficient to cause favorable attachment of NOM moieties on membrane surfaces,

except at extreme alkaline pHs. This was consistent with the UV_{254} rejection data obtained in the filtration experiments (Figure 4-10 versus Figure 4-12). When the ionic strength is in the range of 0.0001, these particles are stable and thus can penetrate through the membrane without retention, similar to the 19 nm latex particles that were stable with respect to deposition. On the other hand, the variations in solution pH can affect the depositional and coagulational stabilities of this NOM component simultaneously. This was directly observed by AFM; as shown in Figure 4-3 for deposition/adsorption (clustering at low pH) and Figure 4-8 for association and dispersion. Therefore, the fouling of the PVDF membrane by this NOM component was variable with solution chemistry. Their contributions to membrane fouling are less at low ionic strengths or alkaline pHs, and greater at acidic pHs, higher ionic strength, or high calcium concentrations. This difference probably contributed significantly to the variations of membrane fouling observed under different chemical conditions.

Table 4-2. Characteristics and contents of three NOM components

Component	Stabilities[1]	Size[2]	Density (g/cm^3)[3]	Mass Content (%)[4]	Conc. (mg/L)[5]
A	Stable/unstable	80 ± 40 nm	1	~ 5	~ 0.5
B	Variable/variable	1 nm ~ 1 μm	1	~ 25	~ 2.5
C	Variable/variable	~ 1 nm	1	~ 70	~ 7.0

Note: [1] Stabilities described include coagulational/depositional (adsorptive) stabilities, and "variable" indicates the stability depend on solution chemistry; [2] characteristic sizes were estimated on the basis of E-SEM for Component A, AFM, E-SEM and SEC-DOC for Component B, and AFM and SEC-DOC for Component C; [3] the density used in model simulation, the real density should be slightly higher; [4] mass contents were estimated based on corresponding DOC and UV rejections measured in fouling experiments, some preliminary runs are not discussed in this chapter; [5] the concentration of each component was calculated based on the total NOM concentration of 10 mg/L (5 mg C/L) and their respective mass content.

The final relevant NOM component, Component C, is probably fulvic acid. Fulvic acids in the solution are the smallest in the three components, and their sizes are estimated to be less than 2 nm based on the SEC-DOC/UV results. In comparison, the

reported hydrodynamic radii of aquatic fulvic acids from other sources were consistently lower than 3 nm regardless of the solution chemistry, including the presence of calcium ions, as determined using different techniques [86-88]. They consist primarily of aromatic compounds, and cause the majority of the measured UV_{254} absorbance. Fulvic acids in Dismal Swamp water are negatively charged due to the presence of phenol and/or carboxylic acid groups on their molecular structures [15]. Their adsorption on a membrane or its surrogate surfaces is strongly affected by solution chemical conditions, including pH and calcium concentrations; as found in other studies [89]. Due to their small sizes, the direct contribution of fulvic acids to the loss of membrane permeability is expected to be very limited as discussed later. However, the adsorption of fulvic acids alters the surface property of hydrophobic membranes by increasing surface charges and hydrophilicity [89]. It may affect the coagulational and/or depositional stabilities of other NOM moieties (both in Components A and B) in the MF system studied and hence alter their fouling behaviors. Similar effects were observed in the fouling of the PVDF membrane by 19 nm latex particles as introduced in Chapter 3. However, without a suitable technique to comprehensively distinguish the roles of other NOM components, such an effect in NOM fouling remains a speculation in current study.

Table 4-2 summarizes the properties of the three components of the Dismal Swamp water NOM. With this general picture of NOM composition, the experimental results on subsequent filtration and fouling may be interpreted as follows. NOM of Component A served as the primary foulants of the PVDF membrane, and was removed very efficiently by the membrane regardless of solution chemistry, due to their relatively large sizes and potential strong affinity to membrane surfaces. Whether or not additional

fouling can occur depended on the aggregation and attachment of the NOM moieties in Component B on membrane surfaces. The rejection of Component B and the resulting membrane fouling are strongly related to the existence of favorable chemical conditions for chemical attachment. If the chemical conditions are consistent in the two sequential filtrations, large and/or unstable moieties in Component B should be removed efficiently in the first filtration step, either via size exclusion or chemical adsorption/deposition. Thus, the fraction of Component B moieties left after this step is small and chemically stable. They are no longer capable of attaching to membrane surfaces and causing additional fouling in the second filtration, regardless of the solution chemistry. In comparison, if the solution chemistry is changed such that the stability of the remaining Component B moieties is reduced, additional retention of Component B will occur and additional fouling will be observed. This explains the phenomenon discovered in Runs 8 and 9 as shown in Figure 4-15.

Table 4-3. Summary of fouling experiment results

Run No.	Feed water quality			Relative TMP		Relative UV_{254} Absorbance	
	I	pH	$[CaCl_2]$ (M)	Total[1]	After backwash[2]	Permeate[3]	Backwash water[4]
1	0.0001	8.2	0	1.50	1.47	0.93	1.01
2	0.0001	7.5	0	1.49	1.44	0.93	1.00
3	0.003	4.0	0	1.70	1.62	0.75	1.00
4	0.003	7.0	0	1.60	1.52	0.88	1.00
5	0.003	11.2	0	1.43	1.43	0.93	1.00
6	0.003	7.0	0.001	1.57	1.51	0.83	1.00
7	0.03	7.0	0.01	1.67	1.64	0.73	1.00
8	0.0001	7.0	0	1.57	n.a.	0.93	n.a.
9	0.003	7.0	0	1.23	n.a.	0.86	n.a.

Note: [1] Relative TMP observed in the end of the first filtration step, corresponding to a permeate throughput of 150 L/m^2; [2] Relative TMP measured at one minute of filtration after returning from the hydraulic backwash; [3] Permeate UV_{254} absorbance was determined with the composite permeate sample collected during the first filtration step; [4] Backwash water sample was the mixture of the feedwater in the feedwater column in the end of the first filtration step and the backwashing water generated from the hydraulic backwash.

A comparison of all fouling results is presented in Table 4-3. It is noticeable that the relative UV_{254} absorbance in the "backwash" water samples always equaled that of the feedwater, suggesting that there was not concentration of UV_{254}- related NOM in the feedwater column during the MF processes. This is consistent with the view of the importance of NOM moieties in Component A in the fouling of the PVDF membrane.

4.4.2 Model Simulation versus Experimental Data

By dividing the DSW NOM into three major components, it becomes possible to assess their individual contributions to the total fouling using the model established in the study. First, it is necessary to estimate their contents, characteristic sizes, and stickiness, based on existing experimental evidence. The corresponding information is presented in Table 4-2.

The model simulation results for the fouling of the PVDF membrane by DSW NOM of Component A are illustrated in Figure 4-25. As shown in the figure, the fouling is predominated by pore blocking and is irreversible in the presence of favorable particle-membrane attachment. The increase in the relative TMP is approximately 1.60 at a throughput of 150 L/m^2. This is comparable to the results of Run 5, which was approximately 1.43 (see Table 4-3). The fouling observed experimentally in Run 5 was completely irreversible, consistent with the modeling results.

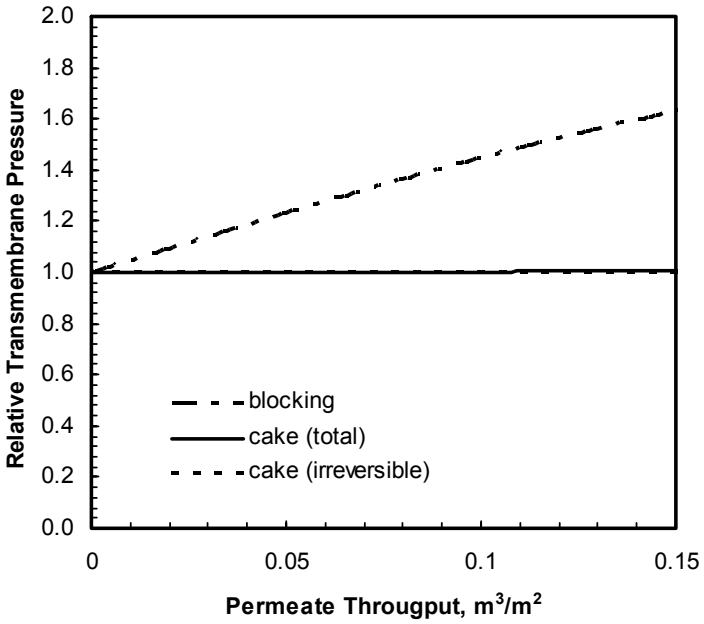

Figure 4-25. Increase of relative transmembrane pressure as a function of permeate throughput. Model setting is similar to that used in Chapter 2, except that the mass concentration of foulants (Component A) is reduced to 5×10^{-4} kg/m^3 or 0.5 mg/L. $\alpha_{pm} = 1$, and $\alpha_{pp} = 0$.

The application of the model to the fouling by NOM of Component B is very difficult without additional experimental information, because both the size and the stabilities of NOM moieties are altered with varying solution chemistry. Therefore, it is only possible to explore some boundary conditions for their fouling behaviors. First, it is noted that the molecular size of this NOM component was measured as 20 to 30 kD with SEC-DOC/UV at neutral pH and low ionic strength, which is equivalent to a hydrodynamic radius of approximately 5 nm. This is less than one sixth of the mean diameter of membrane pores (58 nm). Therefore, the dominant fouling mechanism should be internal pore constriction (standard pore blocking) according to the model. If the particle concentration was 2.5 mg/L as estimated (see Table 4-2), the predicted relative TMP should be merely 1.02 at a permeate throughput of 150 L/m^2, which is much less than that caused by Component A. This result appears to disagree with the

speculation that materials with this molecular size are the dominant foulants for low pressure membranes as introduced in Chapter One. This may be explained from two aspects. First, the membrane pore size of the low pressure membranes used in other studies was smaller than that of the PVDF membrane used in the study. If the diameter of membrane pores decreases to less than 30 nm, NOM moieties with a radius of 5 nm will become large enough to participate in surface pore blocking and/or cake layer formation. Second, the magnitude of fouling is extremely sensitive to the particle/membrane pore size ratio in this region. Even if only a small fraction of NOM moieties of Component B have radii of larger than a sixth of membrane pore size, their contribution to fouling will be substantial. As the solution chemistry become more favorable for the formation of NOM aggregates, the fouling also becomes severe. On the other hand, if the coagulational stability of NOM moieties is completely eliminated, such as the addition of 0.01 M $CaCl_2$ into 5 mg C/L of DSW solution, micron-sized NOM aggregates are formed. The fouling caused by those "macroscopic" substances is primarily cake layer formation. Overall, only qualitative comparison between experimental and modeling results can be made for NOM moieties of Component B.

Finally, the role of NOM moieties of Component C can be estimated using the model. At a concentration of 7 mg/L, the relative TMP is calculated to be approximately 1.05, which is slightly more than that of Component B at low ionic strength, but still significantly less than that of Component A. Additionally, unlike Component B, the fouling caused by Component C can hardly exceed this level since their sizes cannot reach the threshold of a sixth of membrane pore size, regardless of the solution chemistry.

4.5 CONCLUSION

The fouling of the PVDF MF membrane by Dismal Swamp water NOM was investigated under different solution chemical conditions in this work. This NOM sample was characterized using different chemical techniques. It was found that it is likely comprised of three major components that are relevant to the fouling of the membrane. The first component (Component A) was not measurable by UV spectrophometer and has particle diameters of around 80 nm according to the electron microscopic results. It appeared to be sticky to membrane surfaces and thus act as a consistent foulant of the membrane, regardless of the solution chemistry. The second component (Component B) was measurable by UV spectrophotometer and underwent deposition/aggregation depending on the solution chemistry. The particle diameter varied substantially under different chemical conditions. This component was presumably responsible for the variable amounts of fouling observed under varying chemical conditions. Its contribution was slightly greater as lower pH, higher ionic strengths, or higher calcium concentrations. The last component (Component C) consists of fulvic acids. The permeate of each filtration run contained predominantly this component, but had little fouling potential, regardless of solution chemistry. Therefore, its direct contribution to membrane fouling was insignificant.

The model validated in Chapter 3 was used to assess the possible contribution of the three components to the fouling of the MF membrane. The modeling results confirmed that: (1) NOM with the size and concentration of Component A is capable of causing the extent of fouling comparable to the experiment results; (2) NOM like Component C cannot cause significant amount of fouling, regardless of its concentration

in the feedwater, due to its small molecular size. Meanwhile, the model supports the view that the fouling caused by component B would be important if their size distributions shift to larger range as a result of particle aggregation or molecular association. Overall, consistencies between the modeling and the experimental results were found with respect to the fouling of the MF membrane by Dismal Swamp water NOM. However, a quantitative comparison was difficult to make limited by the information on the properties of Components A and B.

The study presented in this chapter suggests that the model developed is useful for us to understand the roles of different NOM components in membrane fouling processes.

Chapter Five

SUMMARIES AND CONCLUSION

5.1 INTRODUCTION

The onset of the twenty-first century has been accompanied by a dramatic increase in the research and application of low pressure membrane filtration (LPMF) in the area of water and wastewater treatment due to its advantages over the conventional techniques. The LPMF mentioned herein include traditionally named microfiltration (MF) and ultrafiltration (UF) that have relatively large membrane pore sizes (10 – 100 nm) and low operating transmembrane pressures (typically less than 0.5 bar). These membranes are robust and effective in removing turbidity and pathogens in the feedwater at competitive costs. However, a major technical problem encountered during the application of LPMF is the loss of membrane permeability as a result of the accumulation of aquatic contaminants on or inside the membranes, i.e., membrane fouling. The goal of the study was to investigate the mechanisms of membrane fouling observed during the MF of natural surface waters.

Based on the review of existing engineering experience and scientific understandings, it was hypothesized in the study that *the fouling of MF membranes, including hydrophobic polyvinylidene fluoride (PVDF) membranes, is primarily ascribed to the existence of favorable chemical attachments among foulant entities (coagulational attachment) and between foulants and membrane surfaces (depositional attachment); the conditions of the two attachments are dependent not only on the properties of the foulants and the membranes, but also on solution chemistry*.

The nature of these attachments was unclear, mostly as a result of the variable compositions of aquatic contaminants and their complicated properties. Therefore, this study did not try to explore the rigorous theoretical foundations of these attachments and the surface interactions behind the scene, but focused on the assessment of the impact of the attachments on the fouling of MF membranes.

5.2 Model Development and Simulation Results

A mathematical model was developed based on the aforementioned hypothesis on the fouling of MF membranes in water treatment. In order to employ simple mathematical analyses, the structural properties of commercial MF membranes were simplified as chemically identical films consisting of evenly distributed uniform-sized circular cylindrical pores. Meanwhile, aquatic contaminants were modeled as mono-dispersed spherical particles that possess uniform sizes and variable physiochemical stabilities. The physiochemical stabilities of the model particles include two aspects during MF of particle suspensions: one is the coagulational stability that is dependent on inter-particle interactions, and the other is the depositional stability that is governed by particle-membrane interactions. The two types of physiochemical stabilities were quantitatively described in the model using two collision efficiency (or sticking probability) coefficients, respectively.

The mathematical derivation of the model was established by revising the classical Hermia model that was developed for the fouling observed in constant pressure membrane filtration. The relationship between membrane fouling and the permeate production used in the Hermia model was replaced with that between fouling and the

accumulated mass of foulants. Next, the correlation between the accumulation of various types of foulants and the permeate throughput was determined by analyzing the migration of particles towards membrane surfaces or inside membrane pores, as well as their attachment probabilities to each other and to membrane surfaces. The combination of the two steps yielded a set of mathematical equations that are capable of predicting the fouling caused by particles with different chemical stabilities and sizes.

Three major scenarios were considered for the simulation of the fouling of MF membranes based on the sizes of particles relative to the membrane pore size: 1) particles are larger than the membrane pore size, 2) particles are less than, but greater than a third of the membrane pore size; and 3) particles are smaller than a third of the membrane pore size.

Through model simulation, it was found that membrane fouling caused by particles larger than the membrane pore size could be dominated by two types of surface fouling. One fouling mechanism was cake layer formation, resulting from the attachment of particles on solid membrane surface and other particles. Cake layer formation for large particles can occur in the absence of favorable physiochemical conditions for particle attachment. However, the fouling was completely hydraulically *reversible* in this case. The other fouling mechanism was the blockage of membrane pore entrances by particles. This type of fouling only occurred in the presence of favorable particle-membrane attachments, and was in general hydraulically *irreversible* once it occurred. Pore blocking appeared to be more effective in reducing membrane permeability than cake layer formation for rigid hydrophobic particles. Overall, the model simulation results showed that the total fouling of MF membranes by large particles increased with

increasing particle-membrane sticking probability, and decreased with increasing particle-particle sticking probability because of the existence of competitions between two types of attachments. On the other hand, the hydraulic reversibility of membrane fouling decreased monotonously with increasing probabilities of particle attachments to both other particles and membrane surfaces.

If caused by particles with radii ranging from 1/6 to 1/2 of the diameter of membrane pores, the fouling proceeded in two sequential steps. First step was the deposition of unstable particles at pore entrances, which resulted in the constriction of membrane pores to such an extent that other incoming particles could no longer enter these pores. As the next step, those incoming particles were retained on the outside surface of the membrane although they were smaller than the original pore size of the membrane, which in turn caused surface fouling similar to that caused by large particles as mentioned previously. The loss of membrane permeability was, on the other hand, dominated by pore constrictions that occurred in the first step. In comparison, the major effect of the second step was an increase of particle removal by the membrane; this effect is also relevant to the industrial application of MF membranes.

As the last scenario, MF membranes can be fouled by particles with radii smaller than a sixth of the diameter of membrane pores. Using the model, the maximum possible extent of fouling was calculated as a function of the particle sizes. The results showed that these small particles contributed to much less amount of fouling compared to the others, even under the most favorable chemical conditions. Therefore, they were less important than relatively large particles in regard to the direct reduction of membrane permeability.

Overall, the model mathematically established the quantitative relationship between membrane fouling and the size and stabilities of aquatic contaminants. The fouling was predicted to be the severest in the second scenario when the chemical conditions are favorable to particle-membrane attachment but unfavorable to particle aggregation. The modeling results also indicate that hydraulically irreversible fouling can not happen in the absence of favorable particle-membrane attachment. The results are consistent with the hypothesis that chemical attachment plays a primary role in the fouling of MF membranes. The relevant sizes of foulants determined in model simulation are comparable to those found in other experimental studies for the fouling of MF membranes. The model and the simulation results are probably applicable to other low pressure membranes given the versatile approach used in modeling.

5.3 MODEL VALIDATION: COLLOIDAL FOULING OF MF MEMBRANES

In order to validate the mathematical model, polystyrene latex particles with two representative sizes were used to challenge a commercial hollow fiber MF membrane made of polyvinylidene fluoride (PVDF) under three different calcium concentrations. As found in preliminary experiments, those latex particles had three different levels of physiochemical stabilities at three calcium concentrations and neutral pHs: 1) in the absence of calcium, they were stable with respect to both deposition and aggregation, 2) in the presence of 0.001 M calcium, they were stable with respect to aggregation but unstable with respect to deposition, and 3) in the presence of 0.01 M calcium, they were unstable with respect to both aggregation and deposition.

The fouling observed with the 93 nm latex particles agreed with the model simulation results for particles larger than membrane pore sizes. The fouling was the least and completely reversible by hydraulic backwash in the absence of calcium, for lack of favorable particle-membrane attachment. As the calcium concentration increased to 0.001 M, the particles unstable in deposition but stable in aggregation fouled the membrane to the greatest extent because pore blocking became possible and competition from cake layer formation was insignificant. Once the calcium concentration increased to 0.01 M, the particles unstable in both deposition and aggregation caused less total fouling than that occurred at 0.001 M calcium due to the decrease in the probability of pore blocking caused by the competition from cake layer formation. However, the fouling observed under this condition was completely irreversible since all particle attachments involved in this process were physiochemically favorable.

The fouling observed with the 19 nm latex particles was consistent with the model prediction for particles with radii in the range of 1/6 to 1/2 of the membrane pore diameter. For stable particles, the fouling was insignificant and more than 90 percent of the particles penetrated through the membrane. In the presence of 0.001 M calcium, the particles unstable in deposition caused substantial amounts of fouling, approximately nine times as much as that by 93 nm latex particles. This trend agrees to the effect of particle sizes on the magnitude of fouling predicted by the model. On the other hand, the increase of calcium concentration to 0.01 M resulted in immediately aggregation of those 19 nm particles. The aggregates were much larger than membrane pores, thereby forming a very fairly permeable cake layer on the external surface of the outside-in membrane. Therefore, the consequent fouling effect (loss of membrane permeability)

was negligible although all the particle attachments involved were favorable (as evidenced by the cake layer remaining in place after permeate backwash).

The fouling mechanisms predicted by the model were further tested by examining the scanning electron micrographs obtained with fouled membrane fibers under representative conditions. Positive evidences were found.

In addition to the validation of the model, it was also found that the presence of 1 mg C/L of natural organic matter (NOM) reduced the attachment of latex particles on the PVDF membrane (and the surrogate) surfaces, and led to an extensive decrease of membrane fouling caused by the 19 nm particles. This result indicates that NOM in natural surface waters may modify the interfacial properties of hydrophobic membranes and the suspended particles, and alter the fouling behavior of colloidal particles.

5.4 MODEL APPLICATION: NOM FOULING OF MF MEMBRANES

NOM fouling has been considered the major type of fouling for microfiltration membranes. Application of the model improved our understandings on the mechanism of NOM fouling and pointed out directions for future research.

Controlled fouling experiments were conducted with the same membrane used in the colloidal fouling study and a representative type of pedogenic aquatic NOM sample under systematically varied chemical conditions. The physical and chemical properties of the NOM were determined using a variety of analytical techniques. These works revealed that this type of NOM likely consists of three major components related to membrane fouling. Component A includes colloidal particles that have broad size distribution and a mean diameter of around 80 nm. These particles appeared to be sticky

to the surface of the PVDF membrane, regardless of the solution chemistry. Component B is comprised of a group of particles with dimensions of 5 nm and above and physiochemical stabilities variable with changing solution chemistry, similar to the latex particles tested in the colloidal fouling study. Finally, Component C includes mainly fulvic acids that are small in sizes (around 1 nm) but reactive with protons and calcium ions in the water. They can be adsorbed at the PVDF/water interface as well, depending on the solution chemistry.

In the fouling experiments, 5 mg C/L of NOM solution consistently fouled the PVDF membrane to a certain extent, regardless of solution chemistry. This is explained by the attachment of Component A on membrane surfaces under all conditions. The model predicted fouling for 80 nm sticky particles was comparable to the fouling obtained at alkaline pHs, conditions under which the impacts of Components B and C were suppressed. The dominant fouling mechanism was pore blocking in this case according both to the model calculation and environmental scanning electron (E-SEM) micrographs. At moderate ionic strength, Component B attached to the membrane surface, which resulted in additional amount of membrane fouling observed experimentally. The magnitude of the fouling by component B varied dramatically with solution chemistry. It was the greatest at a pH of 4.0 and the least at a pH of 11.2, likely resulting from the aggregation of Component B at such a low pH. This aggregation effect was most noticeable at a calcium concentration of 0.01 M, where the formation of cake layers was observed with the E-SEM.

The relevance of Component C in membrane fouling was indirect compared to the other components. According to the model calculation, particles with the sizes of

Component C can only cause minor fouling on MF membranes, regardless of their concentrations and solution chemistry. The major impact of the attachment of Component C on membrane surfaces was expected to be the modification of the properties of the membrane/water interface. Similar to what was found in the colloidal fouling study, the adsorption of Component C on membrane surfaces introduced reactive functional groups on the hydrophoblic surface of PVDF membranes. This effectively made the attachment of other larger particles less stable, thus increased the hydraulic reversibility of their fouling. Such a trend was indeed found in the experiments conducted at moderate ionic strengths and/or calcium concentrations.

5.5 CONCLUSION

The results of the study elucidated a simple truth that is relevant to the fouling of MF membranes in water treatment by aquatic contaminants, i.e., the existence of favorable chemical or physiochemical attachments is the primary condition for the occurrence of colloidal and NOM fouling. In comparison, the size of aquatic contaminants plays a secondary but important role in the fouling process. Therefore, both should be considered simultaneously.

In all the chemical or physiochemical attachments involved, particle-membrane attachments were found to be competitive with particle-particle attachments in determining the magnitude of total fouling. On the other hand, they functioned jointly in governing the hydraulic reversibility of the fouling. The fouling was completely irreversible by hydraulic backwash when all particle attachments involved became favorable, regardless of particle size.

The size of aquatic contaminants affected the mechanism and magnitude of the fouling once they attached onto membrane surfaces under favorable chemical conditions. Of all the contaminants, those with radii of 1/6 to 1/2 of the diameter of membrane pores were found to be the most effective in blocking membrane pores and causing membrane fouling.

The experimental work in the study also showed that the presence of NOM had significant impacts to the attachment of particles to membrane surfaces, thereby changing their fouling behaviors.

In short, this study distinguished the roles of particle size and stabilities (or affinities) and their relative importance in the fouling of MF membranes. This is beneficial to the understanding of the fouling mechanisms and the application of low pressure membrane filtration (including MF) in water and wastewater treatment. More discussions on the implications of the study are given in next chapter, together with proposed future works.

CHAPTER SIX

IMPLICATIONS AND FUTURE WORKS

6.1 IMPLICATIONS FOR THE FOULING OF OTHER LOW PRESSURE MEMBRANES

The engineering background of the study is the widespread application of low pressure, hollow fiber (LPHF) membrane filtration in water and wastewater treatment since the beginning of the 21st century. At the onset of the study, the PVDF membrane used in the experimental work was widely used by industries. Later on, however, another generation of LPHF membranes has emerged and been used in large-scale applications. These new membranes are typically so-called "hydrophilized" PVDF or PES (polyether sulfone) membranes. They not only possess the good chlorine and acid tolerance of the previous generation, but also provide better removal of some aquatic contaminants, such as viruses, and better resistance to hydraulically irreversible fouling [90]. Therefore, the applicability of the model established in the study to these membranes is important to the overall value of the study.

Figure 6-1 presents membrane fouling results conducted with five representative types of LPHF membranes and DSW NOM under similar chemical and hydrodynamic conditions. The standard PVDF MF membrane is the one used throughout the study as introduced in Chapters 3 and 4, while the other four belong to the new generation of proprietarily modified commercial membranes. As shown in the figure, the observed total fouling varied substantially among different membranes, as did the hydraulic reversibility of fouling. However, the fouling of the four new membranes was consistently more hydraulically reversible than the standard PVDF MF membrane. Two modified PVDF membranes (one MF and one UF) had very little irreversible fouling

after the backwash, significantly less than that of the standard PVDF MF membrane. Meanwhile, the hydraulically irreversible fouling of the two PES membranes was close to that of the standard PVDF MF membrane, but the total fouling was greater, indicating greater reversibility of fouling. This experimental comparison demonstrates the advance of LPHF membranes in regard to the control or reduction of NOM fouling. It is especially true for the PVDF UF membrane, which has a pore size rating of approximately 0.025 μm, substantially smaller than that of the standard PVDF MF membrane. Its fouling by DSW NOM, however, was almost negligible after hydraulic backwash.

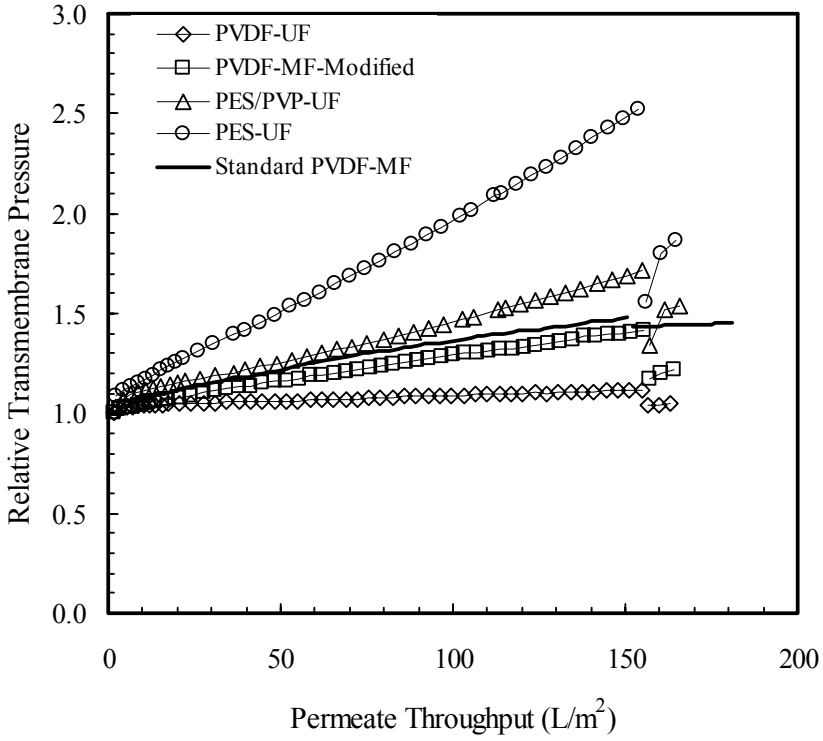

Figure 6-1. Fouling of five representative LPHF membranes by DSW NOM. The feedwater contained 5 mg C/L DOC and 10^{-4} M $NaHCO_3$. pH was around 6.9. No calcium added. The filtration and backwashing flux was controlled at 109 LMH, except for the standard PVDF (90 LMH). The break in each data curve represents a hydraulic backwash.

What is the relationship between these results and the proposed model? First, it generally confirms the relevance of chemical attachment in membrane fouling. By hydrophilizing the membrane surface and/or introducing additional negative surface charges, the attachment of aquatic contaminants on membrane surfaces can be reduced. According to the proposed model, the only dominant fouling mechanism is cake layer formation in the absence of favorable particle-membrane attachment, regardless of the pore size of the membranes. This cake layer is hydraulically reversible, given the absence of favorable particle-particle attachment, a condition reasonable for DSW NOM at low ionic strength and in the absence of calcium.

Second, the results likely show the secondary effect of membrane pore size on fouling. All four new membranes (including the modified PVDF MF membrane as called by the manufacturer) have smaller pores than the standard PVDF membrane, ranging approximately from 0.01 to 0.03 μm. Based on the model simulation results and experimental evidence, most of aquatic materials responsible for the fouling of the standard PVDF MF membrane (Components A and B) should be retained on the external surface of these new membranes, which results in surface fouling of the membrane, even before the formation of the aggregates of Component B. This effectively limits the area of the membrane surfaces that is subject to particle-membrane attachment and the occurrence of hydraulically irreversible fouling. The potential difference in the fouling of MF and UF membranes has also been found in other studies [58].

On the basis of these discussions, the implication of the study for other low pressure membranes can be summarized by envisioning an ideal membrane that is "least" vulnerable to membrane fouling as follows. This membrane should, first of all, have

good clean membrane permeability that is suitable for low pressure operation (i.e., to reduce the formation of a gel-like layer on the membrane surface). Second, its external and internal surfaces should be well hydrophilized and negatively charged in order to minimize the attachment of the retained materials, as well as the surface conditioning effect caused by the adsorption of fulvic acids. Third, it should have suitable surface pore size (less than 0.03 μm), thereby being capable of retaining a majority of unstable colloidal materials on its external surface (i.e., to mitigate particle-membrane attachment).

6.2 Implications for Membrane Fouling and Its Reduction in Water Treatment

This study was focused on the chemical aspects of membrane fouling in part because they are more readily scaled up than physical ones. The findings of the study are likely to be helpful in answering three associated questions that are relevant to the reduction of membrane fouling in large-scale MF systems.

First question: what types of aquatic contaminants are most problematic in the fouling of low pressure membranes? The results from the study imply that the major foulants in natural waters are primarily those that are "sticky" to membrane surfaces. Their sizes relative to membrane pore size can then determine the extent of the fouling under favorable attachment conditions. The fouling is the most severe if the radii of particles are approximately a sixth to a half of the diameter of the membrane pores. For MF membranes with pore diameters of 0.05 to 0.1 μm, the radii of such contaminants are approximately in between 0.01 to 0.02 μm. Aquatic contaminants with such dimensions are mostly high molecular weight macromolecules (e.g., proteins and polysaccharides)

and other organic colloidal particles. Their contributions to the fouling of particular membranes depend primarily on their affinity to membrane surfaces. Such a conclusion is consistent with the importance of colloidal NOM found in many other experimental studies as introduced in Chapter 4.

Second question: what types of membranes are least vulnerable to fouling? The implications of the study to this question have been elucidated previously. It is noteworthy, however, that the modeling approaches used in the study did not fully consider the irreversible fouling caused by gel layer formation. Studies conducted by Elimelech and co-workers [91-93] suggested that the formation of such a gel layer by the complexes of calcium and alginate can cause serious fouling on NF and RO membranes (high pressure membranes). In this case, the dominant interaction is the intermolecular interactions among alginate molecules, rather than between alginate and the membrane surfaces. Therefore, the structural properties of the membrane become less important. Nevertheless, this type of fouling is expected to be less important to the fouling of low pressure membranes used in water treatment due to the difference in the structural properties of low pressure and high pressure membranes and the resulting mechanisms of solute retention.

The last question: what measures should be taken in order to reduce/control membrane fouling? There is not a simple answer to this engineering question. The aforementioned advance in membrane preparation has dramatically improved the resistance of membranes to fouling. Despite this remarkable achievement in membrane preparation, membrane fouling is still a universal phenomenon encountered on large-scale systems. This is to a great extent related to the diverse nature of aquatic foulants.

Therefore, pretreatment of the feed water is usually necessary for fouling control. The results of the study suggest that the removal of some components of aquatic contaminants with certain physical and chemical properties is critical for this purpose. In them, the removal of aquatic contaminants that are sticky to membrane surfaces and larger than 0.01 μm should have immediate and positive improvement on membrane productivity. For this purpose, coagulation or the combination of ion exchange and coagulation has been found effective [78]. On the other hand, processes that remove smaller aquatic materials may also be capable of mitigating fouling indirectly if the affinity of large materials to membrane surfaces is reduced as a result. This is especially important for the understanding of the role of calcium hardness in membrane fouling discussed in previous chapters. However, fundamental studies in this area are still missing.

6.3 IMPLICATIONS FOR THE FOULING OF MEMBRANE BIOREACTORS

With the coupling of biological treatment and membrane filtration, membrane bioreactor (MBR) is an important advance in the application of low pressure membranes in wastewater treatment. Membrane fouling is also an important problem for its application. As reviewed by Yang *et al.* [94], membrane fouling studies accounted for more than a third of the published fundamental studies on MBR. The strategies developed for fouling control include: 1) modification of membrane module designs to optimize aeration and hydraulic conditions, 2) operation of MBRs under critical filtration flux, 3) enhancement of cake layer permeability and dislodge by adding powdered activated carbons (PAC), and 4) physical and chemical cleaning. However, the occurrence of fouling of MBR still appears to be unavoidable. As pointed out by the

authors, permanent fouling caused by the deposition of solute and colloids on membrane surfaces should be better understood, together with the characterization of the foulants.

The results of this study can assist in the understanding of membrane fouling in MBRs although it was based on the MF of natural surface waters. First, it provides a possible fundamental explanation why colloidal sized biomaterials are relatively important for the fouling of low pressure membranes used in MBRs, as found in some recent experimental studies [95, 96]. Second, the results of this study showed the existence and the distinctive role of two types of attachments in membrane fouling process. Therefore, operation of a MBR under the so-called "critical flux" level where the formation of cake layers (particle-particle attachment) is suppressed cannot prevent particle-membrane attachment, thereby reducing the related fouling. This phenomenon is noticed in different bench and pilot-scale systems according to Yang *et al.* [94]. Overall, the coupled effects of particle size and stabilities identified in this study should be applicable to both natural waters and wastewaters, and both MF and MBR. However, MBR is more likely to subject to biofouling than normal MF. The formation of biofilms on membrane surfaces is beyond the scope of the model as it involves not only particle deposition, but also biological activities. In this case, the model and this study should be considered as a partial description of the early phase of biofouling in MBRs.

6.4 IMPLICATIONS FOR THE UNDERSTANDING OF NOM COMPOSITIONS

Based on the model developed in this study, the possible presence of three NOM components affecting membrane fouling has been elucidated in Chapter 4. Although more rigorous studies are needed to validate this approach, the limited success of this

classification of NOM indicates the merit of studies of membrane fouling for the theoretical understanding of NOM composition. Historically, the study of aquatic NOM has been focused predominantly on their chemical compositions, rather than their dispersity and interfacial properties. Therefore, little is known about the properties of aquatic NOM that are larger than 0.01 μm or so since they only account for a very small fraction of the total NOM; e.g., less than 5 percent of the total DOC of DSW NOM is classified as Component A as estimated from the MF results. This is compared to a typical DOC removal of less than 10 percent found by Shafer *et al.* [6].

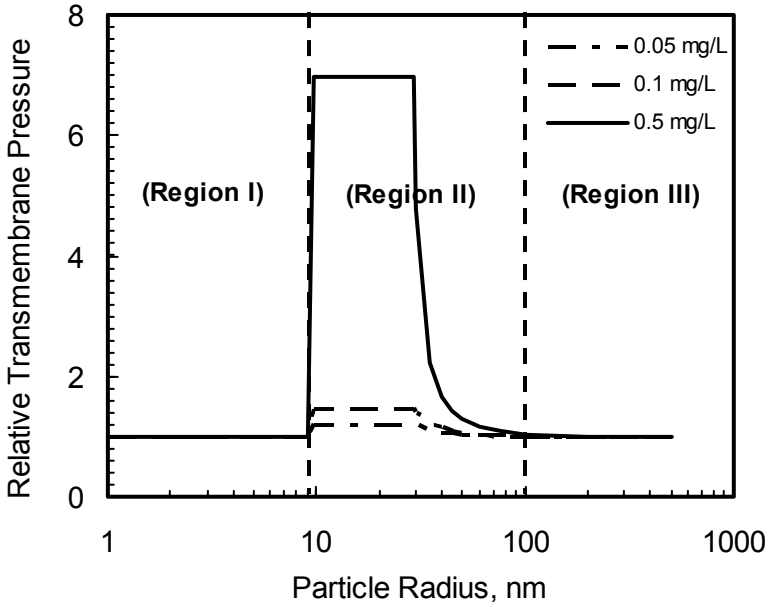

Figure 6-2. Model prediction of the increase of relative transmembrane pressure as a function of NOM size at low concentrations. Model inputs: $\alpha_{pm} = 1$, $\alpha_{pp} = 0$, D_m (pore diameter) = 58 nm, and V_s (permeate throughput) = 150 L/m^2; comparable to experimental conditions. Only fouling by pore blocking and pore constriction were considered. Regions I, II, and III are dominated by pore constriction, pore blocking, and cake layer formation, respectively.

Figure 6-2 illustrates the simulated relationship between the size of NOM moieties and the magnitude of membrane fouling as a result of irreversible pore blocking

and constriction at different NOM concentrations. The results show that substantial irreversible fouling (i.e., approximately 50 percent increase in the transmembrane pressure) can occur even when the concentration of the NOM moieties is as low as 0.1 mg/L or 0.05 mg/L as DOC; given suitable sizes. NOM moieties at such a low concentration are easily ignored in conventional analyses. However, they are extremely important for proper understanding of NOM fouling of MF membranes. This becomes a new challenge to the techniques employed to study the composition of aquatic NOM, including those "minor" fractions that don't contribute much to the total carbon pool.

6.5 Implications for the Transport of Colloids and NOM in Synthetic Porous Media

The fouling of polymeric membranes is in principle a special transport phenomenon involving different aquatic materials and their physical, chemical, and biological properties at the interface of water and polymeric porous media. An important finding of this study was the important role of NOM moieties in such systems. Based on the study, the role of NOM includes two major aspects: one is as part of the colloids that directly participate in the transport processes, and the other is as "conditioners" of the polymer/water interfaces that affect the chemical attachment and transport of colloids.

The existence and relevance of colloidal sized NOM moieties with radii of dozens of nm have been discussed again and again in previous sections. The transport and attachment of these particles inside the porous body of MF membranes result in the change of membrane pore structures, thereby reducing their hydraulic permeability. This was considered the origin of membrane fouling in this study. Due to their relative small

sizes and low permeation velocities, the transport of these particles in membrane pores is dominated by Brownian diffusion in the radial direction and by convection in the axial direction. In contrast to this relatively simple picture of physical transport, the mechanism for their chemical attachment to polymeric surface remains unclear although the trend observed experimentally appears consistent with the concept of so-called "hydrophobic" interaction.

The role of aquatic NOM as surface "conditioners" was clearly demonstrated in the colloidal fouling experiments. For 19 nm latex particles, the presence of 1 mg C/L DSW NOM and 0.001 M $CaCl_2$ significantly reduced their attachment on the hydrophobic PVDF membrane surfaces and therefore reduced membrane fouling. This finding implies that the sorption of aquatic NOM is likely to have strong impacts on the physicochemical properties of polymer/water interfaces. As a result, the chemical attachment and transport of colloids smaller than pore dimensions may be different with/without aquatic NOM. The presence of such effects is possibly relevant to other studies related to the colloidal stability and environmental fate of "nanoparticles" (diameter < 100 nm). Given the ubiquitous presence of NOM in natural aquatic systems, model systems in the absence of NOM may or may not properly reflect the true natural processes. Consequently, some results reported in other studies may be misleading. This is an important question as the environmental impact of nanoparticles is drawing more and more attention from scientists and policy makers.

6.6 RECOMMENDATION FOR FUTURE WORKS

Based on these discussions, the following works are proposed to be conducted in the future.

6.6.1 Membrane Fouling in Heterogeneous Systems

Throughout the entire study, MF membrane fouling was treated as the behaviors of monodisperse particle suspensions applied to membranes with uniform pore structures, for the purpose of simplicity. The potential impacts of system heterogeneity were overlooked. For instance, the change of membrane porosity due to the attachment of one type of material may directly affect the rejection of another type of material and their fouling behavior, which has been proposed by other researchers [54, 97]. On the other hand, the pore size distribution of MF membranes is very likely to influence the magnitude of membrane fouling, which is understandable based on the importance of relative particle sizes found in the study.

In order to investigate this question, it is proposed, from a modeling aspect, to improve the current model by taking into account the heterogeneity of membrane pores and aquatic particles in three steps: 1) considering particle and pore size distributions, 2) considering particles and pores with identical sizes but different chemical attachment probabilities, and 3) combining 1) and 2). Given the availability of model particles, polystyrene latex particles are recommended as the surrogate of natural colloids in model validation. The mixture of different latex particles from the three size ranges with different fouling mechanisms is suitable for the study of the size heterogeneity of particle foulants, whereas the mixture of particles with different surface properties and physiochemical stabilities is good for the investigation of chemical heterogeneity. Size

fractionation technique is also necessary in order to identify the removal of different sized particles in a mixture. The effect of NOM and calcium on membrane fouling can also be experimentally assessed.

6.6.2 Characterization of Colloidal Materials in Aquatic Environment

In aquatic environments, the presence of colloidal materials, including colloidal NOM, has been observed by many researchers. In addition to those introduced in Chapter One, Ledin *et al.* [98] reviewed several works in this area. It was found that a combination of different analytical techniques is imperative in order to overcome their individual defects. This is true based on this study. In the analyses conducted, the prefiltration using GF/C glass fiber provided a coarse separation of micron and submicron sized aquatic materials. At the next level, environmental SEM revealed the presence of colloidal particles (20 μm and above) in the prefiltered Dismal Swamp water, and their attachment on the surfaces of PVDF membranes. After that, AFM operated in the tapping mode showed the accumulation of small aquatic materials (a few nm in height) at a graphite/water interface under different chemical conditions. Unfortunately, these techniques focused on different particle size ranges, and did not provide information on the chemistry of these materials. In comparison, the combination of size exclusion chromatography (SEC) and a variety of analytical tools (e.g., UV, TOC, fluorescence spectrometry, TON, and NMR) generated information on both apparent size and chemistry of aquatic materials, from small organic acids to high molecular weight macromolecules or organic colloids. Some shortcomings of this technique are, however, the limitation on the upper detectable size range, inadequate sensitivity for dilute organic

fractions, and lack of interpretation of physiochemical stability of aquatic materials. Therefore, future studies should be conducted in order to find a suitable approach to quantify the amount of aquatic colloidal materials (especially those in the size range of 10 – 100 nm) in a given water sample and their "stickiness" to different surfaces of concern. If the results of this study are assessed in an opposite way, a low pressure membrane filtration system with well characterized physical and chemical properties may be a plausible choice for the separation and quantification of these aquatic colloidal materials. If proper techniques can be developed to effectively recover these materials from the membrane surfaces, additional chemical tools may be applied to probe their physiochemical, chemical, and biological properties.

6.6.3 Understanding the Nature of Physiochemical Interactions at Polymer/Water Interfaces

The study clearly showed the importance of chemical attachment in the fouling of MF membranes. However, the nature of the physiochemical interactions involved is still to be determined. A deep understanding in this area is beneficial to the development of effective strategies for fouling control.

Lacking clear theoretical information, experimental work is proposed as the first step in this regard. Column experiment may be used to study the attachment and detachment of surrogate colloidal particles under systematically varied hydrodynamic and chemical conditions. The use of surrogate colloidal particles, such as latex particles, can simplify the techniques required for quantitative measurement of particle concentration in each filtration region. The packing materials of the column can be

polymeric resins that have compositions similar to those of the membranes. The size of the resin grains should be in millimeters so that the dimension of inter-grain space is significantly greater than that of surrogate particles. The role of aquatic NOM on the deposition of colloidal particles can be addressed in such tests as well. Experimental particle-membrane attachment probabilities can be obtained from this test, together with their dependence on media properties and solution chemistry.

More fundamental study may be performed by direct determination of related interfacial interactions in aqueous systems. Potential techniques for this purpose include AFM and the cohesive force apparatus. AFM is probably the best available technique. The key issues in this regard may include the availability of smooth base materials that are chemically comparable to the membranes and the fixture of NOM and/or colloidal materials on the tip. Unlike nanofiltration (NF) and reverse osmosis (RO) membranes, MF and other low pressure membranes have relatively rough surfaces for AFM measurement as found in other studies [58]. Therefore, direct force measurement for MF membranes is not as convenient as that for NF or RO membranes. This is perhaps why the related reports (e.g, [53]) have been almost exclusively on the latter. As a result of this difference, a surrogate material with smooth surfaces, such as polymeric thin films, should be used in the place of real MF membranes.

The aforementioned advance in the chemical modification of MF membranes makes the task more difficult. These proprietary modifications substantially changed the interfacial properties of MF membranes. In consequence, suitable surrogate materials are unlikely to exist for these modified membranes. Therefore, information obtained from column experiment and direct force measurement may or may not be applicable to these

new membranes. However, a comparison of two sets of information will still be valuable for the understanding of fouling mechanisms.

6.6.4 Membrane Modification Study

The problems mentioned in the previous section may be to a certain extent addressed by modifying the surface properties of the standard PVDF membranes. The most convenient approach is probably to cover the membrane surface using a surfactant such as SDS. The work of Bielska and Szymanowski [99] showed that filtration of SDS and another surfactant, even above their critical micelle concentrations, did not change the permeability of three UF membranes after their surfaces were coated. It is expected that the adsorption of SDS should hydrophilize the hydrophobic membrane and introduce negative charged sulfate groups on its surface. Thus, it will be interesting to investigate if this physiochemical modification can reduce the attachment of negatively charged hydrophobic colloidal particles, as well as different NOM components on membrane surfaces, thereby reducing membrane fouling.

For practical purposes, the hydrophilization of membrane surfaces by physiochemical adsorption is unlikely to be permanent since the surfactant can be slowly released into the aqueous phase. Therefore, the introduction of sulfate and other functional "non-reactive" (with respect to, e.g., divalent ions) functional groups chemically should be a better choice. How to achieve this goal is an interesting topic for long-term study.

6.6.5 Understanding the Hydrodynamic Aspects of Membrane Fouling

In order to be able to focus on the chemical aspects of membrane fouling, the hydrodynamic conditions were fixed throughout the study. On the other hand, the importance of permeation flux on the fouling of MF and UF membranes has been reported for both colloidal and macromolecular fouling of these membranes. Some related studies have been introduced in Chapter One. The preliminary work performed at the beginning of the study showed some positive correlation between NOM fouling and permeation flux at a relative low flux range (less than 8.5 LMH) and in the absence of calcium. However, the effect seemed to be insignificant when the permeation flux was above this level where the majority of the fouling experiments were conducted.

Overall, it is anticipated that the existence of the critical flux for membrane fouling is dependent on the balance between hydrodynamic drag and repulsive surface interactions, as found on NF membranes [100]. For MF membranes, this coupled chemical and hydrodynamic effect is more likely to occur when surface fouling (pore blocking and/or cake layer formation) is the dominant fouling mechanism. In comparison, the effect should be less extensive when the fouling is predominantly pore constriction caused by aquatic contaminants with radii smaller than a sixth of the pore diameter. It will be interesting and practically useful to test this assumption in future studies. It would be easier to start with colloidal fouling than with NOM fouling since the properties of synthetic particles are better known. Theoretically, the results of this type of study can provide insight into the relationship of particle-membrane attachment probability and hydrodynamic drag force, and improve the model established in this study.

Appendix: a Modified Hermia Model for Constant Flux Microfiltration

A.1 INTRODUCTION

A blocking model based simply on some ideal fouling conditions have been used in evaluating the fouling of membranes by various types of dispersions with complex compositions since it was first established by Hermia [63]. The characteristic form of the model is:

$$\frac{d^2t}{dV^2} = k\left(\frac{dt}{dV}\right)^n$$

where t and V are the filtration time and cumulative permeate volume, respectively, and k and n are two model parameters. In them, n is the most important one that is directly related to blocking mechanisms; t and V can be easily obtained in membrane filtrations. Schematic diagrams of the four fouling modes proposed by Hermia are presented in Figure A-1.

A feature or advantage of the model is that they clearly define several ideal but relevant fouling conditions (or boundaries for non-ideal situations) as a result of various types of pore blockages and cake layer formation. The deviation of real fouling data from these ideal conditions is attributed to the complicated nature of membrane filtration systems and the coincidence of different types of fouling. Another feature of the model is that it does not explicitly reply on the information of foulant rejection. For constant pressure filtration, experimental data on cumulative permeate volume and filtration time are sufficient in implementation of the model for the purpose of data evaluation. Although unable to give us detailed pictures of membrane fouling, mostly as a result of lack of foulant rejection information, the model provides a useful tool to evaluate the real

data and point out the directions needed for further mechanistic studies. Indeed, the combination of the model with other experimental techniques, such as in-situ characterization of fouling layers, may be used to explore the fouling mechanism relevant to membrane filtration of natural waters.

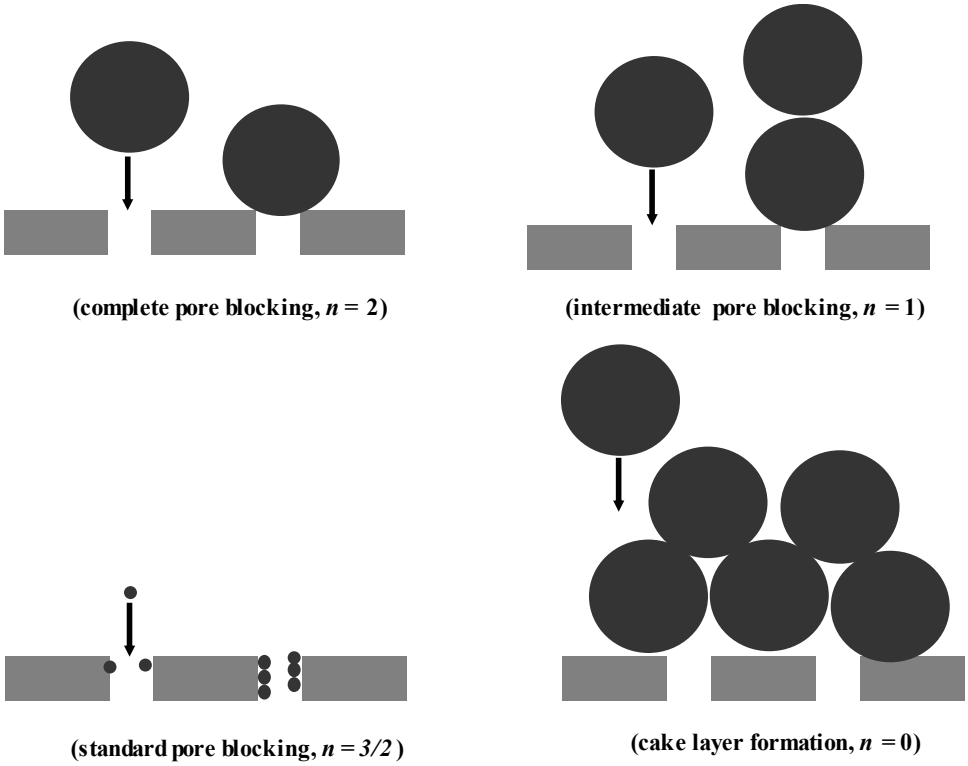

Figure A-1. Schematic diagrams of the four modes of membrane fouling proposed by Hermia.

An important limitation of the original model developed by Hermia is, however, that it was derived solely for constant pressure systems. Therefore, (dt/dV) is used as the basic parameter to evaluate fouling rate. In contrast, most low pressure membrane filtration systems nowadays are designed and operated in the constant flow mode, i.e., the permeate flow rate remains constant throughout the filtration process. In this case, (dt/dV) is constant, and the secondary derivative d^2t/dV^2 becomes zero, regardless of the variation

of other model parameters. Therefore, the abovementioned original form of Hermia model becomes invalid. In order to apply the model to constant flow filtration, the basic expressions of the model has to be revised by integrating the constant flow condition. This is elucidated step by step in this Appendix.

A.2 THE MODIFIED HERMIA MODEL FOR CONSTANT FLUX FILTRATION

A.2.1 Complete Pore Blocking

Complete pore blocking occurs when all particles reaching the membrane only participate in the "sealing" of membrane pores (see Figure A-1). This idealized assumption assumes that none of these particles would stay on top of other particles. Therefore, the area of membrane surfaces with open pores (A_t) decreases linearly with the amount of particles reaching the membrane or with the projected area of the particles on membrane surface (A_p). For a given particle suspension, the latter can be expressed as:

$$A_p = \sigma m_f \tag{A1}$$

where m_f [kg] is the mass of particles that attach to membrane surfaces and cause fouling, σ [m^2/kg] is the projected area of these particles on membrane surface normalized to unit mass of particles, a characteristic of the suspension.

For a monodisperse suspension,

$$\sigma = \frac{1.5}{\rho d \psi} \tag{A2}$$

where ρ [kg/m^3] is the particle density, d [m] is the diameter of particles, and ψ [dimensionless] is the shape factor ($0 < \psi \leq 1$). As an example, if the membrane pores are completely blocked by a model water containing monodispersed spherical particles

with a density of 1.055×10^3 kg/m^3 and a diameter of 10^{-7} m, the corresponding value of σ is then 1.42×10^4 m^2/kg. For non-spherical particles, σ becomes greater as ψ is less than unity.

Further, A_t can be expressed as:

$$A_t = A_0 - A_p = A_0 - \sigma m_f \tag{A3}$$

here A_0 is the initial surface area of the membrane. Hence,

$$\frac{dA_t}{dm_f} = -\sigma \tag{A4}$$

The transmembrane pressure required to drive the permeate through the membrane (P) is related to the permeate flowrate (Q) and A_t following Darcy's law:

$$Q = \frac{PA_t}{\mu R_m} \tag{A5}$$

where R_m [m^{-1}] is the hydraulic resistance of the membrane. For constant flow membrane filtration, Q remains constant during filtration and P increases as a result of membrane fouling. At any time during the filtration, $PA_t = P_0A_0$ as shown in Eqn (A5), where P_0 and A_0 are the initial transmembrane pressure and the pore area of the membrane surface, respectively. Now, we can define the characteristic rate of fouling in constant flow membrane filtration as dP/dm_f, which states how fast the transmembrane pressure would increase per unit mass of aquatic materials being filtered. It is related to the decrease of membrane open area as follows:

$$\frac{dP}{dm_f} = \frac{d}{dm_f}\left(\frac{\mu R_m Q}{A_t}\right) = -\left(\frac{\mu R_m Q}{A_t^2}\right)\frac{dA_t}{dm_f} = -\left(\frac{P^2}{P_0 A_0}\right)\frac{dA_t}{dm_f} \tag{A6}$$

By inserting Eqn (A4) into Eqn (A6), we have:

$$\frac{dP}{dm_f} = \left(\frac{\sigma}{P_0 A_0}\right) P^2 \qquad \text{(A7)}$$

Eqn (A7) can be further simplified by introducing two normalized parameters, P' and m_f':

$$\frac{dP'}{dm_f'} = \sigma P'^2 \qquad \text{(A8)}$$

where P' and m_f' are defined as follows:

$$P' = \frac{P}{P_0} \text{ and } m_f' = \frac{m_f}{A_0}$$

A.2.2 Intermediate Pore Blocking Model

In the case of intermediate pore blocking (see Figure A-1), each particle reaching the membrane may not only block membrane pores as in the case of complete pore blocking, but also attach to other particles that have already been on the membrane surface. It is assumed, however, that the fouling is only contributed by particles blocking membrane pores. This means that the existing particles on the membrane surface serve as competitors to membrane pores and reduce the actual number of approaching particles that can indeed block pores. Therefore, we only need to incorporate an analysis of pore blocking probability into the previous discussion of complete pore blocking. The probability for a particle to block membrane pores at any time is equivalent to the ratio of the remaining open area, A_t, to the initial total open area, A_0. Hence, the decrease of the membrane open area as a unit mass of particles being retained can be expressed as:

$$\Delta A_t = -\sigma \Delta m_f \left(\frac{A_t}{A_0}\right) \qquad \text{(A9)}$$

Eqn (A9) can be written in a differential form:

$$\frac{dA_t}{dm_f} = -\sigma\left(\frac{A_t}{A_0}\right) \tag{A10}$$

Solving this equation with a boundary condition of $A_t = A_0$ at $V = 0$, we have:

$$A_t = A_0 \exp\left(-\frac{\sigma m_f}{A_0}\right) \tag{A11}$$

By bringing Eqn (A11) into Eqn (A6) and also recognizing that:

$$\frac{P_0}{P} = \frac{A_t}{A_0} = \exp\left(-\frac{\sigma m_f}{A_0}\right) \tag{A12}$$

the fouling rate in the case of intermediate blocking is thus obtained:

$$\frac{dP}{dm_f} = \left(\frac{\sigma}{A_0}\right)P \tag{A13}$$

Or:

$$\frac{dP'}{dm_f'} = \sigma P' \tag{A14}$$

A.2.3 Standard Pore Blocking

As shown in the figure, standard pore blocking results from the shrinkage of membrane pores by particles attached to the pore walls. We first assume that the membrane consists of N uniform cylindrical pores with a radius of r_0 and a length of L. Next, it is assumed that the radius of the pores decreases at the same rate as particles attach to their walls. Then, the following mass balance relationship is established to determine the effective pore radius after fouling (r):

$$N\pi\left(r_0^2 - r^2\right)L = \frac{m_f}{\rho} \tag{A15}$$

With aforementioned assumptions, the transmembrane pressure of the membrane is invertly proportional to the radius of the pores following Poiseuille's equation:

$$P = \frac{8\mu LQ}{N\pi} \cdot \frac{1}{r^4} \tag{A16}$$

Consequently, the normalized transmembrane pressure is simply:

$$P' = \frac{P}{P_0} = \frac{r_0^4}{r^4} \tag{A17}$$

By combining Eqns (A15)–(A17), we obtain:

$$\frac{dP'}{dm_f'} = \left(\frac{2}{L\rho}\right) P'^{3/2} \tag{A18}$$

A.2.4 Cake Filtration Model

Unlike pore blocking, the cake filtration type of fouling does not involve any changes to the pore structure of membranes. Instead, the increase of hydraulic resistance encountered during membrane filtration is caused by the formation of a cake layer on top of the membrane surface (see Figure A-1). The cake layer resistance, R_c [m^{-1}] , is usually expressed as:

$$R_c = \hat{R}_c \frac{m_f}{A_0} \tag{A19}$$

where $\hat{R}_c$ [m/kg] is the specific resistance of cake layers. Again, by applying Darcy's law, we have:

$$P = \frac{Q\mu\left(R_m + R_c\right)}{A_0} \text{ and } P_0 = \frac{Q\mu R_m}{A_0} \tag{A20}$$

Since R_m remains constant, it is easy to obtain the fouling rate by combining Eqns (A19) and (A20):

$$\frac{dP}{dm_f} = \frac{Q\mu\hat{R}_c}{A_0^{\,2}} \tag{A21}$$

or the normalized form:

$$\frac{dP'}{dm_f'} = \frac{\hat{R}_c}{R_m} \tag{A22}$$

The RHS of the expression above is independent of the transmembrane pressure if the cake is incompressible and $\hat{R}_c$ remains constant. R_m is usually independent of the pressure for low pressure membranes, while for high pressure membranes, it is also more or less stable as constant pressure filtration is commonly used in these cases.

A.2.5 The Unified Expression

Eqns (A8), (A14), (A18), and (A22) can be written into a unified simple expression as follows:

$$\frac{dP'}{dm_f'} = kP'^{n} \tag{A23}$$

The meanings of k and n in different types of fouling are presented in Table A-1. It is noteworthy that the n values are the same as those found in the constant pressure model developed by Hermia for all types of membrane fouling. This indicates that the operating conditions (constant pressure versus constant flow) do not affect the way in which membranes are fouled as long as the assumed conditions used to obtain the model are met. Moreover, as seen in the table, the fouling rate always increases with increasing transmembrane pressure during membrane filtration except for cake filtration. On the

other hand, the k parameter is a function of the physical properties of both the suspension (e.g., $\hat{R}_c$ and ρ) and the membrane (e.g., L and R_m) for cake filtration and standard blocking. Comparatively, its value is solely dependent on σ, a physical parameter describing suspension properties for complete and intermediate blocking, and the properties of membranes appears unimportant if they reject the same foulants in water at the same efficiency. As seen in Eqn (A23), the efficiency of complete or intermediate pore blocking becomes greater as the size of foulants decreases, given the same mass concentration.

Table A-1. The meanings of paramters k and n in the generalized fouling model

Fouling Type	k	n
Cake filtration	$\frac{\hat{R}_c}{R_m}$	0
Intermediate blocking	σ	1
Standard blocking	$\frac{2}{L\rho}$	3/2
Complete blocking	σ	2

A.2.6 Incorporation of Foulant Rejection Relationship

In the absence of foulant rejection data, Hermia implicitly assumed that the rejection of foulants by the membrane is *always complete* throughout the filtration process. This assumption leads to a simple relationship of:

$$m_f' = \left(C_{feed} - C_{permeate}\right)V_s = C_f V_s \qquad \text{(A24)}$$

Here C_f is the concentration of foulants in the feedwater and remains constant during filtration. By introducing this relationship into Eqn (A23), we have:

$$\frac{dP'}{dV_s} = k'P'^n \qquad \text{(A25)}$$

where V_s is the cumulative volume of the permeate normalized to membrane surface area and is usually called permeate throughput, and k' is simply C_f multiplied by the corresponding expressions given in Table A-1.

A.2.7 A Unified Function for Constant Pressure/Flux Filtration

Eqn (A25) may be further converted into a function of normalized specific permeate flux, J_s', by introducing the definition of specific flux:

$$J_s = \frac{J}{P} \tag{A26}$$

where J is the permeate flux; now we have:

$$J_s' = \frac{J_s}{J_{s0}} = \frac{1}{P'} \tag{A27}$$

Bringing Eqn (A27) into Eqn (A25), we obtain:

$$-\frac{dJ_s'}{dV'} = k' J_s'^{2-n} \tag{A28}$$

Due to the definition of specific flux, the Hermia model for constant pressure systems can also be easily converted into a form like Eqn (A28). Therefore, Eqn (A28) is a unified form of the Hermia model applicable to both constant flux and constant pressure systems.

A.2.8 Model Linearization

If the value of n is introduced based on the above-mentioned fouling mechanisms, Eqns (A25) and (A28) can be converted into two sets of linear equations after integration.

The results are summarized in Table A-2. It is worth mentioning again that the linear equations derived from Eqn (A28) are also valid for constant pressure filtration.

Table A-2. Linear Forms of the modified Hermia Model for Constant Flux Membrane Filtration

Fouling Mechanism	n	Eqn (A25)	Eqn (A28)
Cake Formation	0	$P' = 1 + k'V_s$	$1/J_s' = 1 + k'V_s$
Intermediate blocking	1	$\ln P' = k'V_s$	$\ln J_s' = -k'V_s$
Standard blocking	3/2	$P'^{-\frac{1}{2}} = 1 - \frac{k'}{2}V_s$	$J_s'^{\frac{1}{2}} = 1 - \frac{k'}{2}V_s$
Complete blocking	2	$\frac{1}{P'} = 1 - k'V_s$	$J_s' = 1 - k'V_s$

List of Symbols

Symbol	Unit	Physical Meaning
α_{pm}	dimensionless	the probability for a particle to attach onto the membrane surface after the collision
α_{pp}	dimensionless	the probability for a particle to attach another particle after collision
β_S	dimensionless	the probability for a particle to collide with the solid area of membrane external surfaces
β_P	dimensionless	the probability for a particle to collide with the pores on membrane external surfaces
β_{pp}	dimensionless	the probability for a particle to collide with other particles on membrane external surfaces
ε_s	dimensionless	surface porosity of membrane outside surfaces
Φ_{out}	M	outer diameter of membrane fibers
Φ_{in}	M	inner diameter of membrane fibers
ρ_m	kg/m^3	bulk density of membrane materials
ρ	kg/m^3	density of foulants
σ	m^2/kg	the projected area of a unit mass of the particles on membrane
a	M	foulant particle radius
A_m	m^2	total geometric area of the membrane outside surface (for outside-in membranes)
A_t	dimensionless	the total uncovered membrane surface area
$A_{w,1}$	m^2	the total open area on the wall of one membrane pore
B	m^{-2}	a mass transfer coefficient for particles inside membrane pores
C_a	kg/m^3	mass concentration of particles at a distance of the particle radius from the centerline of the membrane pores, $r=a$

Symbol	Unit	Physical Meaning
$C_{a,l}$	kg/m^3	particle concentration C_a at a distance of l from the pore entrance
C_f	kg/m^3	mass concentration of particles in the feedwater
C_{in}	kg/m^3	the mean mass concentration of particles at the inlet of a membrane pore
C_{out}	kg/m^3	the mean mass concentration of particles at the outlet of a membrane pore
D_m	M	membrane pore diameter
D_p	m^2/s	diffusion coefficient of particles in water
J	m/s	permeate flux used in dead-end membrane filtration
$J_{p,r}$	kg/m^2-s	particle flux moving towards membrane pore walls in the radial direction at a radius of r from the centerline
l	M	distance inside from the entrance of a cylindrical pore
L_m	M	effective length of membrane pores
m_c	kg/m^2	the total mass of particles in the cake layer per unit membrane surface area
m_f'	kg/m^2	total mass of foulants per unit membrane surface area
m_p	kg/m^2	the total mass of particles attaching to membrane pores per unit membrane surface area
m_t	kg/m^2	the total mass of particles delivered to a unit membrane surface area
$m_{w,1}$	Kg	the total mass of particles attaching to the wall of one membrane pore
m_w	kg/m^2	the total mass of particles attaching to membrane pore walls per unit membrane surface area
N_m	m^{-2}	number density of membrane pores per a unit membrane surface area
P'	dimensionless	relative transmembrane pressure (transmembrane pressure during filtration normalized to that of clean membranes)

Symbol	Unit	Physical Meaning
Q_1	m^3/s	permeate flowrate in one membrane pore
Q	m^3/s	permeate flowrate through the entire membrane or module
r	M	radial distance from the centerline of a cylindrical membrane pore
R_m	m^{-1}	hydraulic resistance of clean membranes without fouling
V_1	m^3	cumulative permeate volume through one membrane pore
V_s	m^3/m^2	permeate throughput (cumulative volume of permeate per unit membrane surface area)

References

[1] Baker, R.W., *Membrane Technology and Applications*. 1 ed. Vol. 1. 2000: McGraw-Hill. 509.

[2] US-EPA, *Low-pressure membrane filtration for pathogen removal: application, implementation and regulatory issues*. 2001, United States Environmental Protection Agency: Cincinnati, Ohio.

[3] Laine, J.M., D. Vial, and P. Moulart, *Status after 10 years of operation - overview of UF tehcnology today.* Desalination, 2000. **131**: p. 17-25.

[4] Madaeni, S.S., *The application of membrane technology for water disinfection.* Water Research, 1999. **33**(2): p. 301-308.

[5] Fiksdal, L. and T. Leiknes, *The effect of coagulation with MF/UF membrane filtration for the removal of virus in drinking water.* Journal of Membrane Science, 2006. **279**: p. 364-371.

[6] Schafer, A.I., *Natural Organics Removal Using Membranes: Principles, Performance and Cost*. 1 ed. Vol. 1. 2001, Lancaster, PA 17604: Technomic Publishing Company, Inc. 406.

[7] Shih, M.C., *An overview of arsenic removal by pressure-driven membrane processes.* Desalination, 2005. **172**(1): p. 85-97.

[8] Wend, C.F., P.S. Stewart, W. Jones, and A.K. Camper, *Pretreatment to membrane water treatment systems, a laboratory study.* Water Research, 2003. **37**(14): p. 3367-3378.

[9] Marina, B.J., *Reverse-osmosis technology for waste-water reuse.* Water Science and Technology, 1991. **24**(9): p. 215-227.

[10] Mulder, M., *Basic Principles of Membrane Technology*. 2 ed. Vol. 1. 1996, The Netherlands: Kluwer Academic Publishers. 52-58.

[11] Wilkinson, K.J., A. Joz-Roland, and J. Buffle, *Different Roles of Pedogenic Fulvic Acids and Aquagenic Biopolymers on Colloid Aggregation and Stability in Freshwaters.* Limnology and Oceanography, 1997. **42**(8): p. 1714-1724.

[12] Biber, M.V., F.O. Gulacar, and J. Buffle, *Seasonal variations in principal groups of organic matter in a eutrophic lake using pyrolysis/GC/MS.* Environmental Science & Technology, 1996. **30**(12): p. 3501-3507.

[13] Meyer, J.L., *Production and utilization of dissolved organic carbon in riverine ecosystems*, in *Organic Acids in Aquatic Ecosystems*, E.M. Perdue and E.T. Gjessing, Editors. 1989, Wiley-Interscience: New York. p. 281-299.

[14] Wilkinson, K.J., E. Balnois, G.G. Leppard, and J. Buffle, *Characteristic features of the major components of freshwater colloidal organic matter revealed by transmission electron and atomic force microscopy.* Colloids and Surfaces a-Physicochemical and Engineering Aspects, 1999. **155**(2-3): p. 287-310.

[15] Dempsey, B.A. and C.R. O'Melia, *Proton and calcium complexation of four fulvic acid fractions*, in *Aquatic and Terrestrial Humic Materials*, R.F. Christeins and E.T. Gressing, Editors. 1983, Ann Arbor Science. p. 239-273.

[16] Elkins, K.M. and D.J. Nelson, *Fluorescence and FT-IR spectroscopic studies of Suwannee river fulvic acid complexation with aluminum, terbium and calcium.* Journal of Inorganic Biochemistry, 2001. **87**: p. 81-96.

[17] Meier, M., K. Namjesnik-Dejanovic, P.A. Maurice, Y.-p. Chin, and G.R. Aiken, *Fractionation of Aquatic Natural Organic Matter upon Sorption to Goethite and Kaolinite.* Chemical Geology, 1999. **157**: p. 275-284.

[18] Perminova, I.V., F.H. Frimmel, A.V. Kudryavtsev, N.A. Kulikova, G. Abbt-Braun, S. Hesse, and V.S. Petrosyan, *Molecular weight characteristics of humic substances from different environments as determined by size exclusion chromatography and their statistical evaluation.* Environmental Science & Technology, 2003. **37**(11): p. 2477-2485.

[19] Au, K.-K., A. Penisson, S. Yang, and C.R. O'Melia, *Natural organic matter at oxide/water interfaces: Complexation and conformation.* Geochimica et Cosmochimica Acta, 1999. **63**(19/20): p. 2903-2917.

[20] Jones, K.L. and C.R. O'Melia, *Protein and humic acid adsorption onto hydrophilic membrane surfaces: effects of pH and ionic strength.* Journal of Membrane Science, 2000. **165**(1): p. 31-46.

[21] Dumon, S. and H. Barnier, *Ultrafiltration of Protein Solutions on Zro2 Membranes - the Influence of Surface-Chemistry and Solution Chemistry on Adsorption.* Journal of Membrane Science, 1992. **74**(3): p. 289-302.

[22] Zydney, A.L. and N.S. Pujar, *Protein transport through porous membranes: effects of colloidal interactions.* Colloids and Surfaces a-Physicochemical and Engineering Aspects, 1998. **138**(2-3): p. 133-143.

[23] Tipping, E., *Cation Binding by Humic Substances*. Cambridge Environmental Chemistry Series, ed. P.G.C. Campbell, R.M. Harrison, and S.J. de Mora. Vol. 12. 2002, Cambridge: Cambridge University Press. 434.

[24] Carroll, T., S. King, S.R. Gray, B.A. Bolto, and N.A. Booker, *The fouling of microfiltration membranes by NOM after coagulation treatment.* Water Research, 2000. **34**(11): p. 2861-2868.

[25] Fan, L.H., J.L. Harris, F.A. Roddick, and N.A. Booker, *Influence of the characteristics of natural organic matter on the fouling of microfiltration membranes.* Water Research, 2001. **35**(18): p. 4455-4463.

[26] Lee, N., G. Amy, J.-P. Croué, and H. Buisson, *Identification and understanding of fouling in low-pressue membrane (MF/UF) filtration by natural organic matter (NOM).* Water Research, 2004. **38**: p. 4511-4523.

[27] Lee, N., G. Amy, and J.P. Croue, *Low-pressure membrane (MF/UF) fouling associated with allochthonous versus autochthonous natural organic matter.* Water Research, 2006. **40**(12): p. 2357-2368.

[28] Howe, K.J. and M.M. Clark, *Fouling of microfiltration and ultrafiltration membranes by natural waters.* Environmental Science & Technology, 2002. **36**(16): p. 3571-3576.

[29] Carroll, T., N.A. Booker, and J. Meier-Haack, *Polyelectrolyte-grafted microfiltration membranes to control fouling by natural organic matter in drinking water.* Journal of Membrane Science, 2002. **203**(1-2): p. 3-13.

[30] Chen, V., A.G. Fane, S. Madaeni, and I.G. Wenten, *Particle deposition during membrane filtration of colloids: Transition between concentration polarization and cake formation.* Journal of Membrane Science, 1997. **125**(1): p. 109-122.

[31] Chan, R. and V. Chen, *The effects of electrolyte concentration and pH on protein aggregation and deposition: critical flux and constant flux membrane filtration.* Journal of Membrane Science, 2001. **185**(2): p. 177-192.
[32] Yuan, W. and A.L. Zydney, *Humic acid fouling during microfiltration.* Journal of Membrane Science, 1999. **157**: p. 1-12.
[33] Kelly, S.T. and A.L. Zydney, *Mechanisms for Bsa Fouling during Microfiltration.* Journal of Membrane Science, 1995. **107**(1-2): p. 115-127.
[34] Ho, C.C. and A.L. Zydney, *Effect of membrane morphology on the initial rate of protein fouling during microfiltration.* Journal of Membrane Science, 1999. **155**(2): p. 261-275.
[35] Kim, A.S. and E.M.V. Hoek, *Cake structure in dead-end membrane filtration: Monte Carlo simulations.* Environmental Engineering Science, 2002. **19**(6): p. 373-386.
[36] Zhang, M. and L. Song, *Mechanisms and parameters affecting flux decline in cross-flow microfiltration and ultrafiltration of colloids.* Environmental Science & Technology, 2000. **34**(17): p. 3767-3773.
[37] Chellam, S., J.G. Jacangelo, and T.P. Bonacquisti, *Modeling and experimental verification of pilot-scale hollow fiber, direct flow microfiltration with periodic backwashing.* Environmental Science & Technology, 1998. **32**(1): p. 75-81.
[38] Endo, Y. and M. Alonso, *Physical meaning of specific cake resistance and effects of cake properties in compressible cake filtration.* Filtration and Separation, 2001(9): p. 43-46.
[39] Babel, S., S. Takizawa, and H. Ozaki, *Factors affecting seasonal variation of membrane filtration resistance caused by Chlorella algae.* Water Research, 2002. **36**(5): p. 1193-1202.
[40] Foley, G., *A review of factors affecting filter cake properties in dead-end microfiltration of microbial suspensions.* Journal of Membrane Science, 2006. **274**: p. 38-46.
[41] Kosvintsev, S., R.G. Holdich, I.W. Cumming, and V.M. Starov, *Modelling of dead-end microfiltration with pore blocking and cake formation.* Journal of Membrane Science, 2002. **208**: p. 181-192.
[42] Kosvintsev, S., I.W. Cumming, R.G. Holdich, D. Lloyd, and V.M. Starov, *Sieve mechanism of microfiltration separation.* Colloids and Surfaces A: Physicochemical and Engineering Aspects, 2004. **230**: p. 167-182.
[43] Yuan, W., A. Kocic, and A.L. Zydney, *Analysis of humic acid fouling during microfiltration using a pore blockage-cake filtration model.* Journal of Membrane Science, 2002. **198**(1): p. 51-62.
[44] Ho, C.C. and A.L. Zydney, *Transmembrane pressure profiles during constant flux. microfiltration of bovine serum albumin.* Journal of Membrane Science, 2002. **209**(2): p. 363-377.
[45] Srebnik, S., *Polymer adsorption on multicomponent surfaces with relevance to membrane fouling.* Chemical Engineering Science, 2003. **58**(23-24): p. 5291-5298.
[46] Israelachvili, J., *Intermolecular & Surface Forces*. 2nd ed. 1992, San Diego, CA 92101, USA: Academic Press Inc. 450.
[47] van Oss, C.J., *Interfacial Forces in Aqueous Media*. 1994, New York, New York 10016: Marcel Dekker, Inc. 440.

[48] Taniguchi, M., J.E. Kilduff, and G. Belfort, *Low fouling synthetic membranes by UV-assisted graft polymerization: monomer selection to mitigate fouling by natural organic matter.* Journal of Membrane Science, 2003. **222**: p. 59-70.
[49] Hester, J.F. and A.M. Mayes, *Design and performance of foul-resistant poly(vinylidene fluoride) membranes prepared in a single-step by surface segregation.* Journal of Membrane Science, 2002. **202**(1-2): p. 119-135.
[50] Wavhal, D.S. and E.R. Fisher, *Membrane surface modification by plasma-induced polymerization of acrylamide for improved surface properties and reduced protein fouling.* Langmuir, 2003. **19**(1): p. 79-85.
[51] Liu, Z.M., Z.K. Xu, J.Q. Wang, Q. Yang, J. Wu, and P. Seta, *Surface modification of microporous polypropylene membranes by the grafting of poly(gamma-stearyl-L-glutamate).* European Polymer Journal, 2003. **39**(12): p. 2291-2299.
[52] Yu, H.-Y., Y.-J. Xie, M.-X. Hu, J.-L. Wang, S.-Y. Wang, and Z.-K. Xu, *Surface modification of polypropylene microporous membranes to improve its antifouling property in MBR: CO_2 plasma treatment.* Journal of Membrane Science, 2005. **254**(1-2): p. 219-227.
[53] Brant, J.A. and A.E. Childress, *Colloidal adhesion to hydrophilic membrane surfaces.* Journal of Membrane Science, 2004. **241**(2): p. 235-248.
[54] Taniguchi, M., J.E. Kilduff, and G. Belfort, *Modes of natural organic matter fouling during ultrafiltration.* Environmental Science & Technology, 2003. **37**: p. 1676-1683.
[55] Causserand, C., M. Nystrom, and P. Aimar, *Study of Streaming Potentials of Clean and Fouled Ultrafiltration Membranes.* Journal of Membrane Science, 1994. **88**(2-3): p. 211-222.
[56] Ricq, L., A. Pierre, J.C. Reggiani, S. ZaragozaPiqueras, J. Pagetti, and G. Daufin, *Effects of proteins on electrokinetic properties of inorganic membranes during ultra- and micro-filtration.* Journal of Membrane Science, 1996. **114**(1): p. 27-38.
[57] Maartens, A., P. Swart, and E.P. Jacobs, *Humic membrane foulants in natural brown water: characterization and removal.* Desalination, 1998. **115**(3): p. 215-227.
[58] Lee, N., G. Amy, J.P. Croue, and H. Buisson, *Morphological analyses of natural organic matter (NOM) fouling of low-pressure membranes (MF/UF).* Journal of Membrane Science, 2005. **261**(1-2): p. 7-16.
[59] Schafer, A.I., U. Schwicker, M.M. Fischer, A.G. Fane, and T.D. Waite, *Microfiltration of colloids and natural organic matter.* Journal of Membrane Science, 2000. **171**: p. 151-178.
[60] Saha, N.K., M. Balakrishnan, and M. Ulbricht, *Polymeric memrane fouling in sugarcane juice ultrafiltration: role of juice polysaccharides.* Desalination, 2006. **189**: p. 59-70.
[61] Bowen, W.R. and A.O. Sharif, *Prediction of optimum membrane desig: pore entrance shape and surface potential.* Colloids and Surfaces A: Physicochemical and Engineering Aspects, 2002. **201**: p. 207-217.
[62] Brant, J.A., K.M. Johnson, and A.E. Childress, *Characterizing NF and RO membrane surface heterogeneity using chemical force microscopy.* Colloids and Surfaces a-Physicochemical and Engineering Aspects, 2006. **280**(1-3): p. 45-57.

[63] Hermia, J., *Constant pressure blocking filtration laws - application to power-law non-newtonian fluids.* Trans IChemE, 1982. **60**: p. 183-187.
[64] Laabs, C., G. Amy, and M. Jekel, *Organic colloids and their influence on low-pressure membrane filtration.* Water Science and Technology, 2004. **50**(12): p. 311-316.
[65] Sahimi, M., G.R. Gavalas, and T.T. Tsotsis, *Statistical and continuum models of fluid-solid reactions in porous media.* Chemical Engineering Science, 1990. **45**(6): p. 1443-1502.
[66] Clark, M., M, *Transport Modeling for Environmental Engineers and Scientists*. Environmental Science and Technology, ed. J.L. Schnoor and A. Zehnder. 1996, New York: John Wiley & Sons, Inc. 559.
[67] Chellam, S. and M.R. Wiesner, *Particle back-transport and permeate flux behavior in crossflow membrane filters.* Environmental Science & Technology, 1997. **31**(3): p. 819-824.
[68] Polyakov, Y.S., *Particle deposition in outside-in hollow fiber filters and its effect on their performance.* Journal of Membrane Science, 2006. **278**(1-2): p. 190-198.
[69] Kang, S.T., A. Subramani, E.M.V. Hoek, M.A. Deshusses, and M.R. Matsumoto, *Direct observation of biofouling in cross-flow microfiltration: mechanisms of deposition and release.* Journal of Membrane Science, 2004. **244**(1-2): p. 151-165.
[70] Huang, H., N. Lee, C.R. O'Melia, G. Amy, and J.G. Jacangelo. *Bench scale evaluation of the fouling of low pressure, hollow fiber membranes by different types of natural organic matter*. in *American Water Works Association Membrane Technology Conference*. 2005. Phoenix, Arizona, USA: American Water Works Association.
[71] Tiller, C.L. and C.R. O'Melia, *Natural organic matter and colloidal stability: models and measurements.* Colloids and Surfaces A: Physiochemical and Engineering Aspects., 1993. **73**: p. 89-102.
[72] Duclos-Orsello, C., W.P. Kelly, D.C. Grant, J. Zahka, and V. Thom, *Neutral adsorptive capture of particles by membranes: network modeling near the membrane isoelectric point.* Journal of Membrane Science, 2004. **237**: p. 167-180.
[73] Polyakov, Y.S., *Deadend outside-in hollow fiber membrane filter: Mathematical model.* Journal of Membrane Science, 2006. **279**(1-2): p. 615-624.
[74] Leenheer, J.A. and J.P. Croue, *Characterising aquatic dissolved organic matter.* Environmental Science & Technology, 2003. **37**(1): p. 18A-26A.
[75] Spinette, R., *(Unpublished)*. 2003, Johns Hopkins University.
[76] Gorham, J. and H. Fairbrother, *(Unpublished)*. 2005, Johns Hopkins University.
[77] Shin, J.Y., *Packed bed filtration in potable water treatment: Pretreatment chemistry for the removal of particles and natural organic matter*, in *Department of Geography and Environmental Engineering*. 2005, Johns Hopkins University: Baltimore, Maryland. p. 311.
[78] Allpike, B.P., A. Heitz, C.A. Joll, R.I. Kagi, G. Abbt-Braun, F.H. Frimmel, T. Brinkmann, N. Her, and G. Amy, *Size exclusion chromatography to characterize DOC removal in drinking water treatment.* Environmental Science & Technology, 2005. **39**(7): p. 2334-2342.

[79] Peuravuori, J. and K. Pihlaja, *Molecular size distribution and spectroscopic properties of aquatic humic substances.* Analytica Chimica Acta, 1997. **337**(2): p. 133-149.
[80] Berestovsky, G.N., V.I. Ternovsky, and A.A. Kataev, *Through pore diameter in the cell wall of Chara corallina.* Journal of Experimental Botany, 2001. **52**(358): p. 1173-1177.
[81] Au, K.K., S.L. Yang, and C.R. O'Melia, *Adsorption of weak polyelectrolytes on metal oxide surfaces: A hybrid SC/SF approach.* Environmental Science & Technology, 1998. **32**(19): p. 2900-2908.
[82] Redwood, P.S., J.R. Lead, R.M. Harrison, I.P. Johnes, and S. Stoll, *Characterization of humic substances by environmental scanning electron microscopy.* Environmental Science & Technology, 2005. **39**(7): p. 1962 - 1966.
[83] Danilatos, G.D., *Foundations of Environmental Scanning Electron Microscopy.* Advances in Electronics and Electron Physics, 1988. **71**: p. 109-250.
[84] Yuan, W. and A.L. Zydney, *Effects of solution environment on humic acid fouling during microfiltration.* Desalination, 1999. **122**: p. 63-76.
[85] Koh, M., M.A. Clark, and K.J. Howe, *Filtration of lake natural organic matter: Adsorption capacity of a polypropylene microfilter.* Journal of Membrane Science, 2005. **256**(1-2): p. 169-175.
[86] Lead, J.R., K.J. Wilkinson, E. Balnois, B.J. Cutak, C.K. Larive, S. Assemi, and R. Beckett, *Diffusion coefficients and polydispersities of the Suwannee River fulvic acid: Comparison of fluorescence correlation spectroscopy, pulsed-field gradient nuclear magnetic resonance, and flow field-flow fractionation.* Environmental Science & Technology, 2000. **34**(16): p. 3508-3513.
[87] Schimpf, M.E. and M.P. Petteys, *Characterization of humic materials by flow field-flow fractionation.* Colloids and Surfaces A: Physicochemical and Engineering Aspects, 1997. **120**(1-3): p. 87-100.
[88] Hosse, M. and K.J. Wilkinson, *Determination of electrophoretic mobilities and hydrodynamic radii of three humic substances as a function of pH and ionic strength.* Environmental Science & Technology, 2001. **35**(21): p. 4301-4306.
[89] Jucker, C. and M.M. Clark, *Adsorption of Aquatic Humic Substances on Hydrophobic Ultrafiltration Membranes.* Journal of Membrane Science, 1994. **97**: p. 37-52.
[90] Ulbricht, M., *Advanced functional polymer membranes.* Polymer, 2006. **47**: p. 2217-2262.
[91] Lee, S., J. Cho, and M. Elimelech, *A novel method for investigating the influence of feed water recovery on colloidal and NOM fouling of RO and NF membranes.* Environmental Engineering Science, 2005. **22**(4): p. 496-509.
[92] Lee, S., J.W. Cho, and M. Elimelech, *Combined influence of natural organic matter (NOM) and colloidal particles on nanofiltration membrane fouling.* Journal of Membrane Science, 2005. **262**(1-2): p. 27-41.
[93] Li, Q.L. and M. Elimelech, *Organic fouling and chemical cleaning of nanofiltration membranes: Measurements and mechanisms.* Environmental Science & Technology, 2004. **38**(17): p. 4683-4693.

[94] Yang, W.B., N. Cicek, and J. Ilg, *State-of-the-art of membrane bioreactors: Worldwide research and commercial applications in North America.* Journal of Membrane Science, 2006. **270**(1-2): p. 201-211.
[95] Rosenberger, S., C. Laabs, B. Lesjean, R. Gnirss, G. Amy, M. Jekel, and J.C. Schrotter, *Impact of colloidal and soluble organic material on membrane performance in membrane bioreactors for municipal wastewater treatment.* Water Research, 2006. **40**(4): p. 710-720.
[96] Jarusutthirak, C. and G. Amy, *Role of soluble microbial products (SMP) in membrane fouling and flux decline.* Environmental Science & Technology, 2006. **40**(3): p. 969-974.
[97] Schafer, A.I., A.G. Fane, and T.D. Waite, *Fouling effects on rejection in the membrane filtration of natural waters.* Desalination, 2000. **131**(1-3): p. 215-224.
[98] Ledin, A., S. Karlsson, A. Duker, and B. Allard, *Characterization of the Submicrometer Phase in Surface Waters - a Review.* Analyst, 1995. **120**(3): p. 603-608.
[99] Bielska, M. and J. Szymanowski, *Removal of methylene blue from waste water using micellar enhanced ultrafiltration.* Water Research, 2006. **40**(1027-1033).
[100] Hong, S. and M. Elimelech, *Chemical and physical aspects of natural organic matter (NOM) fouling of nanofiltration membranes.* Journal of Membrane Science, 1997. **132**: p. 159-181.